Universitat Autònoma de Barcelona

Ruthenium Complexes with Polynucleating Ligands and their Capacity to Catalytically Oxidize Water to Dioxyen.

PhD Thesis presented by

LAIA FRANCÀS FORCADA

Supervised by

Prof. Antoni Llobet Dalmases, Dr. Lluís Escriche Martínez and Dr. Xavier Sala Román

Programa de doctorat de "Catálisis Homogénea"

Departament de Química

Facultat de Ciències

2011

Universitat Autònoma de Barcelona

Memòria presentada per aspirar al Grau de Doctor per Laia Francàs Forcada.

Laia Francàs Forcada

Vist i plau

Prof. Antoni Llobet Dalmases

Institut Català d'Investigació Química (ICIQ), Tarragona
Universitat Autònoma de Barcelona, Bellaterra, Barcelona

Dr. Lluís Escriche Martínez

Dept. Química
Facultat de Ciències
Universitat Autònoma de Barcelona

Dr. Xavier Sala Román

Dept. Química
Facultat de Ciències
Universitat Autònoma de Barcelona

Bellaterra, 1 de Setembre de 2011

PREFACE

According to the decision of the PhD commission of the UAB taken on June 15th, 2011, this PhD Thesis is presented as a compendium of publications. In addition two new manuscripts that have been part of this PhD research, are also included.

In the following part all the publications and manuscripts are presented (following the order of their appearance from the first to the last chapter):

Publications presented to the PhD commission on June 15th, 2011:

Paper A: "Ru Complexes That Can Catalytically Oxidize Water to Molecular Dioxygen" Isabel Romero, Montserrat Rodríguez, Cristina Sens, Joaquim Mola, Mohan Rao Kollipara, Laia Francàs, Elena Mas-Marza, Lluís Escriche, and Antoni Llobet. "Ru Complexes That Can Catalytically Oxidize Water to Molecular Dioxygen." *Inorg. Chem.* **2008**, 47, 1824-1834.

Paper B: "Synthesis, Structure and Reactivity of New Tetranuclear Ru-Hbpp Based Water Oxidation Catalysts" Laia Francàs, Xavier Sala, Eduardo Escudero-Adán, Jordi Benet-Buchholz, Lluís Escriche and Antoni Llobet. *Inorg. Chem.* **2011***,* 50, 2771-2781.

Paper C: "A Ru-Hbpp-Based Water-Oxidation Catalyst Anchored on Rutile TiO_2" Laia Francàs, Xavier Sala, Jordi Benet-Buchholz, Lluís Escriche, and Antoni Llobet. *ChemSusChem* **2009**, 2, 321-329.

Additional manuscripts:

Paper D: "Ru-Hbpp-Based Water-oxidation Catalysts anchored on FTO-TiO_2" Laia Francàs, Xavier Sala, Jordi Benet-Buchholz, Lluís Escriche and Antoni Llobet. IN PREPARATION

Paper E: "Synthesis, Characterization and Linkage Isomerism in Mono- and Dinuclear Ruthenium Complexes Containing the New Pyrazole Based ligand Hpbl" Laia Francàs, Daniel Moyano, Jordi Benet-Buchholz, Xavier Fontrodona, Lluís Escriche, Antoni Llobet and Xavier Sala. IN PREPARATION

Acknowledgements

In the following part I express in Catalan, my mother tongue, my acknowlgments to all the people that in a way or another have given support to my PhD Thesis.

Al posar-me davant de l'ordinador per escriure els agraïments, em venen al cap tantes i tantes persones que han fet possible aquest moment, que és impossible que hi surtin totes reflectides. Han estat 5 anys i mig molt intensos a nivell professional, però també a nivell personal, que fan que si ara tornés enrere en el temps, tornaria a començar aquesta aventura, que està apunt d'acabar.

En primer lloc m'agradaria agrair als meus tres directors: Dr. Lluís Escriche, Dr. Antoni Llobet i Dr. Xavier Sala, al haver-me permès treballar amb ells, la seva paciència i la seva disponibilitat, realment ha estat un plaer treballar amb vosaltres. Lluís moltes gràcies, pel dia a dia, per ser-hi sempre que he tingut un dubte. Toni, moltes gràcies per la teva proximitat tot i estar a Tarragona i per donar-me l'oportunitat de fer aquesta tesi. I Xavi, moltes gràcies, per tots els teus consells i la teva confiança, la veritat és que he après moltes coses treballant al teu costat.

Tampoc em puc descuidar als altres membres del grup: Al Dr. Jaume Casabó per estar sempre disposat a compartir la seva saviesa i bon humor; Al Dr. Jordi García-Anton, per escoltar sempre els meus dubtes, tant químics com personals.

Al servei tècnic i administratiu de la unitat de química inorgànica per la seva ajuda i eficàcia. Agraïment que vull fer extensiu als diferents científico-tècnics de la Universitat Autònoma de Barcelona: Al Servei d'Anàlisi Química, especialment a la Dra. Alba Estaquio i la Ma Jesús Ibarz; Al servei de Ressonància Magnètica Nuclear, Pau gràcies per barallar-te amb mi amb els nitrògens.

També em cal donar les gràcies als cristal·lògrafs que han resolt les estructures cristal·lines d'aquesta tesi, al Dr. Jordi Benet i al Dr. Eduardo Escudero de l'ICIQ i al Dr. Xavier Fontrodona de la UdG.

Tampoc em puc descuidar de donar les gràcies a la Dra. Isabel Romero i la Dra. Montserrat Rodríguez de la UdG, pels seus consells i el seu ajut sempre que l'he necessitat.

Durant la tesi he tingut la sort que de tenir sempre les portes obertes per anar al Institut Català d'Investigació Química (ICIQ). Gràcies al seu servei tècnic i administratiu. Però sobretot no puc descuidar de donar les gràcies als meus companys de laboratori d'allà, per fer-me sentir una més del grup i ajudar-me en tot allò que he necessitat. Moltes gràcies Lydia, Carlo, Nora, Isidoro, Stephan, Pau, Laura i Sonnath. En especial a la Lydia amb qui vaig començar aquesta aventura i amb qui sempre he pogut comptar, moltes gràcies per tot.

I would like to thank prof. Franc Meyer from Göttingen University, for accepting me in his big group during three months and for his support and to the whole Meyer's group. My stage in Göttingen it would not be the same without my friends: Asia, Katrin, Daniel and Maria. Thanks for all the great moments we spent together.

I tornant a casa, no em puc descuidar a la gent del meu grup, amb qui he compartit hores i hores de laboratori, congressos, preocupacions i alegries. Gràcies a tots els que hi han passat: Sílvia, Abel, Lydia, Sergi, Gavin, Joan, Josep, Raquel, Daniel, Jonathan i Fernando. Però evidentment molt especialment en Joan amb qui més temps he passat entre aquestes quatre parets, moltíssimes gràcies per tot, sense tu aquesta aventura no hagués estat igual. Moltes gràcies Mercè per ser la millor companya de laboratori "consorte" que podia tenir.

Gemma, Jordi, Dani, Ori, Nacho, Karen, Meri, Joan, Josep, Mònica, Miguel, Xavi. Diuen que tota aventura té un tresor, doncs la vostra amistat n'és un dels millors que m'enduc d'aquesta. Moltíssimes gràcies de tot cor, per tots els moments que hem passat junts al laboratori i fora, que en són molts i que espero que seguim ampliant. Un trosset d'aquesta tesi també és vostre. Sònia, Aldonza, Mercè, Albert, això també va per vosaltres.

A la resta de companys de la planta d'inorgànica (Joan, Adaris, Lourdes, Alba, Eduardo, Miquel, Leo, Adu, Ma Angeles, Fran, Mireia, Sílvia, Cata, Katia, Jordi), moltes gràcies per tot, de debò que sou els millors que he pogut trobar.

A les meves amigues de tota la vida Carme, Anna, Cris, Marta, Mireia, Ester, Gemma, Sílvia, per poder comptar sempre amb vosaltres, per compartir tantes i tantes aventures, sense vosaltres no seria la mateixa. Als de Monis per tots els sopars i moments de desconnexió. A les Sisonetes per omplir de música la meva vida. Gràcies Jordi per deixar-me fer servir les teves fotos de les gotes per la portada i a tu Albert, pels teus retocs finals de professional.

A les químiques, per preocupar-se sempre de mi i intentar no perdre mai el contacte. Gràcies Rut per compartir amb mi aquest tram final de tesi sense les nostres hores de teràpia al cotxe no hagués estat el mateix.

I per últim però no per això els menys importants, a la meva família, sense ells us puc ben assegurar que no seria qui sóc. Gràcies pel futris, la millor medicina pels moments baixos. Molt i molt especialment als meus pares i la meva germana per ser-hi i fer-me costat sempre, sense vosaltres res d'això hagués estat possible, moltíssimes gràcies.

A totes aquelles persones que d'una manera o altre m'han ajudat a créixer com a persona.

The work performed in the present doctoral thesis has been possible thanks to the funding of:

Institut Català d'Investigació Química (ICIQ).

Grups de Recerca reconeguts de la Generalitat de Catalunya.

Ministerio de Ciencia e Inovacion (MICINN).

Comission of the European Union throgh project SOLAR-H2.

American Chemical Society through the Petroleun Research Fund.

Finally I would also like to thank Universitat Autònoma de Barcelona for the pre-doctoral FI-UAB grant.

GRAPHICAL ABSTRACTS

I. Introduction (pages 1- 40):

Photosynthesis is the biological process by which photons from the sun are captured and the energy is stored into the energy rich carbon molecules needed to power life. Inspired by this process, artificial photosynthesis seeks to use water and sunlight to obtain H_2 as a carbon free fuel. In this context the polypyridilic ruthenium aqua/oxo systems are interesting in order to carry out the water oxidation reaction. All these concepts are developed in this chapter.

II. Objectives (pages 41-44)

III. Results and discussion (pages 45-114)

1. **Ruthenium-Hbpp based complexes capable to oxidize water. Deactivation pathway.** Including the works:

A. Synthesis, Structure and Reactivity of New Tetranuclear Ru-Hbpp Based Water Oxidation Catalysts

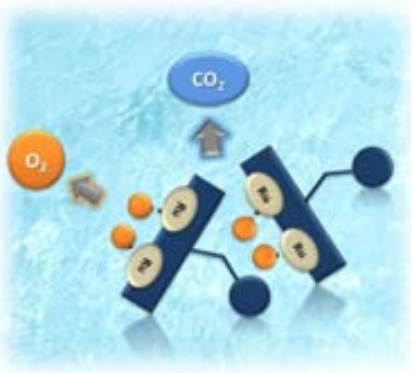

The synthesis of new tetra- and octadentate Hbpp modified ligands have been described. In addition, their corresponding di- and tetranuclear complexes have been synthesized and thoroughly characterized. The catalytic activity of these Ru-OH_2/Ru=0 systems towards water oxidation has been tested, and their deactivation pathway has been studied.

B. A Ru-Hbpp-Based Water-Oxidation Catalyst Anchored on TiO_2-rutile

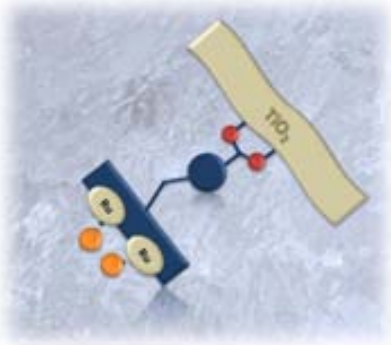

Aiming the anchoring of the dinuclear active complex onto rugged inorganic supports such us TiO_2 the Hbpp-Bz ligand has been modified by the addition of a carboxylic moiety. The corresponding complexes have been synthesized, characterized and supported onto the surface of TiO_2-rutile powder. The new heterogeneous catalyst has been used to oxidize water using Ce(IV) as chemical oxidant.

C. Ru-Hbpp-Based Water-oxidation Catalysts Anchored on FTO-TiO_2

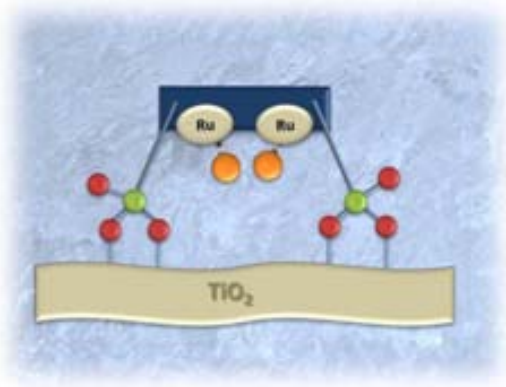

Complexes ***$[Ru^{II}_2(L\text{-}L)(bpp)(trpy\text{-}Pe)_2]^{n+}$*** *(L-L= μ-Cl and n = 2; L-L= μ-Ac and n = 2, L-L = $(H_2O)_2$ and n = 3) have been prepared in order to anchor them onto FTO-TiO_2 films. The properties of the homogeneous and the supported catalysts have been studied. Together with the modified electrode* ***FTO-TiO_2-$[Ru^{II}_2(bpp\text{-}Ra)(H_2O)_2(trpy)]^{2+}$****, they have been tested as water oxidation catalysts by electrochemical activation.*

2. Synthesis, characterization and linkage isomerism in mono- and dinuclear ruthenium complexes containing the new Hpbl ligand with different coordination sites

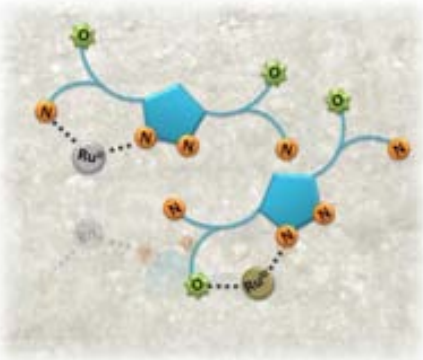

The synthesis and coordinating abilities in front of Ru of a new hemilabile bridging ligand are described. The aim of the work is to develop a new family of ruthenium complexes capable to perform linkage isomerism in order to stabilize the Ru high oxidation states. This linkage isomerism is based on the different N/O affinity of the Ru(II) and Ru(III) oxidation states

VI. Summary and conclusions

(pages 115-120)

TABLE OF CONTENTS

GLOSSARY OF TERMS AND ABBREVIATIONS

1D	Monodimensional
2D	Bidimensional
ATP	Adenosine TriPhosphate
bpea	N,N-bis(2-pyridyl)ethylamine
bpy	Bipyridine
CASPT2	Complete Active Space Perturbation Theory
CB	Conduction Band
COSY	Correlation Spectroscopy
CPE	Controlled potential electrolysis
CV	Cyclic Voltammetry
d (NMR)	Doublet
DFT	Density Functional Theory
DOSY	Diffusion-Ordered NMR spectroscopy
E	Potential
$E_{1/2}$	Half potential
ET	Electron transfer
E^0	Standart potential
FTO	Fluorine-doped tin oxide
HMBC-N	Heteronuclear multiple-bond correlation spectroscopy proton-nitrogen
ia	Anodic current
ic	Cathodic current
ITO	Indium Tin Oxide
J	Coupling Constant
M	Molar
MLCT	Metal to Ligand Charge Transfer
MS	Mass Spectroscopy
NHE	Normal Hydrogen Electrode
NMR	Nuclear Magnetic ressonance
NADPH	Nicotinamide Adenine Dinucleotide Phosphate

OAc^-	Acetate
OEC	Oxygen Evolving Center
PCET	Proton Coupled Electron Transfer
PEM	Proton Exchange Membrane
POM	Polyoxometalate
POV-Ray	Persistent of Vision- Raytracer
ppm	Parts per million
PSI	Photosystem I
PSII	Photosystem II
PT	Proton Tranfer
Py	Pyridine
Pz	Pyrazole
q (NMR)	Quadruplet
RT	Room Temperature
s (NMR)	Singlet
SSCE	Standart Saturated Calomel Electrode
t (NMR)	Triplet
TBAH	Tetra(n-butyl)ammonium hexafluorophosphate
TLC	Thin Layer Chromatography
TMSBr	Trimethylsilyl bromide
TOF	Turn Over Frequency
TON	Turn Over Number
Trpy	Terpyridine
UV-vis	Ultraviolet-visible spectroscopy
Vs.	Versus
WOC	Water Oxidation Catalyst
Yz	Tyrozine Z
δ (NMR)	Chemical shift
ε	Extintion coefficient
λ	Wavelength

I. INTRODUCTION

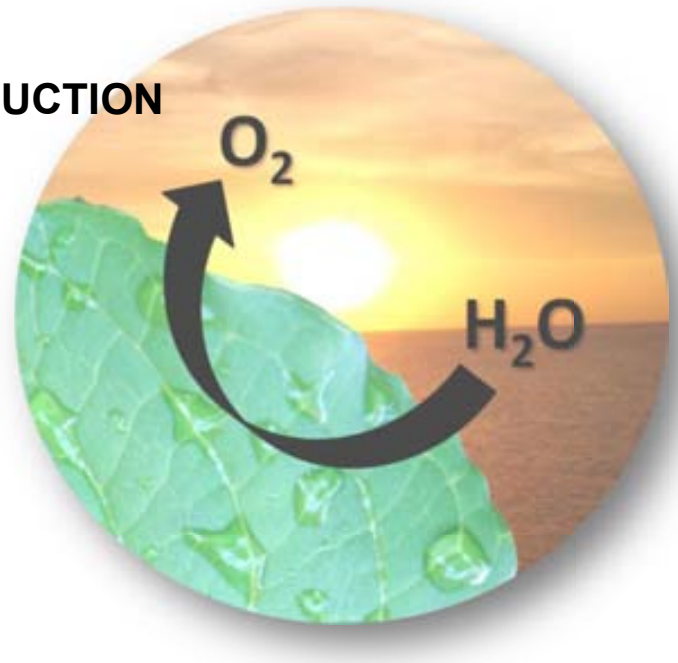

I.1. Abstract

This starting chapter presents the bases for the work performed in this PhD thesis, from the general properties of ruthenium chemistry to the specific water oxidation mechanism of a ruthenium complex.

Furthermore, it constitutes and updated and extended version of the following review included in this work:

- "Ru Complexes That Can Catalytically Oxidize Water to Molecular Dioxygen" Isabel Romero, Montserrat Rodríguez, Cristina Sens, Joaquim Mola, Mohan Rao Kollipara, Laia Francàs, Elena Mas-Marza, Lluís Escriche, and Antoni Llobet. "Ru Complexes That Can Catalytically Oxidize Water to Molecular Dioxygen." *Inorganic Chemistry* **2008**, 47, 1824-1834.

I.2. An Introduction to the ruthenium chemistry

Ruthenium is a metal situated in the d group of the periodic table. The electronic configuration [Kr] $4d^7$ $5s^1$ confers its very unique redox properties, together with osmium, displaying the widest range of oxidation states in their complexes. This gives way to various ruthenium complexes having oxidation states from -2 as in $[Ru(CO)_4]^{2-}$ to +8 as in RuO_4, which corresponds to d^0 to d^{10} electronic configurations, each with different coordination geometries.[1] Consequently, ruthenium complexes are redox-active and their application as redox reagents in various chemical reactions is a topic of much current interest. Other general characteristics of ruthenium coordination compounds are their high electron transfer capacity[2] and their ability to stabilize reactive species like oxo-metals[3] and metal-carbene complexes.[4]

Ruthenium complexes are widely used and studied in different chemical fields. They attract the attention of researchers due to their high stability and the easy modification of their properties by employing carefully controlled synthetic methods. In ruthenium complexes, clear correlations can be observed between their properties and the nature of the ligands bound to the central metal ion. This correlation allows us to classify them according to their applications. Complexes bearing π-conjugated ligands or systems that enable electronic delocalization have shown specific properties in nonlinear optics,[5] magnetism,[6] molecular sensing[7] and liquid crystals.[8] On the other hand, sulfoxide complexes have been extensively studied due to their relevant usefulness in chemotherapy.[9] However, the most employed are ruthenium complexes with heterocyclic N-donor ligands due to their interesting spectroscopic, photophysical and electrochemical properties.[10] These may be taken into advantage for their application as photosensitizers for photoactive conversion of solar energy,[11] molecular electronic devices[12] and photoactive DNA cleavage agents for therapeutic purposes.[13] In the present work, catalysis is the most important application of the prepared ruthenium complexes.[1,14] Characteristics that make them suitable catalysts are: the synthetic versatility, the availability of high oxidation states and the robust character of their coordination sphere. Above all, polypyridyl ruthenium complexes with aqua ligands have been extensively employed in oxidation reactions of organic[15] and inorganic[16] substrates, C-H insertion[17] and proton-coupled electron transfer.[18]

Complexes with phosphine ligands are used in hydrogenation reactions[19] as well as in addition reactions[20] and metathesis.[21] Other ligands like carbonyl, tertiary phosphines, cyclopentadienyl, arenes and dienes have proven to serve effectively as the activating factors such as in hydrogen abstraction[22] or generation.[23]

I.3. Ruthenium polypyridyl aqua complexes

During 1940s to 1960s, the Australian coordination chemist Frances P. Dwyer and his collaborators published a series of papers developing the synthetic chemistry of polypyridyl ruthenium complexes.[24] The synthetic procedures firstly described in these initial publications have been used, expanded and improved enormously. This background allows varying the properties of these complexes by rationally combining the ruthenium surrounding ligands and expands their application to different fields of science. In the late 1960s, Thomas J. Meyer and collaborators started a systematic study of these complexes and pointed attention to their relevant reactive properties based on their accessibility to long-lived excited states and oxidation states varying from Ru(II) to Ru(VI).[25] It is important to notice that these redox properties can be modulated by varying the ancillary ligands.[26]

A particularly interesting situation arises when the water molecule is directly bound to the metal centre. These Ru-aqua complexes have very special redox properties as they are affected by proton exchange. As shown in Scheme 1, the successive oxidations from Ru(II) to Ru(IV) are accompanied by a sequential proton losing favoured by the enhanced acidity of the bonded aqua ligand.

$$Ru^{II}\text{-}OH_2 \underset{+H^+ +1e^-}{\overset{-H^+ -1e^-}{\rightleftharpoons}} Ru^{III}\text{-}OH \underset{+H^+ +1e^-}{\overset{-H^+ -1e^-}{\rightleftharpoons}} Ru^{IV}{=}O$$

Scheme 1

The redox pH dependence shifts the Ru(III/II) and Ru(IV/III) transitions to lower potentials when a drop in the medium acidity takes place. This fact is attributed to the increase of proton acidity in higher oxidation states. The Nernst equation, see equation 1, correlates pH with redox potential in such a way that, for a monoprotic and

monoelectronic transfer, the redox potential diminishes in 59 mV by every pH unit increased.

$$E_{1/2}=E^{0}_{1/2}-0.059(m/n)\cdot pH \qquad (1)$$

$E_{1/2}$= half wave redox potential at a given pH, $E^{0}_{1/2}$= half wave redox potential at standard conditions, m= number of transferred protons, n= number of transferred electrons.

The graphical representation of this pH dependence in front of the redox potential is known as Pourbaix diagram. This diagram combine the redox equilibria with the acid-base equilibrium of all the thermodynamically stable species involved and represents the dependence of the half wave redox potential, $E_{1/2}$, with respect to the complete pH range.

The most significant trends of these ruthenium aqua complexes can be observed in Scheme 2, which shows the Latimer diagrams for two different polypyridylic ruthenium complexes containing (b) and non-containing (a) a water molecule as an ancillary ligand. In this scheme, the electronic configurations were point out due to their importance in redox processes where electrons are gained and lost from dπ levels. Changes in the electron content do not occur in the σ-bonding framework, which is the reason for the observed coordinative stability in the three consecutive oxidation states and explains the relevance of these complexes in the study of electron transfer and redox reactions in general.

$$\underset{(d\pi^4)}{cis\text{-}[Ru^{IV}(bpy)_2(Cl)_2]^{2+}} \xrightarrow{1.7\ V} \underset{(d\pi^5)}{cis\text{-}[Ru^{III}(bpy)_2(Cl)_2]^{2+}} \xrightarrow{0\ V} \underset{(d\pi^6)}{cis\text{-}[Ru^{II}(bpy)_2(Cl)_2]^{2+}} \qquad (a)$$

$$\underset{(d\pi^4)}{cis\text{-}[Ru^{IV}(bpy)_2(py)(O)]^{2+}} \xrightarrow{0.78\ V} \underset{(d\pi^5)}{cis\text{-}[Ru^{III}(bpy)_2(py)(OH)]^{2+}} \xrightarrow{0.67\ V} \underset{(d\pi^6)}{cis\text{-}[Ru^{II}(bpy)_2(py)(H_2O)]^{2+}} \qquad (b)$$

(V versus NHE, M=0.1 at pH=7)

Scheme 2. Latimer diagrams of Ru polypyridyl complexes (a) non-containing and (b) containing a coordinated water molecule.

Diagram (a) of Scheme 2 shows the typical redox behaviour observed in ruthenium chloro polypyridyl complexes. For these compounds, the Ru(III/II) oxidation takes place at low and accessible potentials (0 V) but, an increase in charge and oxidation state shifts the Ru (IV/III) oxidation to highly positive potentials (1.7 V).[27] When the anionic chloro ligands are replaced by neutral pyridine and water ligands, diagram (b), an increase in the Ru(III)-OH/Ru(II)-H_2O potential (from 0 to 0.6 V) is observed whereas the Ru(IV)-O/Ru(III)-OH redox couple decreases to 0.67 V.[28] This data point to a dramatic stabilization of the Ru(IV) species when the aqua ligand coordinates the metal centre. This in turn is caused by its successive deprotonation and subsequent electronic stabilization to the higher oxidation states by the oxo complex formation. As shown in Figure 1, the $d\pi_{Ru}$-$2p\pi,_O$ multiple bond interaction is the key factor favouring the stabilization of Ru(IV). The final result of this process is the near overlap of the Ru(IV/III) and Ru(III/II) redox couples, which has important reactivity implications; thermodynamically, at pH=7, the Ru(IV) species can behave with almost the same efficiency as two-electron or one-electron oxidants.[29]

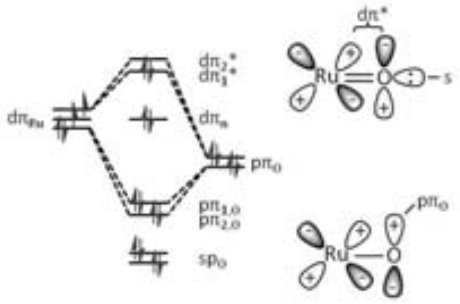

Figure 1. Ru^{IV}=O schematic energy orbital diagram.

The special properties that the Ru^{IV}=O group exerts to its complexes enable them to operate as efficient oxidants for a wide range of substrates. Firstly, as mentioned above, the oxo groups stabilize high oxidation states and make them accessible at fairly low potentials. In addition, from the mechanistic point of view, its ability to accept two electrons can avoid radicalary reaction pathways of high energy and reactivity.[29] Finally, the robust character of its first coordination sphere makes possible the easy exchange between Ru(II) and Ru(IV) without any dramatic changes in the catalyst structure, the oxo group being the only that modifies its composition.

Another interesting point of these high oxidation state oxo complexes is the possible modulation of its reactivity by tuning their redox potentials, a fact that is easily accomplished by modifying the accompanying ligands. Table 1[26] shows this

strong ligand effect over the Ru(IV/III) and Ru(III/II) redox couples potentials in different families of ruthenium complexes with N-containing ligands.

Table 1. Electrochemical Parameters for aqua complexes of Ru[a].

Entry	Complex	$E_{1/2}$(V) [b]			$\Delta E_{1/2}$ [c]
		Ru(III/II)	Ru(IV/III)	Ru(IV/II)	
1	$[Ru(NH_3)(H_2O)]^{2+}$	-0.33	0.01	0.01	0.68
2	$[Ru(tpy)(H_2O)_3]^{2+}$ [c]	0.35	0.64	0.50	0.29
3	$[Ru(tpy)(acac)(H_2O)]^{+}$	0.16	0.45	0.31	0.29
4	$[Ru(tpy)(C_2O_4)(H_2O)]^{+}$	0.19	0.56	0.38	0.37
5	*trans*-$[Ru(tpy)(pic)(H_2O)]^{+}$	0.21	0.45	0.33	0.24
6	*cis*-$[Ru(tpy)(pic)(H_2O)]^{+}$	0.38	0.56	0.47	0.22
7	$[Ru(tpy)(tmen)(H_2O)]^{2+}$	0.36	0.59	0.48	0.13
8	$[Ru(tpy)(phen)(H_2O)]^{2+}$	0.50	0.60	0.55	0.10
9	$[Ru(tpy)(bpy)(H_2O)]^{2+}$	0.49	0.62	0.56	0.13
10	$[Ru(tpy)(4,4'\text{-}((CO_2Et)_2bpy))(H_2O)]^{2+}$	0.66	0.80	0.73	0.13
11	$[Ru(tpy)(4,4'\text{-}Me_2\text{-}bpy)_2(H_2O)]^{2+}$	0.47	0.61	0.54	0.14
12	*cis*-$[Ru(6,6'\text{-}Me_2\text{-}bpy)_2(H_2O)]^{2+}$ [d]	0.57	0.73	0.65	0.16
13	*cis*-$[Ru(bpy)_2(py)(H_2O)]^{2+}$	0.43	0.53	0.48	0.11
14	*cis*-$[Ru(bpy)_2(AsPh_3)(H_2O)]^{2+}$	0.50	0.67	0.59	0.17
15	*cis*-$[Ru(bpy)_2(PPh_3)(H_2O)]^{2+}$	0.50	0.76	0.63	0.36
16	*cis*-$[Ru(bpy)_2(PEt_3)(H_2O)]^{2+}$	0.46	0.67	0.57	0.21
17	*cis*-$[Ru(bpy)_2((P(i\text{-}Pr)_3)(H_2O)]^{2+}$	0.45	0.68	0.57	0.23
18	*cis*-$[Ru(bpy)(biq)(PEt_3)(H_2O)]^{2+}$	0.45	0.63	0.54	0.18
19	$[Ru(tpm)(4,4'\text{-}(NO_2)_2\text{-}bpy)(H_2O)]^{2+}$	0.56	0.75	0.66	0.19
20	*cis*-$[Ru(bpy)(biq)(PPh_3)(H_2O)]^{2+}$	0.48	0.70	0.59	0.22

[a] In H_2O at pH=7.0, T=22±2 ºC, I=0.1 M vs SSCE. [b] $E_{1/2}$ values for Ru^{III}-OH/Ru^{II}-OH_2, Ru^{IV}=O/Ru^{III}-OH, and Ru^{IV}=O/Ru^{II}-OH_2 couples. [c] $\Delta E_{1/2}=E_{1/2}(Ru(IV/III)-E_{1/2}/Ru(III/II)$. [d] pH=4.0. [e] In CH_2Cl_2/H_2O (3:1). Abbreviations: biq= 1,1'-biquinoline; tmen= N,N,N-tetramethylethylenediamine; dppene=cis-1,2-bis(diphenylphosphino)ethylene; pic= picolinate anion; acac= acetyl acetonate anion; phen= phenantroline.

In general, the Ru(III/II) couple is strongly influenced by the ligands. Ru(II) is stabilized by dπ-π*(L) back-bonding in the presence of ligands such as PPh_3 (entries 16 and 18) having low-lying acceptor levels. However, Ru(III) oxidation state is clearly stabilized by electron-donating ligands as $acac^-$ or $C_2O_4^-$ (entries 3 and 4).

On the other hand, Ru(IV/III) couples are, in general, less sensitive to ligand variations than Ru(III/II). This phenomena is observed by comparing the complexes in entries 3 and 9 or 4 and 8, where changes in the accompanying ligands produce only a slight modification in the potential of the Ru(IV/III) couple whereas the Ru(III/II) couple

is strongly influenced. This behaviour is due to the control of the π-binding exerted by the oxo ligand through a $d\pi_{Ru}$-p_o interaction in the Ru(IV) species.

I.4. Catalysis and Ruthenium Complexes

The term catalysis was coined by Berzelius more than 150 years ago and is derived from the greek words *kata* and *loosen*, which means down, and split or break respectively. The current definition is: "A catalyst is a substance that increases the rate of approach to thermodynamic equilibrium of a chemical reaction without being consumed".[30]

In general, catalysis is divided into homogeneous[31] and heterogeneous[32] catalysis; the former applies when the catalyst and the substrate are in the same phase and the later when they are not. Table 2 summarizes the principal differences between homogeneous and heterogeneous catalysis.

Table 2. Homogeneous vs. heterogeneous catalysis. Schematic comparison.

Features	Homogeneous catalyst	Heterogeneous catalyst
Form	Metal complex	Solid, often metal or metal oxide
Active centres	Well defined	Not defined
Activity	High	Variable
Selectivity	High	Variable
Reaction conditions	Mild	Drastic
Average time of life	Variable	Long
Sensitivity to poisons	Low	High
Problems of diffusion	None	Possible
Recycling	Difficult and expensive	Easy
Separation from products	Difficult	Easy
Variation of steric and electronic features	Possible	Difficult
Mechanism studies	Possible	Difficult

Homogeneous catalysts are based on easily characterizable molecular species with well-defined active sites. These active sites are spatially well separated and have self-similar structures. Consequently, there is a constant energetic interaction between each active site and the substrate. The catalytic properties of a given transition metal in homogeneous phase can be tuned through the nature of the ligands bound to the

metal centre making it a suitable catalyst for different types of catalytic reactions. Knowing how the electronic/geometric properties of the ligands can tune metal reactivity will allow us to rationally design better catalysts and achieve good levels of effectiveness and selectivity.

In contrast, heterogeneous catalysts allow easy product/catalyst separation and recovery from the reaction medium, easy handling and potential catalyst recycling. However, they often lack of good characterization at the molecular level, thus difficulting mechanistic studies. The preparation procedures are concerted and consequently not always easy to reproduce.[33] In addition, the fact that active sites are placed in a microporous environment often causes diffusion control of the catalysed reaction and reduces the activity and the selectivity.

Therefore, the development of new catalyst that combines the best features of both kind of systems is an interesting and growing area in catalysis. These hybrid catalysts are named immobilized heterogeneous catalyst or supported catalysts.[34]

I.4.1. Supported catalysts

An immobilized catalyst is the result of the transformation of a homogeneous catalyst to a heterogeneous one. The simplest process to perform this task is by supporting a soluble active molecule on the surface of an insoluble solid.

The aim of supported catalysts is to combine the mentioned advantages of both homogenous and heterogeneous catalysis such as: (1) high activity, selectivity and reaction rates (homogeneous catalysis), (2) easy catalyst recovery and preparation of multifunctional catalysts (heterogeneous catalysis). Among the different techniques described to immobilize catalysts into solid supports here we point some of the most relevant in our field (Figure 2);

a) Post-synthetic covalent functionalization; includes the anchoring or grafting of the catalyst through suitable functional groups.
b) Post-synthetic non-covalent deposition: includes processes like electrostatic immobilization, physisorption and encapsulation.

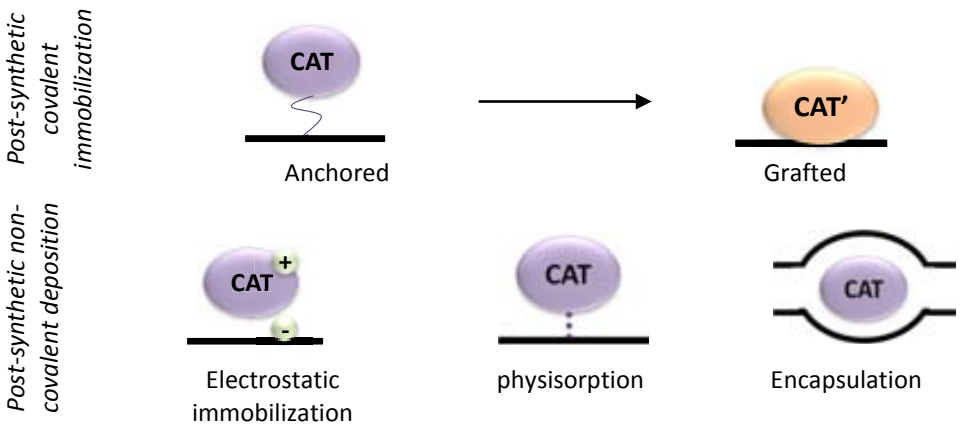

Figure 2. Schematic representation of different types of catalyst immobilization.

In the present work, the most relevant one is the anchoring of a catalyst by covalent tethering.

I.4.1.1. Immobilization by covalent tethering (anchoring)

This immobilization method has been used to support a wide variety of active homogeneous catalysts.[35] One of its advantage is that the chemical surrounding of the metal centre is maintained as in the homogeneous parent precursor, but with all the heterogeneous advantages.[36]

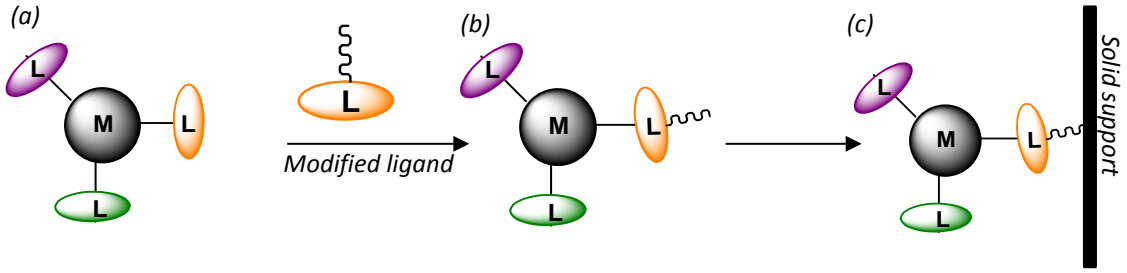

Figure 3. General process for anchoring an homogeneous catalyst into a solid support.

The general covalent immobilization process for an active homogeneous catalyst is represented in Figure 3. A modified ligand is introduced to a well-known active homogeneous catalyst (a) giving a new catalyst (b). This modification, that should be introduced through a peripheral position in order keep the original catalytic activity, allows the catalyst to be anchored by a covalent bond onto the solid support (c). Furthermore, in many cases, the solid support has to be also modified or processed

before the anchoring process. For instance, TiO_2 is generally calcined before being used as solid support.

I.4.2. Titanium dioxide as solid support in catalysis

Titanium dioxide occurs in nature as the minerals rutile, anatase and brookite, being the first two the most common and rutile the thermodynamically most stable form. For the later reason anatase and brookite are both converted into rutile at elevated temperatures, 915 and 750 ^{o}C respectively.[37]

This metal oxide is a semiconductor material that absorbs the UV light component, $\lambda < 377$ for anatase and $\lambda < 397$ for rutile, creating highly oxidative centres. This property has been taken in advantage in photocatalytic redox processes such as waste degradation[38] and alcohol oxidation.[39]

Structural modifications of titanium dioxide can affect its band gap energy allowing it to absorb light in the visible zone, that being of interest in the solar cells research field. These modifications can be carried out by synthesizing new TiO_2-based composite materials,[40] through n-doping or by surface immobilization of sensitizing dyes.[11] The last approach is especially interesting because by introducing adequate functional groups in the organic framework of the ligands, a complex can be easily anchored onto the TiO_2 surface.

The properties that an efficient sensitizer should accomplish are:[41]

- The excited state should have enough thermodynamic driving force for the injection of electrons into the conduction band.
- The oxidized sensitizer should be stable, in order to be quantitatively reduced back by an electron donor or an electron-relay system.
- The dye MLCT absorption should overlap with the solar emission spectrum in order to get the maximum power conversion.

Ruthenium polypyridyl complexes are a versatile family of compounds that exhibit the above-mentioned properties.

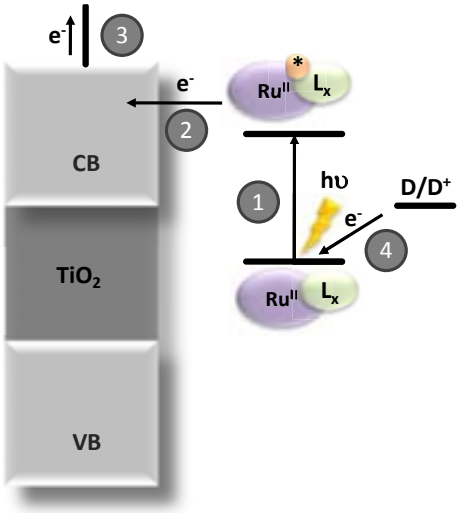

Figure 4. Scheme of visible light induced electron transfer on ruthenium complex sensitized TiO_2.

Figure 4 shows the pathway of a visible light induced electron transfer on a ruthenium complex sensitized TiO_2 device. The ruthenium complex acting as a sensitizer is excited by absorbing visible light (1) and injects an electron into the conduction band (CB) of TiO_2 (2). Once the electron is in the semiconductor it proceeds to an external circuit (3). The oxidized sensitizer can be regenerated by accepting an electron from an electron donor present in the electrolyte (4).[42]

When the sensitizer is a ruthenium (II) complex the first oxidation to ruthenium (III) occurs as a photoinduced electron transfer. However, there is no optimum pathway to obtain the catalytically more interesting oxoruthenium (IV) by the same method, due to the lack of efficient light harvesting ability of the ruthenium (III) complex. The alternative pathway to get TiO_2-$Ru^{IV}=O^{2+}$ is the cross-surface electron transfer between different polypyridyl complexes adsorbed onto TiO_2.[43] This strategy is shown in the Scheme 3.

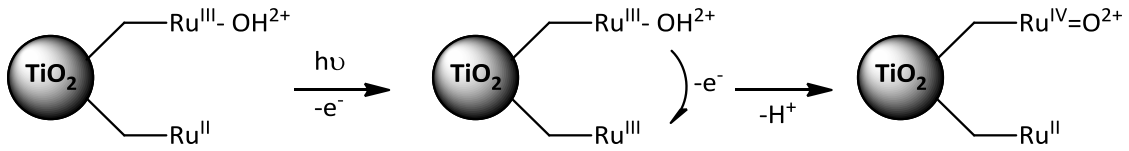

Scheme 3. Indirect route to obtain $Ru^{IV}=O^{2+}$ in an anchored Ru-H_2O complex by a cross surface-electron transfer.

The chemical binding between the molecular sensitizer and the residual OH groups in the TiO_2 surface can be done by reaction with different anchoring groups, being the phosphonate and carboxylate functionalities the most frequently used. Both

functional groups exhibit different binding properties. The carboxylate can behave as monodenate or bidentate linker, whereas phosphonate can also act as a tridentate (Figure 5). Different studies have established that the properties of the sensitized TiO_2 are strongly influenced by the nature and number of the anchoring group[44] and the length of the linkers.[45] These studies concluded that the linkage of a phosphonate moiety is stronger than the carboxylate one. As a consequence when the anchoring group is a carboxylate the efficient electronic coupling between the surface and the sensitizer is dependent on the number of carboxylate groups present in the complex. On the other hand, when the anchoring group is a phosphonate, an additional phosphonate group does not affect the system properties.

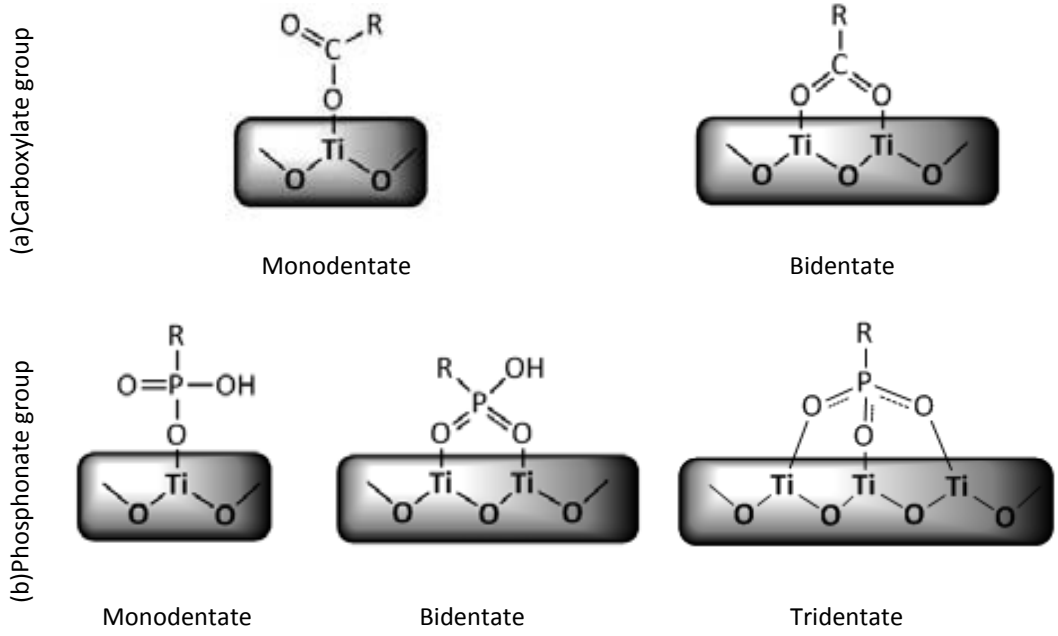

Figure 5. Structure of possible linkages between the complexes with (a) a carboxylate or (b) a phosphonate as anchoring group and the TiO_2 surface.

I.5. Photosynthesis and water oxidation

One of the most important challenges that our society faces in the 21st century is to find a non-contaminant and renewable energy source. Nowadays, by far, fossil fuels are the most used energy sources. However, their reserves are progressively

decreasing at the same time that energy demand continues increasing.[46] Furthermore, a backside in using fossil fuels is the unprecedented rate of carbon dioxide emission into the atmosphere. This increase is known to be closely related to the global climate change.

The earth receives an inexhaustible power flow from the sun. One hour of sunlight is equivalent to all energy humankind uses in a year. So, solar energy has an enormous potential as a clean, abundant and economical energy source, but it cannot be employed such as; it must be captured and transformed into more useful forms, such as a fuel. Green plants have succeeded doing this thanks to photosynthesis. They are capable to take water, sunlight and carbon dioxide to make sugars and starches, which provides the energy they need. Therefore, Nature excels in getting electrons from water and storing them in chemical bonds.

Trying to mimic green plants, scientists are currently developing artificial photosynthetic systems. Cleavage of water into hydrogen and oxygen is the most attractive and environmental friendly (carbon-free) fuel-generating process due to hydrogen combustion produces heat, water and electricity.[47]

In short, the combination of water's availability and hydrogen's cleanliness make water photolysis a great alternative to obtain clean and renewable solar fuels.[48]

I.5.1. Natural photosynthesis

Photosynthesis is the process that converts sunlight energy into the organic molecules of biomass. It takes place in the photosystem II (PSII), cytochrome b_6f, photosystem I (PSI) and ATPsynthase which are spanned along the thylakoid membrane in choroplasts of green plants, algae and oxyphotobacteria (i.e. cyanobacteria) as is shown in Figure 6.

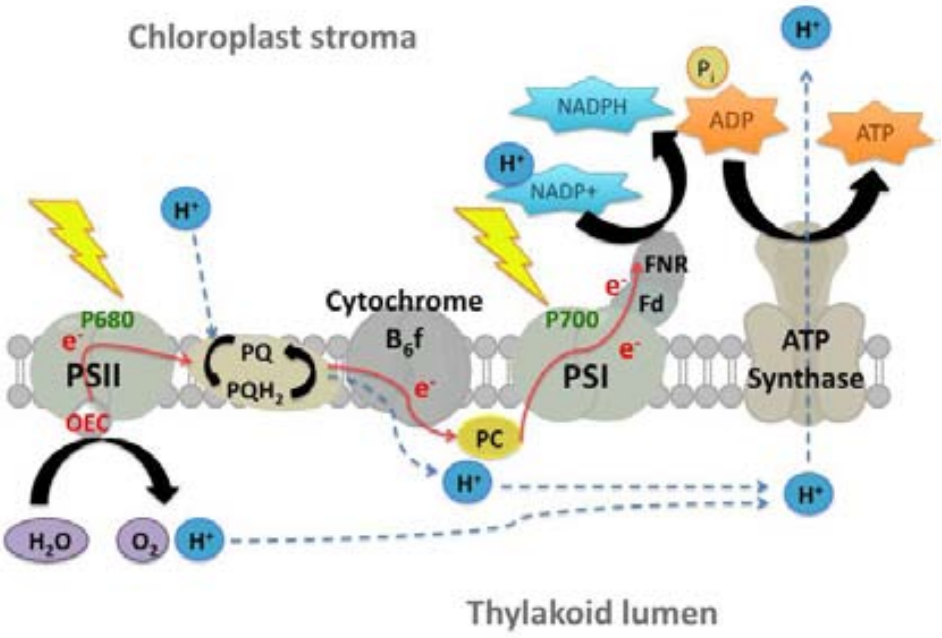

Figure 6. Schematic diagram of the electron-proton transport chain of oxygenic photosynthesis in the thylacoid membrane, showing how PSI and PSII work together to use absorbed light to oxidize water and reduce $NADP^+$.

This figure shows the general process of photosynthesis. The process starts when the chlorophyll and other pigments absorb a photon of solar energy. It is transferred efficiently to the PSII reaction centre. Here is where charge separation takes place generating a high oxidizing species $P680^{\cdot+}$ that drives the water splitting at the Oxygen Evolving Centre (OEC). The reducing equivalent is passed along an electron transport chain through the cytochrome b_6f to PSI where it is excited by a second light photon. At this point, sufficient energy is accumulated to drive the fixation of carbon dioxide, generating first the reduced NADPH (Nicotinamide Adenine Dinucleotide Phosphate) as a hydrogen carrier and the energy rich molecule ATP (Adenosine Triphosphate).[49, 47b]

The most interesting reaction in the context of the present work takes place in the OEC situated in photosystem II that is a multisubunit membrane protein.[50] Although the last decade significant progresses have been done in this field, there remain a lot of unanswered questions especially in the water oxidation mechanism.

One of the breakthroughs achieved this last decade is the refinement of the crystal structure of PSII, which revealed considerable information about the organization of the OEC. The Oxygen Evolving Centre is formed by four manganese

ions and a calcium ion. Figure 7 shows the refined crystal structure published in 2004 by Ferreira et al.[51] The most important outcome is the suggestion that three Mn ions and a Ca ion are forming a cubane-like structure with oxo-bridges linking them. In this proposal, the fourth Mn ion is linked to the cubane moiety by a mono-μ-oxo bridge via one of the oxo groups of the cubane. Surrounding this metal-cluster there are a lot of different amino acid residues. It is important to point tyrosine (Yz), which acts as an intermediate electron carrier between $P680^{\cdot+}$ and the Mn_4Ca-cluster. Nowadays, other studies have been published around the OEC structure, most of them agree with the model proposed by Ferreira et al., and others slightly modify it.[52] However, some important information is still unknown, such as the role and number of water molecules acting as ligands, which hampers a full understanding of the water oxidation mechanism.

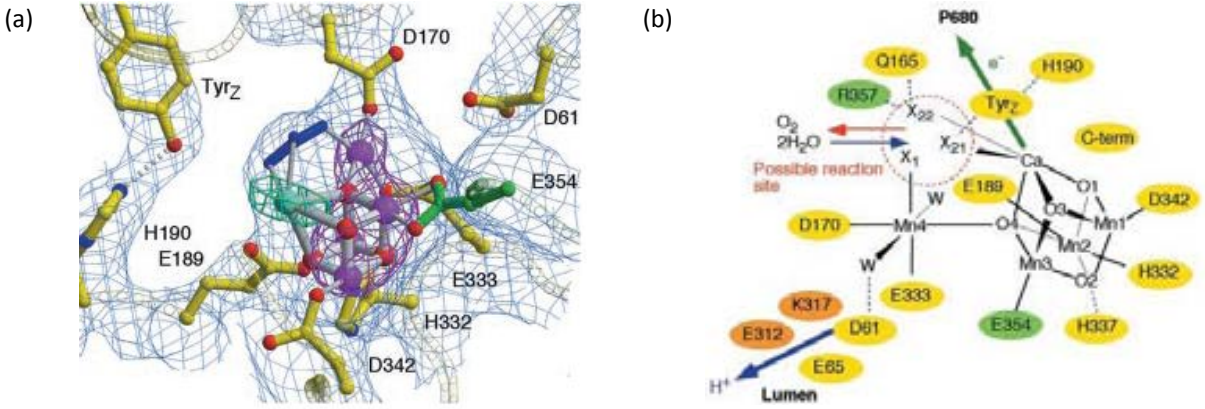

Figure 7. (a) Stereo view of the OEC with side-chain ligands and possible catalytically important side-chain residues. Mn ions, Ca^{2+}, and oxygen atoms are shown in magenta, cyan, and red, respectively. One unidentified nonprotein ligand to the OEC is colored in green. The protein main chain is depicted in light gray. (b) Schematic view of the OEC. Possible water molecules, which are not visible at the current resolution, are indicated as W.

Water oxidation is a four-electron process, therefore four charge-separation steps must be accumulated. The Mn_4Ca-cluster is responsible of carrying out this accumulation through a stepwise oxidation by the tyrosine radical though a series of states S_i (i=0-4). Oxygen formation takes place when the most oxidized cluster state, S_4, returns to the most reduced state, S_0, in a four electron reduction process, as shown in Figure 8. This process involves the oxidation of two water molecules, which have probably been coordinatively bound to the metal centre.[53]

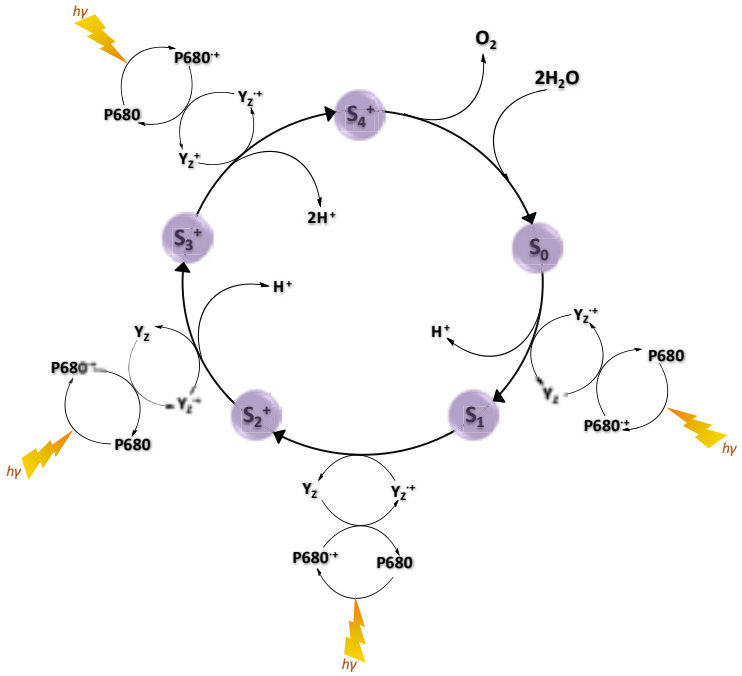

Figure 8. The S-state cycle showing the process that allows oxygen formation.

Some studies[54] suggest that the Ca ion is not only a structural cofactor in the OEC. It could also play an important role as a Lewis acid during the water oxidation process. These studies support the proposed binding of Ca^{2+} to a water molecule affecting its nucleophilic reactivity.

I.5.2. Artificial photosynthesis

The so called artificial photosynthetic process consists in the performance of the water splitting in an electrochemical cell. Only water and sunlight are employed to obtain energy as molecular hydrogen in a way similar to how green plants obtain their energy from water, CO_2 and sunlight.[55]

$$2H_2O \longrightarrow 4e^- + 4H^+ + O_2 \quad (2)$$

$$4e^- + 4H^+ \longrightarrow 2H_2 \quad (3)$$

$$2H_2O \longrightarrow 2H_2 + O_2 \quad (4)$$

Scheme 4. Separation of water splitting reaction into independent half reactions.

The decomposition of water into its elements (H_2 and O_2, (4) in Scheme 4) is a thermodynamically uphill reaction that implies the oxidation of two water molecules to oxygen and the reduction of four protons. To perform the oxidation half reaction a strong oxidant and a suitable redox catalyst are needed (reaction (2), Scheme 4). Similar requirements, a strong reductant and a redox catalyst,

are necessary to reduce protons to H_2 (reaction (3), Scheme 4). The intrinsic complexity of both processes justifies the separation of the overall water cleavage reaction in two compartments, allowing a much easier and independent study of water oxidation and reduction.[56,47,53]

Nowadays another important challenge is the use of sunlight as energy source for this reaction. In the literature, some examples of systems that are capable to split water using ultraviolet radiation[57] can be found. Despite UV radiation is able to promote the desired transformation, systems using it cannot be considered as true artificial photosynthetic devices.

An artificial photosynthetic system should be built by:[58,47] 1) an antenna or photosensitive material for light harvesting and charge separation;[59] 2) a water to oxygen oxidation subcell; 3) a membrane to provide physical separation of the products;[60] 4) a proton to hydrogen reduction subcell.[61]

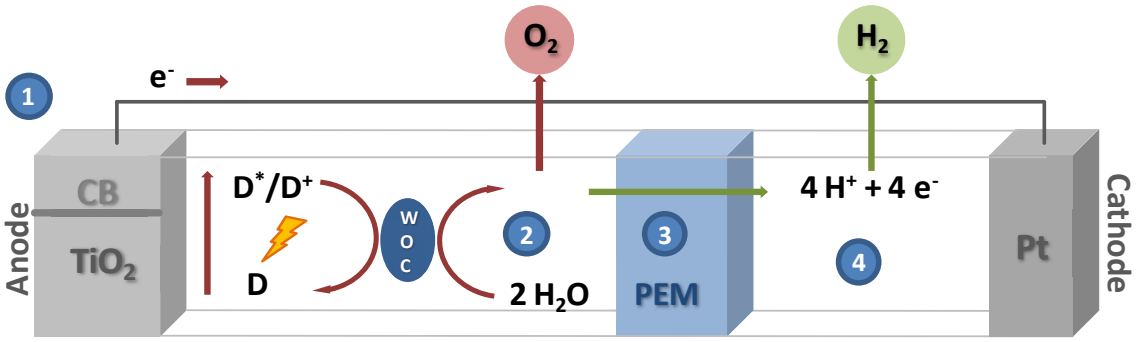

Figure 9. Schematic drawing of a water splitting photochemical cell. 1) Light harvesting device; 2) water oxidation process carried out by a water oxidation catalyst (WOC); 3) proton-exchange membrane; 4) proton reduction process.

Figure 9 shows an example of a water splitting photochemical cell that can be considered as a modification of the Grätzel cell.[56c] In this case, the cell is designed to generate hydrogen as a chemical fuel, instead of electricity, as Grätzel proposed in his original model. The process starts with a photoinduced charge separation. A molecular photosensitizer (D) attached to the TiO_2 absorbs a photon to generate an excited state (D^*), which injects an electron into the TiO_2 conducting band. Some of the most studied photosensitizers in solar energy absorption are polypyridyl complexes of ruthenium (II) such as tris(2,2'-bipyridine)ruthenium (II) that possesses strong absorbance in the visible spectrum and microsecond excited-state lifetimes at room

temperature. The injected electrons are conducted through a wire to the cathode, where protons are reduced to hydrogen by a platinum electrode. The oxidized photosensitizer (D^+) is reduced by the water oxidation catalyst (WOC), regenerating the initial photosensitizer (D). At the same time, the WOC is oxidized accumulating oxidative equivalents. When the oxidation potential is the appropriate one (after 4 absorbed photons), the water oxidation reaction takes place (process 2 in Figure 9). The generated protons go through the proton exchange membrane (PEM) to the cathode where their reduction is carried out. This membrane (3 in Figure 9) which separates the anodic and cathodic cell compartments is not only useful to avoid H_2 / O_2 mixing but also to prevent the short-circuiting of the cell. Note that the PEM must be sufficiently rugged to resist relatively severe conditions of pH and redox potentials. The most difficult process of this complex system is water oxidation.[62]

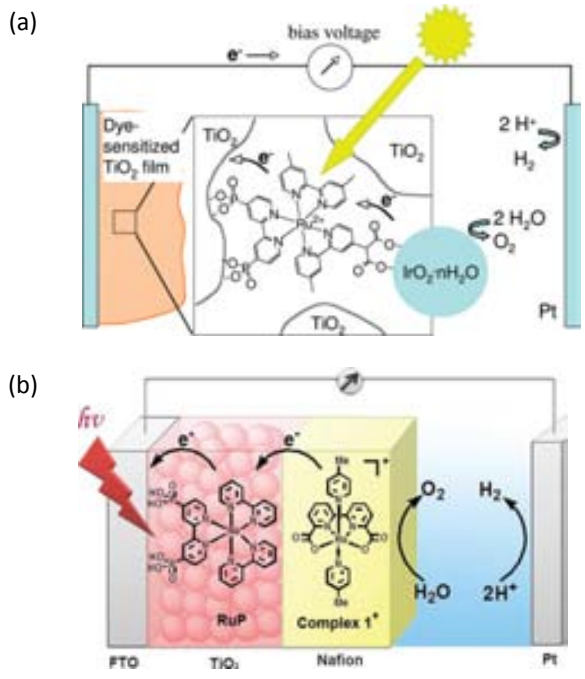

Figure 10. Scheme of the water oxidation dye sensitized solar cell (a) published by Mallouk's group, (b) published by the Sun's group.

Only few practical examples of the overall above-mentioned photoelectrochemical fuel cell have been published in the literature. In 2009, Mallouk's group reported the first device that was capable to carry out the water splitting reaction by sunlight[63] as shown in Figure 10(a). In this device, a ruthenium polypyridylic complex modified with bidentate phosphonates in the bypiridine ligands was used as a photosensitizer attached to a nanocrystalline TiO_2 film deposited on F-SnO_2. In this case the WOC were hydrated iridium oxide nanoparticles ($IrO_2 \cdot nH_2O$) stabilized by the dye carboxylate moieties. A Pt wire was used as a counter electrode and Ag/AgCl as a reference electrode, and they were separated from the working

electrode (TiO_2 film) by a coarse frit. This system shows low quantum efficiency[1] due to the slow electron transfer from $IrO_2 \cdot nH_2O$ nanoparticles to the oxidized dye. Later on, Sun and co-workers[64] published the second fuel cell example in 2010 and Figure 10(b) shows its schematic representation. They used a molecular ruthenium complex as WOC, which was immobilized into a nafion membrane. The anode was based on a tris (2,2'-bipyridine)ruthenium (II) complex modified with phosphonate groups to be attached onto a FTO-TiO_2 film, which was coated by the modified nafion membrane. As in Mallouk's system, a Pt wire was used as counter electrode and Ag/AgCl as reference electrode. In both cases, a small externally applied voltage is needed in order to assists the water splitting reaction.

I.5.3. Mechanisms of the Water Oxidation Process

Water oxidation is the bottleneck process for water splitting. So far, several molecular catalysts have been reported to be capable to oxidize water to oxygen. However, none of them can perform this reaction in an efficient way.[47] In the literature we can find examples containing different metal centres such as iron[65], cobalt[66], iridium[67] and manganese[68] , but the most widely suited is ruthenium, in which the present work is focused.

The root difficulties of this process are that: (1) it is thermodynamically unfavourable (with a E^{o}=1.23 V vs. SHE at pH=0) and (2) There exists an intrinsic molecular complexity because of multiple and synchronized bond rearrangements are needed together with the removal of protons and electrons. For this reasons it is a process difficult to study from a mechanistic point of view. The formation of an oxygen-oxygen bond promoted by transition metal complexes can be classified in the two possible scenarios[69] shown in Figure 11.

[1] Quantum efficiency *is defined as the number of O_2 molecules formed per two absorbed photons.*

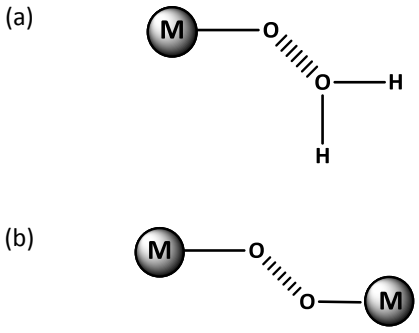

Figure 11. Potential metal based oxygen-oxygen bond formation pathways. (a) Solvent nucleophilic attack. (b) Interaction of two M-O entities.

- Solvent nucleophilic attack to a M-O bond. This is one of the favoured mechanisms for the OEC-PSII[52] and can be found in both mononuclear and polynuclear complexes.
- The interaction between two M-O entities. This reaction can be described as a reductive elimination or as a radical-radical coupling reaction. As in the first mechanism, the nuclearity of the complex can also be variable.

I.5.4. Ruthenium complexes capable to oxidize water

The first reported example of a ruthenium complex capable to oxidize water, the so-called blue dimer, was published by Meyer's group in 1982. This complex, was able to perform 13.2 TN at pH 1 by means of Ce(IV) as chemical oxidant. It consists of two ruthenium centres linked by an oxo bridge, with two bipyridines and one water molecule occupying the remaining coordination positions.[70] This seminal work promoted the preparation and study of a wide and varied family of related compounds with the aim to improve the catalytic properties of the system. The compounds of this family reported until 2007, which can be classified into three different groups: oxo bridged dinuclear complexes (including the polyoxometalates), non-oxo bridged dinuclear complexes and mononuclear species, are summarized in Annex I, Paper A.

Among the compounds described in Paper A (Annex I), the dinuclear complex reported in 2004 by our group showed better activities and efficiencies than those reported previously for the water oxidation process.[71] This complex was a new synthetic approach for a four electrons WOC, which was formed by two ruthenium atoms linked by a more robust and rigid bridging ligand, the Hbpp (Figure 12). This ligand (together with higher stability) also allows the electronic communication between the two metal centres. The latest results concerning this complex are explained in the following section due to their relevance for the present work.

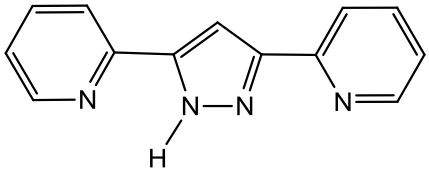

Figure 12. Drawing of the Hbpp ligand.

During the last four years, which is the time devoted to the preparation of this work, an increasing amount of WOC systems based on ruthenium compounds have appeared in the literature, some of them integrated in overall water splitting devices. As a general trend, scientists efforts are nowadays focused on achieve the photo activation of the catalyst instead of the chemical activation. The most significant results are summarised below using the same classification system as Paper A (Annex I).

I.5.4.1. Recent contributions in dinuclear non-oxo bridging ruthenium catalysts

Sun's group achieved one of the most recent and important contributions to this family of diruthenium catalysts. Last year, they reported new dinuclear ruthenium complexes with a bridging ligand containing nitrogen and carboxylate functionalities as donor groups (Figure 13) and *trans*[72] (**a**) and *cis* (**b**) disposition of the Ru metal centres.[73] From a mechanistic point of view both catalysts present an activity dependent on the Ce(IV) concentration and first order kinetics with respect to the catalyst. For complex (**a**), the mechanistic studies based on catalysis performed in labelled water show that water is the main source of the evolved oxygen.

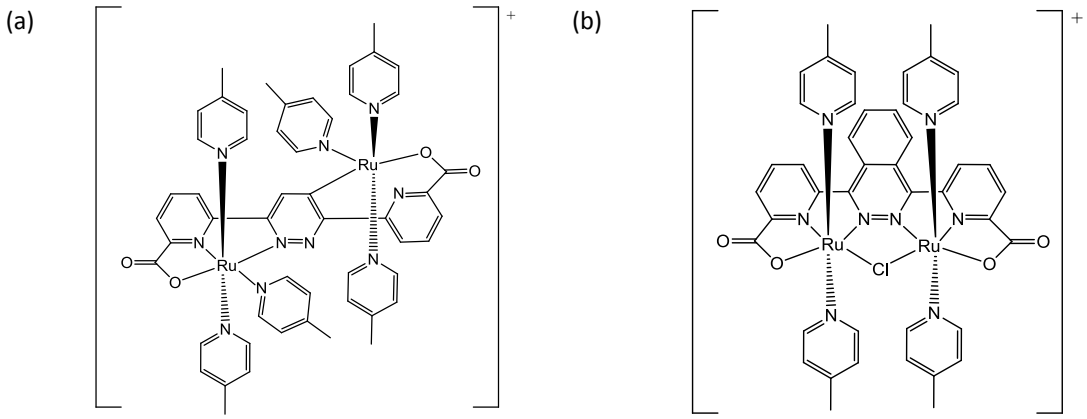

Figure 13. Complexes synthesized by Sun and co-workers (a) *trans* isomer, (b) *cis* isomer.

Complex (**b**) shows the best catalytic results ever reported for a molecular catalyst using Ce(IV) as chemical oxidant at pH=1, with a 0.05 μM catalyst concentration and 5 mM Ce(IV) concentration. In these conditions, a TN of 10.000 could be achieved with TOF values of 1.2 s^{-1}. Moreover, the fact that the potential for catalytic water oxidation is lower than the oxidation potential of $[Ru(bpy)_3]^{3+}$ indicates that this reaction could be produced in a photoinduced manner. To perform this photoinduced water oxidation under neutral conditions, catalyst (**b**) and a sacrificial electron acceptor ($S_2O_8^{2-}$) were used together with $[Ru(bpy)_3]^{3+}$ as photosensitizer. In these conditions and under irradiation at λ>400 nm, a TN of 60 was achieved with a TOF of 0.1 s^{-1}. These results were improved when a stronger photosensitizer, $[Ru(bpy)_2(4,4'\text{-}(CO_2Et)_2\text{-}bpy)]^{2+}$, was used. However, in all cases, the TN and TOF reached were far from those obtained using Ce(IV) as chemical oxidant. This fact has been attributed to the simultaneous consumption of the sensitizer and the acceptor during the catalytic process. Recently, the same group have also reported the coupling of this photoinduced water oxidation system in an overall photoelectrochemical cell for hydrogen production,[63] as already detailed in page 20.

I.5.4.2. New Ruthenium Polyoxometalate Complexes

In 2008, the groups of Bonchio[74] and Hill[75] reported independently and nearly simultaneously the water oxidation activity of the polyoxometalate complex $[Ru^{IV}_4(\mu\text{-}O)_4(\mu\text{-}OH)_2(H_2O)_4(\gamma\text{-}Si\text{-}W_{10}O_{36})_2]^{10-}$, ($Ru_4$-POM; POM is the polyoxometalate ligand γ-Si-$W_{10}O_{36}^{8-}$).

The structure of the reported complex (Figure 14) consists of a tetranuclear unit formed by four Ru^{IV}-OH_2 groups, linked by O^{2-}, OH^- and the POM ligands. We can imagine that the oxygen atoms are occupying the vertices of an octahedron and the ruthenium atoms those of a tetrahedron. The POM units act as tetradentate bridging ligands between two ruthenium centres and finally each metal centre completes its octahedral coordination

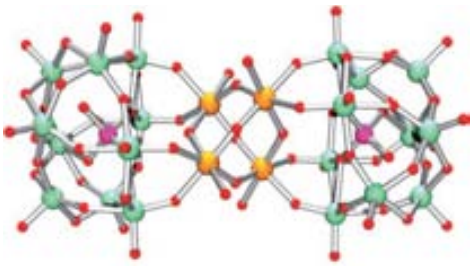

Figure 14. POV-Ray drawing of the X-ray structure of the Hill's and Bonchio's polyoxometalate complex.

with a terminal aqua ligand. Its catalytic activity towards water oxidation is impressive, performing the reaction in a 0.1 M triflic acid solution and with a ratio complex: Ce(IV) of 1: 400 it can achieve 385 TN, which represents an efficiency of 90% in about 2 h.

For this complex, it has been shown that the initial $[Ru^{IV}\text{-}OH_2]_4$ (S_0) core is oxidized in four successive steps to form the $[Ru^{V}\text{-}OH]_4$ (S_4), in analogy with the natural system. The structural, computational and kinetic evidence shows that the nucleophilic attack of a water molecule on the high valent ruthenium centres is the most reasonable mode of O-O bond formation. The intramolecular reaction between two adjacent ruthenium sites is not possible for geometrical constrains and the bimolecular pathway, involving two molecules of catalyst, can be discarded by the first order oxygen evolution kinetics.[76]

Interestingly, this complex has also been reported to be able to oxidize water in homogenous phase with a light-driven strategy involving $[Ru^{II}(bpy)_3]^{2+}$ as photosensitizer and $S_2O_8^{2-}$ as sacrificial oxidant.[77] The most remarkable issue for this photocatalytic system is the high quantum efficiency achieved (9%). However, its main drawbacks are those already described for the corresponding overall water splitting photoelectrochemical cell (see page 20 of this introduction). The competitive oxidation of water and of the photosensitizer (bpy) have been corroborated by kinetic studies.[77b]

In order to improve the initial dispositive, the same authors have replaced the $[Ru(bpy)_3]^{2+}$ sensitizer by the tetranuclear Ru(II) complex $[Ru\{(\mu\text{-}dpp)Ru(bpy)_2\}_3](PF_6)_8$ (dpp= 2,3-bis(2'-pyridyl)pyrazine) (Figure 15). Using this tetranuclear sensitizer a larger portion of the visible light region is absorbed and its decomposition is less than 5% (whereas for the $[Ru(bpy)_3]^{2+}$ sensitizer was higher than 40%).[78]

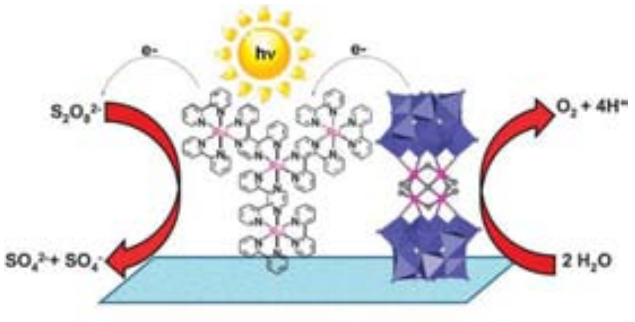

Figure 15. Photocatalytic water oxidation powered by the interplay of the tetraruthenium sensitizer and the polyoxometalate WOC.

This modification also increases the quantum efficiency up to 30%, which is the highest value obtained for photoinduced water oxidation *via* a molecular assembled system.

The last results involving this polyoxometalate complex have promoted the preparation of a nanotube-polyoxometalate material to be used as an electrocatalytic water oxidation system.[79]

I.5.4.3. Recent contributions in Mononuclear Complexes

Until 2008 scientists thought that complexes with multiple metal centres were required to carry out the multiple proton-coupled electron-transfer (PCET) steps associated with water splitting. Recently, it has been demonstrated that mononuclear complexes are also capable to promote the formation of dioxygen from water.

The first mononuclear species reported to be active as WOC were the iridium complexes published by Bernhard and co workers.[67h] Following up this feature the scientific groups of: Thummel,[80] Meyer[81] and Sakai[82] independently reported that polypyridyl ruthenium compounds with only one active site are also competent catalysts for this reaction. The importance of this observation lies in the fact that these mononuclear systems are generally easier to synthesize and study than systems of higher nuclearity.

From these works some important ideas can be extracted. First, a single catalytic site is enough to promote water oxidation with good activities and efficiencies and that is a quite general trend for ruthenium polypyridyl aqua complexes.[83] For example, $[Ru(trpy)(bpy)(H_2O)]^{2+}$ has been reported to be able to generate oxygen, giving a TN of 178 and an efficiency of 89.2%, when dissolved in water:acetonitrile (20:1) with the presence of Ce(IV) as chemical oxidant.[82] The second and mechanistic idea arise from the kinetic studies performed with these complexes. For the aqua complexes or complexes with a labile ligand, the most accepted mechanism for water oxidation begins when the oxidation state (V) is reached. The Ru(V) species become highly reactive and suffers a nucleophilic attack by solvent water molecules that generates the O-O bond, forming a Ru^{III}-OOH intermediate. Then, the Ru^{III}-OOH species undergoes a rapid one-electron oxidation accompanied by proton loss to form a Ru^{IV}-

OO intermediate that finally generates molecular oxygen. The DFT calculations over the peroxo species show that a seven-coordinated structure with a bidentate peroxo ligand is favoured over a six-coordinated structure with a terminal peroxo ligand.[84]

When the catalytically active mononuclear complexes are coordinatively saturated such as in the case of those reported by Thummel,[80] the proposed mechanism proceeds via a metal coordination expansion. Therefore, a water molecule coordinates generating coordination seven around the metal centre. The critical bond formation step is proposed to involve an external water molecule together with the Ru^{IV}-O high oxidation state, which generates a Ru^{IV}-OOH intermediate that finally yields dioxygen and the initial Ru(II) catalyst. Even though there is no detailed experimental evidence, this proposal is also supported by DFT calculations.

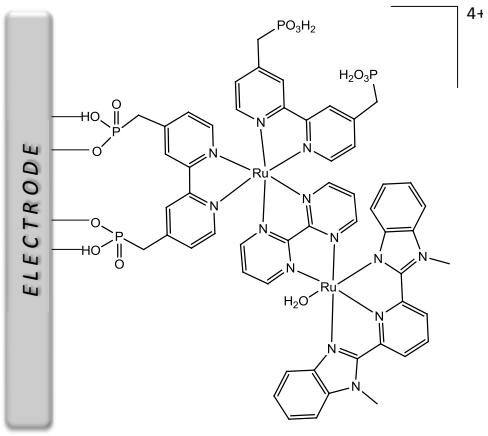

Figure 16. The complex $[(4,4'\text{-}((HO)_2P(O)CH_2)_2bpy)Ru^{II}(bpm)Ru^{II}(Mebimpy)(OH_2)]^{4+}$ supported on an electrode.

For electrocatalytic applications, some mononuclear complexes have been modified and attached to a semiconductor surface[85]. As a general trend, when an ITO-TiO_2 surface is used, faster water oxidation rates can be achieved than when a FTO-TiO_2 is used. This may be due to the rate-limiting cross-surface electron transfer.

The supported version of mononuclear complexes has also been prepared and attached to a dye sensitizer to perform the photoelectrochemical water splitting,[84] as is drawn in Figure 16. The proposed mechanism for this reaction is shown in Scheme 5. It is important to point that the back electron transfer is not an issue in this example because there is no redox carrier.

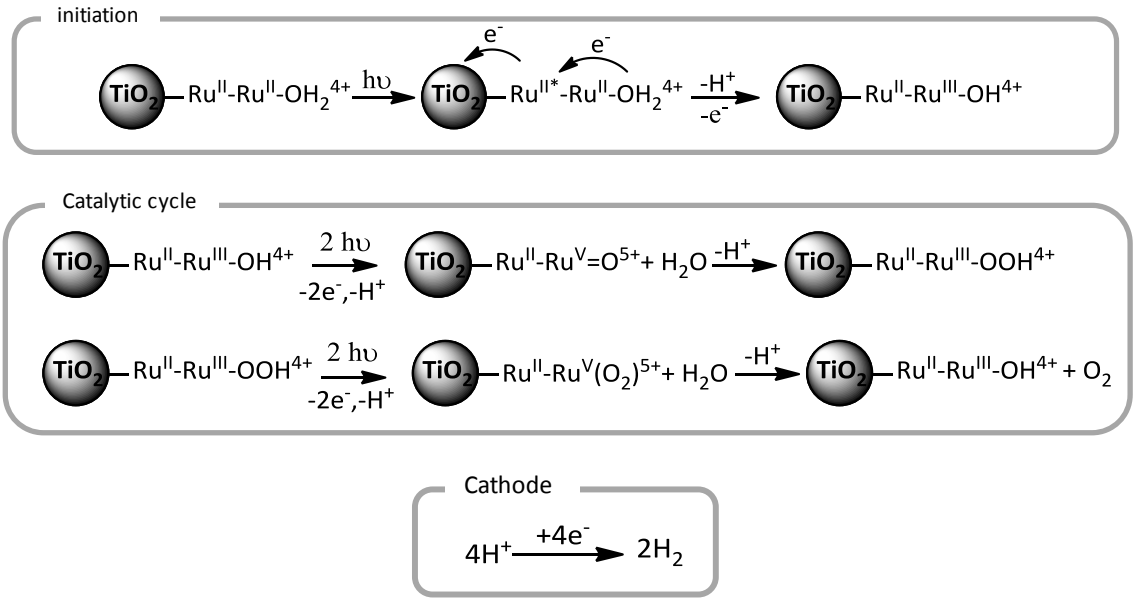

Scheme 5. Proposed photoelectrochemical mechanism for water oxidation.

The groups of Milstein,[86] Sun,[87] and Berlinguette[88] have achieved the most recent results in this field. The latter reported the water oxidation activity of several polypyridylic aquacomplexes, and the kinetic studies of the process suggest that the mechanism that takes place is the one proposed by Meyer and co-workers.[84]

Milstein's group reported a mononuclear ruthenium complex containing an asymmetric tridentate meridional ligand, two OH^- groups in a *cis* facial disposition and a CO ligand completing the octahedral type of coordination (Figure 17). Irradiation of this complex in the 320-420 nm range produces HOOH, which later disproportionate to molecular oxygen and water. Oxygen-labelling experiments and kinetic analyses clearly indicate that the intramolecular reductive elimination process, where the ruthenium metal changes the oxidation state from (II) to (0) is responsible for the O-O bond formation.

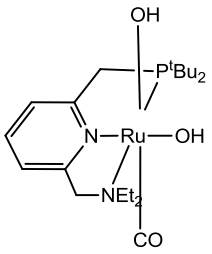

Figure 17. Structure of the neutral complex [Ruᴵᴵ(PNN)(CO)].

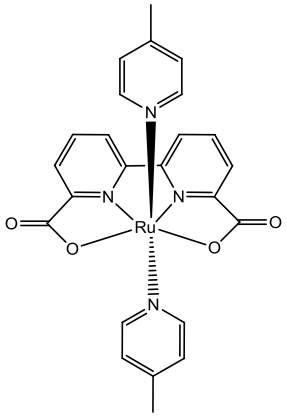

Figure 18. Structure of the complex $[Ru^{II}(bdc)(4\text{-pic})_2]$.

The preparation of an octahedrally distorted ruthenium complex $[Ru^{II}(bdc)(4\text{-pic})_2]$, as is drawn in Figure 18, has been carried out by Sun's group. This complex is capable of oxidizing water by the use of a chemical oxidant such as Ce(IV), electrochemically at relatively low potentials or photochemically using $[Ru(bpy)_3]^{2+}$ or $[Ru(dmbpy)_3]^{2+}$ as sensitizer and $[Co(NH_3)_5Cl]^{2+}$ or $S_2O_8^{2-}$ as sacrificial acceptor.

I.5.5. Water oxidation mechanism of the Ru-Hbpp complex

This is a recent work developed in our group, [89] which is based on the previous knowledge on the ruthenium chemistry of the Hbpp ligand. Most of the complexes presented in this PhD thesis are based on Hbpp ruthenium complexes and, therefore, their WO mechanism is thoroughly described at this point.

To study this mechanism, some previous ideas should be taken into account. First, the substitution kinetics of the labile aqua ligand as function of the oxidation state of the ruthenium centres. This process was studied by monitoring the MeCN substitution of the aqua ligand through UV-vis spectroscopy (Equations (5) and (6)).

$$H_2O\text{-}Ru^{II}Ru^{II}\text{-}H_2O + MeCN \longrightarrow H_2O\text{-}Ru^{II}Ru^{II}\text{-}NCMe + H_2O \qquad k_1=4.0\cdot10^{-2}\ s^{-1} \qquad (5)$$

$$H_2O\text{-}Ru^{II}Ru^{II}\text{-}NCMe + MeCN \longrightarrow MeCN\text{-}Ru^{II}Ru^{II}\text{-}NCMe + H_2O \qquad k_2=5.8\cdot10^{-5}\ s^{-1} \qquad (6)$$

The most important idea obtained from these experiments is that the first substitution for the oxidation state Ru(II, II) (Equation (5)) is faster than the second one (Equation (6)), which shows a decrease of 2 orders of magnitude in the rate constant. In addition, for the first substitution reaction, the rate constant decreases when the Ru oxidation state increases.

It was also established that the Hbpp ligand, when acting as a bridge between two ruthenium metal centres, places them closer and further provides a route for their

electronic coupling. Moreover, the additional ancillary trpy ligands coordinate in a meridional manner in such a way that the oxygen atoms of the aqua groups occupy the sixth coordination position. This arrangement places the two oxygen atoms at 2.48 Å, when the sum of the Van der Waals radii is 3.04 Å (Figure 19.). Recent studies have demonstrated that, in solution and at room temperature, this complex presents dynamic behaviour with the two Ru centres synchronically moving very fast below and above the equatorial plane. As a result, the C_2 symmetry found in the solid state is converted to a C_{2v} symmetry in solution. This fact and the appropriate orientation favour the coupling between the two M-O to generate oxygen in an intramolecular pathway.[90]

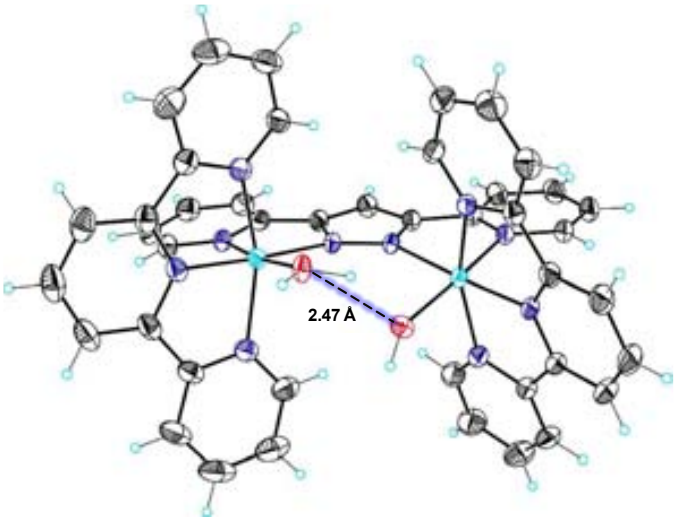

Figure 19. Ortep plots at 50% probability for the cationic part of the complex $[Ru_2^{II}(\mu\text{-bpp})(OH)(H_2O)(trpy)_2]^{2+}$. Colour codes: Ru, cyan; N, blue; O, red; C, grey; H, light blue.

The mechanistic studies were carried out by means of kinetics measurements monitored by UV-vis spectroscopy together with ^{18}O labelling experiments. The analysis of the data obtained suggests that the Ru(II,II) species are sequentially oxidized by one-electron processes with Ce(IV) up to the Ru(IV, IV) oxidation state. The first three electron transfers are fast (to reach Ru(III,IV)) but the last one is slow. A fact which could be associated with the need to remove two protons from the same aqua ligand.

When the Ru(IV,IV) oxidation state is reached, an intramolecular coupling takes place to achieve the oxygen-oxygen bond formation (Figure 20). It is important to point

that this mechanism could be unambiguously assigned as the unique one taking place as a result of the ^{18}O labelling experiments and that it is further supported by a thorough theoretical analysis of intermediates and transition states based on DFT and CASPT2 calculations. These last studies indicates that water molecules in the first solvation shell play an important role stabilizing intermediates or transition-state structures.

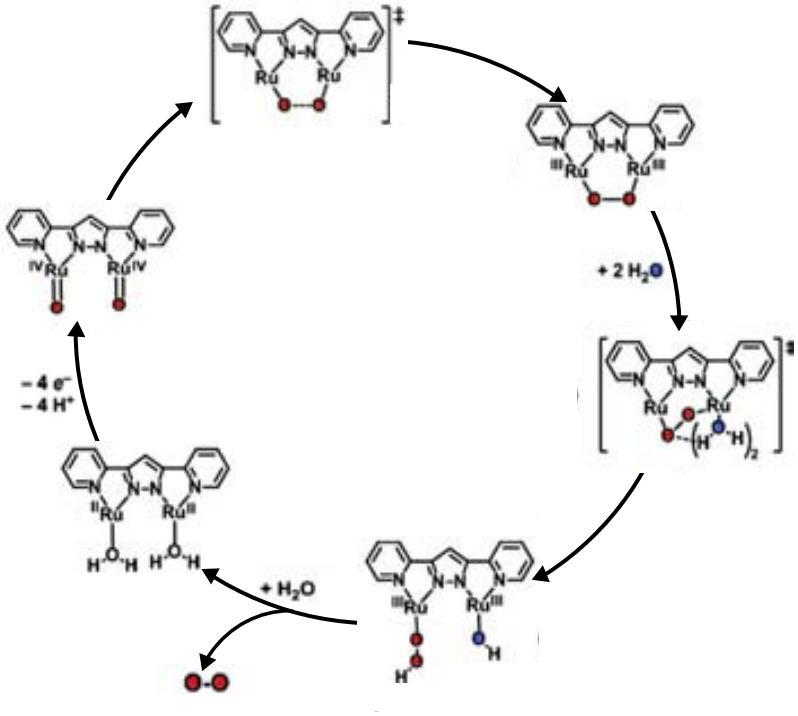

Figure 20. Water oxidation mechanism for the $[Ru_2^{II}(\mu\text{-bpp})(H_2O)(trpy)_2]^{3+}$complex. Terpyridine ligands on ruthenium atoms are not shown for clarity.

There are some potential deactivation pathways for this catalytic system. The first one is the coordination of different anions to the active site generating non-catalytic species. The other important deactivation pathway is studied in the present work and is related to the strong oxidant medium and the high oxidizing species produced during the catalytic process.

I.6. References

[1] Bruneau, C. *Ruthenium catalysts and fine chemistry*; Springer-Verlag: Berlin, **2004**.

[2] (a) Qu, P.; Thompson, D. W.; Meyer, G. J. *Langmuir* **2000**, *16*, 4662-4671. (b) Butler, J.; George, M.; Schoonover, J.; Dattelbaum, D.; Meyer, T. *Coord. Chem. Rev.* **2007**, *251*, 492-514. (c) Meyer, T. J. *Pure Appl. Chem.* **1990**, *62*, 1003-1009.

[3] (a) Goeltz, J. C.; Hanson, C. J.; Kubiak, C. P. *Inorg. Chem.* **2009**, *48*, 4763-4767. (b) Seok, W. K.; Meyer, T. J. *Inorg. Chem.* **2005**, *44*, 3931-3941.(b) Meyer, T. J.; Huynh, M. H. V. *Inorg. Chem.* **2003**, *42*, 8140-8160.

[4] Ley, Steven V.; Norman, Joanne; Griffith, William P.; Marsden, Stephen P. *Synthesis.* **1994**, *7*, 639-66.

[5] (a) Green, K.; Cifuentes, M.; Corkery, T.; Samoc, M.; Humphrey, M. *Angew. Chem. Int. Ed.* **2009**, *48*, 7867-7870. (b) Coe, B. J. *Acc. Chem. Res.* **2006**, *39*, 383-393. (c) Whittall, Ian R.; McDonagh, Andrew M.; Humphrey, Mark G.; Samoc, Marek. *Adv. Organomet. Chem.* **1998**, *43*, 349-405. (d) Whittall, Ian R.; Mcdonagh, Andrew M.; Humphrey, Mark G.; Samoc, Marek. *Adv. in Organomet. Chem.* **1998**, *42*, 291-362.

[6] (a) Mikuriya, M.; Yoshioka, D.; Handa, M. *Coord. Chem. Rev.* **2006**, *250*, 2194-2211. (b) Desplanches, C.; Ruiz, E.; Alvarez, S. *Eur. J. Inorg. Chem.* **2003**, *2003*, 1756-1760. (c) Larionova, J.; Mombelli, B.; Sanchiz, J.; Kahn, O. *Inorg. Chem.* **1998**, *37*, 679-684.

[7] (a) Kizaki, T.; Abe, T.; Matsumoto, T.; Ogo, S. *Chem. Lett.* **2010**, *39*, 128-129. (b) Fillaut, J.; Andriès, J.; Marwaha, R. D.; Lanoë, P.; Lohio, O.; Toupet, L.; Gareth Williams, J. *J.Organomet. Chem.* **2008**, *693*, 228-234.

[8] (a) Aquino, M. A. *Coord. Chem. Rev.* **1998**, *170*, 141-202. (b) Hudson, S. A.; Maitlis, P. M. *Chem. Rev.* **1993**, *93*, 861-885.

[9] (a) Silva, D. D. O. *Anticancer Agents Med. Chem.* **2010**, *10*, 312-323. (b) Bergamo, A.; Sava, G. *Dalton Trans* **2007**, 1267-1272. (c) Groessl, M.; Reisner, E.; Hartinger, C. G.; Eichinger, R.; Semenova, O.; Timerbaev, A. R.; Jakupec, M. A.; Arion, V. B.; Keppler, B. K. *J. Med. Chem.* **2007**, *50*, 2185-2193.

[10] Vos, J. G.; Kelly, J. M. *Dalton Trans***. 2006**, *41*, 4869-4883.

[11] (a) Sirimanne, P.; Winther-Jensen, B.; Weerasinghe, H.; Cheng, Y. *Thin Solid Films* **2010**, *518*, 2871-2875. (b) Chen, C.; Pootrakulchote, N.; Wu, S.; Wang, M.; Li, J.; Tsai, J.; Wu, C.; Zakeeruddin, S. M.; Grätzel, M. *J. Phys. Chem. C.* **2009**, *113*, 20752-20757. (c) Lyon, J. E.; Rayan, M. K.; Beerbom, M. M.; Schlaf, R. *J. Appl. Phys.* **2008**, *104*, 073714. (d) Krebs, F.; Biancardo, M. *Sol. Energ. Mat. Sol. C.* **2006**, *90*, 142-165. (e) Grätzel, M. *Inorg. Chem.* **2005**, *44*, 6841-6851. (f) Islam, A. *J. Photoch. and Photobio. A:*

2003, *158*, 131-138. (g) Balzani, V.; Juris, A.; Venturi, M.; Campagna, S.; Serroni, S. *Chem. Rev.* **1996**, *96*, 759-834. (h) Juris, A. *Coord. Chem. Rev.* **1988**, *84*, 85-277.

[12] (a) Belser, P.; De Cola, L.; Hartl, F.; Adamo, V.; Bozic, B.; Chriqui, Y.; Iyer, V. M.; Jukes, R. T. F.; Kühni, J.; Querol, M.; Roma, S.; Salluce, N. *Adv. Funct. Mater.* **2006**, *16*, 195-208. (b) Newkome, G. R.; Cho, T. J.; Moorefield, C. N.; Mohapatra, P. P.; Godínez, L. A. *Chem. Eur. J.* **2004**, *10*, 1493-1500. (c) Endo, H.; Ogawa, T. *Inter. J. Nanosci.* **2002**, *1*, 631-635. (d) Barigelletti, F.; Flamigni, L. *Chem. Soc. Rev.* **2000**, *29*, 1-12. (e) Balzani, V.; Campagna, S.; Denti, G.; Juris, A.; Serroni, S.; Venturi, M. *Acc. Chem. Res.* **1998**, *31*, 26-34.

[13] (a) Liu, Y.; Zeng, C.; Yao, J.; Wu, F.; He, L.; Huang, H. *Chem. Biodivers.* **2010**, *7*, 1770-1783. (b) Liu, Y.; Liang, Z.; Li, Z.; Zeng, C.; Yao, J.; Huang, H.; Wu, F. *Biometals* **2010**, *23*, 739-752. (c) Schatzschneider, U. *Eur. J. Inorg. Chem.* **2010**, *10*, 1451-1467. (d) Tan, L.; Zhang, S.; Liu, X.; Xiao, Y. *Aust. J. Chem.* **2008**, *61*, 725. (e) Zhang, Q.; Liu, J.; Ren, X.; Zhang, P. *Transition Met. Chem.* **2005**, *30*, 285-289. (f) Zhang, Q.; Liu, J.; Liu, J.; Zhang, P.; Ren, X.; Liu, Y.; Huang, Y.; Ji, L. *J. Inorg. Biochem.* **2004**, *98*, 1405-1412. (g) Delaney, S.; Pascaly, M.; Bhattacharya, P. K.; Han, K.; Barton, J. K. *Inorg. Chem.* **2002**, *41*, 1966-1974. (h) Zhen, Q.; Ye, B.; Zhang, Q.; Liu, J.; Hong Li; Ji, L.; Wang, L. *J. Inorg. Biochem.* **1999**, *76*, 47-53.

[14] Murahashi, S. *Ruthenium in organic synthesis*; Wiley-VCH: Weinheim ;[Great Britain], **2004.**

[15] (a) Singh, P.; Das, D.; Singh, M.; Singh, A. K. *Inorg. Chem. Com.* **2010**, *13*, 223-226. (b) Tada, M.; Muratsugu, S.; Kinoshita, M.; Sasaki, T.; Iwasawa, Y. *J. Am. Chem. Soc.* **2010**, *132*, 713-724. (c) Chatterjee, D.; Nayak, K. A.; Ember, E.; van Eldik, R. *Dalton Trans.* **2010**, *39*, 1695. (d) Murali, M.; Mayilmurugan, R.; Palaniandavar, M. *Eur. J. Inorg. Chem*. **2009**, 3238-3249. (e) Chatterjee, D. *Catal. Surv. Asia* **2009**, *13*, 132-142. (f) Nunes, G.; Alexiou, A.; Toma, H. *J. Catal.* **2008**, *260*, 188-192. (g) Jiang, G.; Chen, J.; Thu, H.; Huang, J.; Zhu, N.; Che, C. *Angew. Chem. Int. Ed.* **2008**, *47*, 6638-6642. (h) Huynh, M. H. V.; Meyer, T. *J. Chem. Rev.* **2007**, *107*, 5004-5064. (i) Punniyamurthy, T.; Velusamy, S.; Iqbal, *J. Chem. Rev.* **2005**, *105*, 2329-2364. (j) Jitsukawa, K.; Oka, Y.; Yamaguchi, S.; Masuda, H. *Inorg. Chem.* **2004**, *43*, 8119-8129. (k) Catalano, V. J.; Heck, R. A.; Immoos, C. E.; Öhman, A.; Hill, M. G. *Inorg. Chem.* **1998**, *37*, 2150-2157. (l) Marmion, M. E.; Takeuchi, K. J. *J. Am. Chem. Soc.* **1988**, *110*, 1472-1480. (m) Thompson, M. S.; De Giovani, W. F.; Moyer, B. A.; Meyer, T. J. *J. Org. Chem.* **1984**, *49*, 4972-4977.

[16] (a) Meyer, Thomas J. Plenum: New York, **1988**; 33-47. (b) Holm, R. H. *Chem. Rev.* **1987**, *87*, 1401-1449. (c) Gulliver, D. *Coord. Chem. Rev.* **1982**, *46*, 1-127.

[17] (a) Doyle, M. P.; Duffy, R.; Ratnikov, M.; Zhou, L. *Chem. Rev.* **2010**, *110*, 704-724. (b) Chatterjee, D.; Mitra, A.; Shepherd, R. E. *Inorg. Chim. Acta* **2004**, *357*, 980-990.

[18] (a) Miyazaki, S.; Kojima, T.; Mayer, J. M.; Fukuzumi, S. *J. Am. Chem. Soc.* **2009**, *131*, 11615-11624. (b) Manner, V. W.; Mayer, J. M. *J. Am. Chem. Soc.* **2009**, *131*, 9874-9875. (c) Miyazaki, S.; Kojima,

T.; Sakamoto, T.; Matsumoto, T.; Ohkubo, K.; Fukuzumi, S. *Inorg. Chem.* **2008**, *47*, 333-343. (d) Concepcion, J. J.; Brennaman, M. K.; Deyton, J. R.; Lebedeva, N. V.; Forbes, M. D. E.; Papanikolas, J. M.; Meyer, T. J. *J. Am. Chem. Soc.* **2007**, *129*, 6968-6969. (e) Kojima, T.; Hayashi, K.; Matsuda, Y. *Inorg. Chem.* **2004**, *43*, 6793-6804.

[19] (a) Aydemir, M.; Baysal, A. *J. Organomet. Chem.* **2010**, *695*, 2506-2511. (b) Adams, R. D.; Trufan, E. *Philos. T. Roy. So. A.* **2010**, *368*, 1473-1493. (c) Kokkinos, N. C.; Lazaridou, A.; Nikolaou, N.; Papadogianakis, G.; Psaroudakis, N.; Chatzigakis, A. K.; Papadopoulos, C. E. *Appl. Catal. A-Gen.* **2009**, *363*, 129-134. (d) Baratta, W.; Chelucci, G.; Herdtweck, E.; Magnolia, S.; Siega, K.; Rigo, P. *Angew. Chem. Int. Ed.* **2007**, *46*, 7651-7654. (e) Skapski, A. C.; Troughton, P. G. H. *Chem. Commun. (London)* **1968**, 1230.

[20] (a) Fernández-Zúmel, M. A.; Kiefer, G.; Thommes, K.; Scopelliti, R.; Severin, K. *Eur. J. Inorg. Chem.* **2010**, 3596-3601. (b) Nair, R. P.; Kim, T. H.; Frost, B. J. *Organometallics* **2009**, *28*, 4681-4688. (c) Dabb, S. L.; Messerle, B. A.; Wagler, J. *Organometallics.* **2008**, *27*, 4657-4665.

[21] (a) Antonucci, A.; Bassetti, M.; Bruneau, C.; Dixneuf, P. H.; Pasquini, C. *Organometallics* **2010**. (b) van der Eide, E. F.; Piers, W. E. *Nature Chem.* **2010**, *2*, 571-576. (c) Nolan, S. P.; Clavier, H. *Chem. Soc. Rev.* **2010**, *39*, 3305. (d) Ben-Asuly, A.; Aharoni, A.; Diesendruck, C. E.; Vidavsky, Y.; Goldberg, I.; Straub, B. F.; Lemcoff, N. G. *Organometallics.* **2009**, *28*, 4652-4655. (e) Ager, D. *Handbook of chiral chemicals; 2n* ed.; Taylor & Francis: Boca Raton, **2006**.

[22] (a) Wada, T.; Tsuge, K.; Tanaka, K. *Chem. Lett.* **2000**, 910-911. (b) Bernhard, P.; Anson, F. C. *Inorg. Chem*. **1988**, *27*, 4574-4577.

[23] (a) Sieffert, N.; Bühl, M. *J. Am. Chem. Soc.* **2010**, *132*, 8056-8070. (b) Fukuzumi, S.; Kobayashi, T.; Suenobu, T. *J. Am. Chem. Soc.* **2010**, *132*, 1496-1497. (c) Morris, D. J.; Clarkson, G. J.; Wills, M. *Organometallics.* **2009**, *28*, 4133-4140.

[24] Dwyer, F. P.; Mellor, D. P. *Chelating Agents and Metal Chelates*; Academic Press: New York, **1964**.

[25] Meyer, T. J.; Huynh, M. H. V. *Inorg. Chem.* **2003**, *42*, 8140-8160.

[26] Dovletoglou, A.; Adeyemi, S. A.; Meyer, T. J. *Inorg. Chem.* **1996**, *35*, 4120-4127.

[27] Eggleston, D. S.; Goldsby, K. A.; Hodgson, D. J.; Meyer, T. J. *Inorg. Chem.* **1985**, *24*, 4573-4580.

[28] (a) Binstead, R. A.; Moyer, B. A.; Samuels, G. J.; Meyer, T. J. *J. Am. Chem. Soc.* **1981**, *103*, 2897-2899. (b) Moyer, B. A.; Meyer, T. J. *Inorg. Chem.* **1981**, *20*, 436-444. (c) Moyer, B. A.; Meyer, T. J. *J. Am. Chem. Soc.* **1978**, *100*, 3601-3603.

[29] (a) Masllorens, E.; Rodríguez, M.; Romero, I.; Roglans, A.; Parella, T.; Benet-Buchholz, J.; Poyatos, M.; Llobet, A. *J. Am. Chem. Soc.* **2006**, *128*, 5306-5307. (b) Meyer, T. J. *J. Electrochem. Soc.* **1984**, *131*, 221C.

[30] P. W. N. M. van Leeuwen. *Homogeneous catalysis: understanding the art*; Kluwer Academic Publishers: Dordrecht;Boston, **2004**.

[31] Cornils, B. *Applied homogeneous catalysis with organometallic compounds : a comprehensive handbook in three volumes*; 2n ed.; Wiley-VCH: Weinheim, **2002**.

[32] (a) Freund, H. *Chem. Eur. J.* **2010**, *16*, 9384-9397. (b) Anastas, P. *Handbook of green chemistry.*; Wiley-VCH: Weinheim, **2009**. (c) Ertl, G. *Handbook of heterogeneous catalysis.*; 2n ed.; Wiley-VCH; John Wiley distributor: Weinheim; Chichester, **2008**. (d) Ding, K. *Handbook of asymmetric heterogeneous catalysis;* Wiley-VCH: Weinheim, **2008**. (e) Kwak, B. S. *Catal. Surv. Asia.* **2005**, *9*, 103-116.

[33] (a) Meille, V. *Appl. Catal. A-Gen.* **2006**, *315*, 1-17. (b) Goodman, D. J. Catal. **2003**, *216*, 213-222. (c) Campanati, M.; Fornasari, G.; Vaccari, A. *Catal. Today*. **2003**, *77*, 299-314.

[34] (a) Dal Santo, V.; Liguori, F.; Pirovano, C.; Guidotti, M. *Molecules* **2010**, *15*, 3829-3856. (b) Thomas, S. M. *ChemCatChem.* **2010**, *2*, 127-132. (c) Dioos, B. M.; Vankelecom, I. F.; Jacobs, P. *Adv. Synth. Catal.* **2006**, *348*, 1413-1446. (d) Thomas, J. M.; Raja, R.; Lewis, D. W. *Angew. Chem. Int. Ed.* **2005**, *44*, 6456-6482. (e) Buchmeiser, M. *Catal. Today.* **2005**, *105*, 612-617. (f) McMorn, P.; Hutchings, G. *J. Chem. Soc. Rev.* **2004**, *33*, 108.

[35] (a) Batail, N.; Bendjeriou, A.; Djakovitch, L.; Dufaud, V. *Appl. Catal. A-Gen.* **2010**, *388*, 179-187. (b) Ribeiro, S. M.; Serra, A. C.; Rocha Gonsalves, A. *J. Mol. Catal. A-Chem*. **2010**, *326*, 121-127. (c) Pugin, B.; Blaser, H. *Top Catal.* **2010**, *53*, 953-962. (d) Pereira, C.; Biernacki, K.; Rebelo, S. L.; Magalhães, A. L.; Carvalho, A. P.; Pires, J.; Freire, C. *J. Mol. Catal. A-Chem.* **2009**, *312*, 53-64. (e) Sayah, R.; Framery, E.; Dufaud, V. *Green Chem*. **2009**, *11*, 1694. (f) Bayramoglu, G.; Kiralp, S.; Yilmaz, M.; Toppare, L.; Arica, M. *Biochem. Eng. J.* **2008**, *38*, 180-188. (g) McDonald, A. R.; Müller, C.; Vogt, D.; van Klink, G. P.; van Koten, G. *Green Chem.* **2008**, *10*, 424. (h) Kuźniarska-Biernacka, I.; Silva, A. R.; Carvalho, A. P.; Pires, J.; Freire, C. *J. Mol. Catal. A-Chem.* **2007**, *278*, 82-91. (i) Ribeiro, S. M.; Serra, A. C.; Rocha Gonsalves, A. *Tetrahedron.* **2007**, *63*, 7885-7891.

[36] Corma, A.; Garcia, H. *Adv. Synth. Catal.* **2006**, *348*, 1391-1412.

[37] (a) Winkler, J. *Titanium Dioxide*; Vincentz Verlag, **2003**. (b) Wiberg, E. *Inorganic chemistry*; 1r ed.; Academic Press ;De Gruyter: San Diego ;Berlin ;New York, **2001**.

[38] (a) Liu, Z.; Wang, Y.; Chu, W.; Li, Z.; Ge, C. *J. Alloy. Compd.* **2010**, *501*, 54-59. (b) Asghar, W.; Qazi, I. A.; Ilyas, H.; Khan, A. A.; Awan, M. A.; Rizwan Aslam, M. *J. Nanomater.* **2010**, 1-9.

[39] (a) Higashimoto, S.; Suetsugu, N.; Azuma, M.; Ohue, H.; Sakata, Y. *J. Catal.* **2010**, *274*, 76-83. (b) Zhang, M.; Wang, Q.; Chen, C.; Zang, L.; Ma, W.; Zhao, J. *Angew. Chem. Int. Ed.* **2009**, *48*, 6081-6084. (c) Hornstein, B. J.; Dattelbaum, D. M.; Schoonover, J. R.; Meyer, T. J. *Inorg. Chem*. **2007**, *46*, 8139-8145. (d) Guo, Y.; Hu, C. *J. Mol. Catal. A-Chem.* **2007**, *262*, 136-148. (e) Köckritz, A.; Sebek, M.; Dittmar, A.; Radnik, J.; Brückner, A.; Bentrup, U.; Pohl, M.; Hugl, H.; Mägerlein, W. *J. Mol. Catal. A-Chem.* **2006**, *246*, 85-99. (f) Drew, K.; Girishkumar, G.; Vinodgopal, K.; Kamat, P. V. *J. Phys. Chem. B.* **2005**, *109*, 11851-11857.

[40] (a) Qiu, X.; Miyauchi, M.; Yu, H.; Irie, H.; Hashimoto, K. *J. Am. Chem. Soc.* **2010**, *132*, 15259-15267. (b) Maeda, K.; Teramura, K.; Lu, D.; Takata, T.; Saito, N.; Inoue, Y.; Domen, K. *Nature.* **2006***, 440*, 295-295.

[41] Nazeeruddin, M. K.; Muller, E.; Humphry-Baker, R; Vlachopoulos, N.; Gratzel, M. *J. Chem. Soc., Dalton Trans.* **1997**, *23*, 4571-4578.

[42] (a) Bae, E.; Choi, W. *J.Phys. Chem. B.* **2006**, *30*, 14792-14799. (b) Rensmo, H.; Westermark, K.; Södergren, S.; Kohle, O.; Persson, P.; Lunell, S.; Siegbahn, H. *J. Chem. Phys*. **1999**, *111,* 2744. (c) Argazzi, R.; Bignozzi, C. A.; Hasselmann, G. M.; Meyer, G. J. *Inorg. Chem.* **1998**, *18*, 4533-4537.

[43] (a) Gallagher, L. A.; Serron, S. A.; Wen, X.; Hornstein, B. J.; Dattelbaum, D. M.; Schoonover, J. R.; Meyer, T. J. *Inorg. Chem.* **2005**, *44*, 2089-2097. (b) Gallagher, L. A.; Meyer, T. J. *J. Am. Chem. Soc.* **2001**, *123*, 5308-5312.

[44] (a) Duprez, V.; Biancardo, M.; Krebs, F. *Sol. Energ. Mat. Sol. C.* **2007**, *91*, 230-237. (b) Bae, E.; Choi, W. *J.Phys. Chem. B.* **2006**, *30*, 14792-14799. (c) Kilså, K.; Mayo, E. I.; Brunschwig, B. S.; Gray, H. B.; Lewis, N. S.; Winkler, J. R. *J. Phys. Chem. B.* **2004**, *108*, 15640-15651. (d) Bae, E.; Choi, W.; Park, J.; Shin, H. S.; Kim, S. B.; Lee, J. S. *J. Phys. Chem. B.* **2004**, *108*, 14093-14101.

[45] (a) Houarner-Rassin, C.; Chaignon, F.; She, C.; Stockwell, D.; Blart, E.; Buvat, P.; Lian, T.; Odobel, F. *J. Photochem. Photobiol. A-Chem.* **2007**, *192*, 56-65. (b) Myahkostupov, M.; Piotrowiak, P.; Wang, D.; Galoppini, E. *J. Phys. Chem. C.* **2007**, *111*, 2827-2829.

[46] Armaroli, N.; Balzani, V. *Angew. Chem. Int. Ed.* **2007**, *46*, 52-66.

[47] (a) Hurst, J. K. *Science.* **2010**, *328*, 315-316. (b) Sanderson, K. *Nature.* **2008**, *452,* 400-402.

[48] (a) McDaniel, N. D.; Bernhard, S. *Dalton Trans.* **2010**. (b) Balzani, V.; Credi, A.; Venturi, M. *ChemSusChem*. **2008**, *1*, 26-58.

[49] Dau, H.; Zaharieva, I. *Acc. Chem. Res.* **2009**, *42*, 1861-1870.

[50] Caffarri, S.; Kouřil, R.; Kereïche, S.; Boekema, E. J.; Croce, R. *EMBO J.* **2009**, *28*, 3052-3063.

[51] Ferreira, K. N. *Science.* **2004**, *303*, 1831-1838.

[52] Renger, G.; Renger, T. *Photosynth. Res.* **2008**, *98*, 53-80. And the references therein.

[53] Barber, J. *Chem. Soc. Rev.* **2009**, *38*, 185. And the reference therein.

[54] Brudvig, G. W. *Philo. T. Roy. Soc. B.* **2008**, *363*, 1211-1219. And the reference therein.

[55] Magnuson, A.; Anderlund, M.; Johansson, O.; Lindblad, P.; Lomoth, R.; Polivka, T.; Ott, S.; Stensjö, K.; Styring, S.; Sundström, V.; Hammarström, L. *Acc. Chem. Res.* **2009**, *42*, 1899-1909.

[56] (a) Kalyanasundaram, K.; Graetzel, M. *Curr. Opi. Biotech.* **2010**, *21*, 298-310. (b) Tinker, L. L.; McDaniel, N. D.; Bernhard, S. *J. Mater. Chem.* **2009**, *19*, 3328. (c) Grätzel, M. *Nature.* **2001**, *414*, 338-344.

[57] (a) Licht, S. *Int. J. Hydrogen Energ.* **2001**, *26*, 653-659. (b) Khaselev, O. *Science.* **1998**, *280*, 425-427. (c) Fujishima, A.; Honda, K. *Nature.* **1972**, *238*, 37-38.

[58] McConnell, I.; Li, G.; Brudvig, G. W. *Chem. Biol.* **2010**, *17*, 434-447.

[59] (a) Wong, W.; Ho, C. *Acc. Chem. Res.* **2010**, *43*, 1246-1256. (b) Lee, H.; Wu, S.; Yang, T.; Yen, T. *Energies.* **2010**, *3*, 784-802. (c) Busche, C.; Comba, P.; Mayboroda, A.; Wadepohl, H. *Eur. J. Inorg. Chem*. **2010**, 1295-1302. (d) Buhbut, S.; Itzhakov, S.; Tauber, E.; Shalom, M.; Hod, I.; Geiger, T.; Garini, Y.; Oron, D.; Zaban, A. *ACS Nano.* **2010**, *4*, 1293-1298. (e) Terazono, Y.; Kodis, G.; Liddell, P. A.; Garg, V.; Moore, T. A.; Moore, A. L.; Gust, D. *J. Phys. Chem. B.* **2009**, *113*, 7147-7155. (f) Staniszewski, A.; Heuer, W. B.; Meyer, G. *J. Inorg. Chem.* **2008**, *47*, 7062-7064. (g) Choi, H.; Baik, C.; Kim, S.; Kang, M.; Xu, X.; Kang, H. S.; Kang, S. O.; Ko, J.; Nazeeruddin, M. K.; Grätzel, M. *New J. Chem.* **2008**, *32*, 2233. (h) Balzani, V. *Sol. Energ. Mat. Sol. C.* **1995**, *38*, 159-173.

[60] (a) Ismail, M.; Damjanovic, T.; Ingham, D.; Ma, L.; Pourkashanian, M. *J. Power Sources.* **2010**, *195*, 6619-6628. (b) Atlam, O. *Int. J. Hydrogen Energ.* **2009**, *34*, 6589-6595. (c) Ünlü, M.; Zhou, J.; Kohl, P. A. *J. Phys. Chem. C* **2009**, *113*, 11416-11423. (d) Kocha, S. S.; Deliang Yang, J.; Yi, J. S. *AIChE J.* **2006**, *52*, 1916-1925.

[61] (a) Kachmar, A.; Vetere, V.; Maldivi, P.; Franco, A. A. *J. Phys. Chem. A.* **2010**, *114*, 11861-11867. (b) Musat, R.; Vigneron, G.; Garzella, D.; LeCaër, S.; Hergott, J. F.; Renault, J. P.; Pommeret, S. *Chem. Commun*. **2010**, *46*, 2394. (c) Tinker, L. L.; Bernhard, S. *Inorg. Chem*. **2009**, *48*, 10507-10511. (d)

Wright, R.; Lim, C.; Tilley, T. *Chem. Eur. J.* **2009**, *15*, 8518-8525. (e) Maeda, K.; Wang, X.; Nishihara, Y.; Lu, D.; Antonietti, M.; Domen, K. *J. Phys. Chem. C.* **2009**, *113*, 4940-4947. (f) Song, L.; Zeng, G.; Lou, S.; Zan, H.; Ming, J.; Hu, Q. *Organometallics.* **2008**, *27*, 3714-3721. (g) Valyaev, D. A.; Peterleitner, M. G.; Semeikin, O. V.; Utegenov, K. I.; Ustynyuk, N. A.; Sournia-Saquet, A.; Lugan, N.; Lavigne, G. *J. Organomet. Chem.* **2007**, *692*, 3207-3211.

[62] (a) Gust, D.; Moore, T. A.; Moore, A. L. *Acc. Chem. Res.* **2009**, *42*, 1890-1898. (b) Herrero, C.; Lassallekaiser, B.; Leibl, W.; Rutherford, A.; Aukauloo, A. *Coord. Chem. Rev.* **2008**, *252,* 456-468.

[63] (a) Youngblood, W. J.; Lee, S. A.; Maeda, K.; Mallouk, T. E. *Acc. Chem. Res.* **2009**, *42*, 1966-1973. (b) Youngblood, W. J.; Lee, S. A.; Kobayashi, Y.; Hernandez-Pagan, E. A.; Hoertz, P. G.; Moore, T. A.; Moore, A. L.; Gust, D.; Mallouk, T. E. *J. Am. Chem. Soc.* **2009**, *131*, 926-927.

[64] Li, L.; Duan, L.; Xu, Y.; Gorlov, M.; Hagfeldt, A.; Sun, L. *Chem. Commun.* **2010**, *46*, 7307.

[65] Ellis, W. C.; McDaniel, N. D.; Bernhard, S.; Collins, T. J. *J. Am. Chem. Soc.* **2010**, *132*, 10990-10991.

[66] (a) Kanan, M. W.; Yano, J.; Surendranath, Y.; Dincă, M.; Yachandra, V. K.; Nocera, D. G. *J. Am. Chem. Soc.* **2010**, *132*, 13692-13701. (b) Gerken, J. B.; Landis, E. C.; Hamers, R. J.; Stahl, S. S. *ChemSusChem* **2010**, *3*, 1176-1179. (c) McAlpin, J. G.; Surendranath, Y.; Dincă, M.; Stich, T. A.; Stoian, S. A.; Casey, W. H.; Nocera, D. G.; Britt, R. D. *J. Am. Chem. Soc.* **2010**, *132*, 6882-6883. (d) Yin, Q.; Tan, J. M.; Besson, C.; Geletii, Y. V.; Musaev, D. G.; Kuznetsov, A. E.; Luo, Z.; Hardcastle, K. I.; Hill, C. L. *Science* **2010**, *328*, 342-345. (e) Jiao, F.; Frei, H. *Energy Environ. Sci.* **2010**, *3*, 1018. Risch, M.; Khare, V.; Zaharieva, I.; Gerencser, L.; Chernev, P.; Dau, H. *J. Am. Chem. Soc.* **2009**, *131*, 6936-6937.

[67] (a) Lalrempuia, R.; McDaniel, N. D.; Müller-Bunz, H.; Bernhard, S.; Albrecht, M. *Angew. Chem. Int. Ed.* **2010**, *49*, 9765-9768. (b) Blakemore, J. D.; Schley, N. D.; Balcells, D.; Hull, J. F.; Olack, G. W.; Incarvito, C. D.; Eisenstein, O.; Brudvig, G. W.; Crabtree, R. H. *J. Am. Chem. Soc.* **2010**, *132*, 16017-16029. (c) Gorlin, Y.; Jaramillo, T. F. *J. Am. Chem. Soc.* **2010**, *132*, 13612-13614. (d) Savini, A.; Bellachioma, G.; Ciancaleoni, G.; Zuccaccia, C.; Zuccaccia, D.; Macchioni, *A. Chem. Commun.* **2010**, *46*, 9218. (e) Blakemore, J. D.; Schley, N. D.; Olack, G. W.; Incarvito, C. D.; Brudvig, G. W.; Crabtree, R. H. *Chem. Sci.* **2010**, *2*, 94. (f) Hull, J. F.; Balcells, D.; Blakemore, J. D.; Incarvito, C. D.; Eisenstein, O.; Brudvig, G. W.; Crabtree, R. H. *J. Am. Chem. Soc*. **2009**, *131*, 8730-8731. (g) Cao, R.; Ma, H.; Geletii, Y. V.; Hardcastle, K. I.; Hill, C. L. *Inorg. Chem*. **2009**, *48*, 5596-5598. (h) McDaniel, N. D.; Coughlin, F. J.; Tinker, L. L.; Bernhard, S. *J. Am. Chem. Soc*. **2008**, *130*, 210-217.

[68] (a) Li, G.; Sproviero, E. M.; McNamara, W. R.; Snoeberger, R. C.; Crabtree, R. H.; Brudvig, G. W.; Batista, V. S. *J. Phys. Chem. B.* **2010**, *114*, 14214-14222. (b) Robinson, D. M.; Go, Y. B.; Greenblatt, M.; Dismukes, G. C. *J. Am. Chem. Soc*. **2010**, *132*, 11467-11469. (c) Brimblecombe, R.; Koo, A.; Dismukes,

G. C.; Swiegers, G. F.; Spiccia, L. *J. Am. Chem. Soc.* **2010**, *132*, 2892-2894. (d) Jiao, F.; Frei, H. *Energy Environ. Sci.* **2010**, *3*, 1018. (e) Dismukes, G. C.; Brimblecombe, R.; Felton, G. A. N.; Pryadun, R. S.; Sheats, J. E.; Spiccia, L.; Swiegers, G. F. *Acc. Chem. Res.* **2009**, *42*, 1935-1943. (f) Brimblecombe, R.; Kolling, D. R. J.; Bond, A. M.; Dismukes, G. C.; Swiegers, G. F.; Spiccia, L. *Inorg. Chem.* **2009**, *48*, 7269-7279. (g) Brimblecombe, R.; Swiegers, G.; Dismukes, G.; Spiccia, L. *Angew. Chem. Int. Ed.* **2008**, *47*, 7335-7338. (h) Tagore, R.; Crabtree, R. H.; Brudvig, G. W. *Inorg. Chem.* **2008**, *47*, 1815-1823. (i) Meelich, K.; Zaleski, C. M.; Pecoraro, V. L. *Philo. T. Roy. Soc. B.* **2008**, *363*, 1271-1281. (j) Mullins, C.; Pecoraro, V. *Coord. Chem. Rev.* **2008**, *252*, 416-443 and the reference therein. (k) Chen, G. Y.; Han, G. Y.; Ling, L.; Huang, D. G.; Li, S. Q.; Khorobrykh, A. A.; Zharmukhamedov, S. K.; Liu, Q. T.; Klimov, V. V.; Kuang, T. Y. *Photosynthetica* **2007**, *45*, 620-627. (l) Tagore, R.; Chen, H.; Zhang, H.; Crabtree, R. H.; Brudvig, G. W. *Inorg. Chim. Acta* **2007**, *360*, 2983-2989.

[69] (a) Wang, L.; Wu, Q.; Van Voorhis, T. *Inorg. Chem.* **2010**, *49*, 4543-4553. (b) Romain, S.; Vigara, L.; Llobet, A. *Acc. Chem. Res.* **2009**, *42*, 1944-1953.

[70] (a) Gilbert, J. A.; Eggleston, D. S.; Murphy, W. R.; Geselowitz, D. A.; Gersten, S. W.; Hodgson, D. J.; Meyer, T. J. *J. Am. Chem. Soc.* **1985**, *107*, 3855-3864. (b) Gersten, S. W.; Samuels, G. J.; Meyer, T. J. *J. Am. Chem. Soc.* **1982**, *104*, 4029-4030.

[71] Sens, C.; Romero, I.; Rodríguez, M.; Llobet, A.; Parella, T.; Benet-Buchholz, J. *J. Am. Chem. Soc.* **2004**, *126*, 7798-7799.

[72] Xu, Y.; Åkermark, T.; Gyollai, V.; Zou, D.; Eriksson, L.; Duan, L.; Zhang, R.; Åkermark, B.; Sun, L. *Inorg. Chem.* **2009**, *48*, 2717-2719.

[73] Xu, Y.; Fischer, A.; Duan, L.; Tong, L.; Gabrielsson, E.; Åkermark, B.; Sun, L. *Angew. Chem. Int. Edit.* **2010**, *49*, 8934-8937.

[74] Sartorel, A.; Carraro, M.; Scorrano, G.; De Zorzi, R.; Geremia, S.; McDaniel, N. D.; Bernhard, S.; Bonchio, M. *J. Am. Chem. Soc.* **2008**, *130*, 5006-5007.

[75] Geletii, Y. V.; Botar, B.; Kögerler, P.; Hillesheim, D. A.; Musaev, D. G.; Hill, C. L. *Angew. Chem. Int. Ed. Engl.* **2008**, *47*, 3896-3899.

[76] Sartorel, A.; Miró, P.; Salvadori, E.; Romain, S.; Carraro, M.; Scorrano, G.; Di Valentin, M.; Llobet, A.; Bo, C.; Bonchio, M. *J. Am. Chem. Soc.* **2009**, *131*, 16051-16053.

[77] (a) Orlandi, M.; Argazzi, R.; Sartorel, A.; Carraro, M.; Scorrano, G.; Bonchio, M.; Scandola, F. *Chem. Commun. (Camb.)* **2010**, *46*, 3152-3154. (b) Geletii, Y. V.; Besson, C.; Hou, Y.; Yin, Q.; Musaev, D. G.; Quiñonero, D.; Cao, R.; Hardcastle, K. I.; Proust, A.; Kögerler, P.; Hill, C. L. *J. Am. Chem. Soc.* **2009**,

131, 17360-17370. (c) Geletii, Y. V.; Huang, Z.; Hou, Y.; Musaev, D. G.; Lian, T.; Hill, C. L. *J. Am. Chem. Soc*. **2009**, *131*, 7522-7523.

[78] Puntoriero, F.; La Ganga, G.; Sartorel, A.; Carraro, M.; Scorrano, G.; Bonchio, M.; Campagna, S. *Chem. Commun. (Camb.)* **2010**, *46*, 4725-4727.

[79] Toma, F. M.; Sartorel, A.; Iurlo, M.; Carraro, M.; Parisse, P.; Maccato, C.; Rapino, S.; Gonzalez, B. R.; Amenitsch, H.; Da Ros, T.; Casalis, L.; Goldoni, A.; Marcaccio, M.; Scorrano, G.; Scoles, G.; Paolucci, F.; Prato, M.; Bonchio, M. *Nat. Chem.* **2010**, *2*, 826-831.

[80] Tseng, H.; Zong, R.; Muckerman, J. T.; Thummel, R. *Inorg. Chem.* **2008**, *47*, 11763-11773.

[81] Concepcion, J. J.; Jurss, J. W.; Templeton, J. L.; Meyer, T. J. *J. Am. Chem. Soc.* **2008**, *130*, 16462-16463.

[82] Masaoka, S.; Sakai, K. *Chem. Lett.* **2009**, *38*, 182-183.

[83] Concepcion, J. J.; Jurss, J. W.; Norris, M. R.; Chen, Z.; Templeton, J. L.; Meyer, T. J. *Inorg. Chem.* **2010**, *49*, 1277-1279.

[84] (a) Concepcion, J. J.; Tsai, M.; Muckerman, J. T.; Meyer, T. J. *J. Am. Chem. Soc.* **2010**, *132*, 1545-1557. (b) Concepcion, J. J.; Jurss, J. W.; Brennaman, M. K.; Hoertz, P. G.; Patrocinio, A. O. T.; Murakami Iha, N. Y.; Templeton, J. L.; Meyer, T. J. *Acc. Chem. Res.* **2009**, *42*, 1954-1965.

[85] Chen, Z.; Concepcion, J. J.; Jurss, J. W.; Meyer, T. J. *J. Am. Chem. Soc.* **2009**, *131*, 15580-15581.

[86] Kohl, S. W.; Weiner, L.; Schwartsburd, L.; Konstantinovski, L.; Shimon, L. J. W.; Ben-David, Y.; Iron, M. A.; Milstein, D. *Science.* **2009**, *324*, 74-77.

[87] (a) Duan, L.; Xu, Y.; Gorlov, M.; Tong, L.; Andersson, S.; Sun, L. *Chem. Eur. J.* **2010**, *16*, 4659-4668. (b) Duan, L.; Xu, Y.; Zhang, P.; Wang, M.; Sun, L. *Inorg. Chem.* **2010**, *49*, 209-215

[88] Wasylenko, D. J.; Ganesamoorthy, C.; Koivisto, B. D.; Henderson, M. A.; Berlinguette, C. P. *Inorg. Chem.* **2010**, *49*, 2202-2209.

[89] Bozoglian, F.; Romain, S.; Ertem, M. Z.; Todorova, T. K.; Sens, C.; Mola, J.; Rodríguez, M.; Romero, I.; Benet-Buchholz, J.; Fontrodona, X.; Cramer, C. J.; Gagliardi, L.; Llobet, A. *J. Am. Chem. Soc.* **2009**, *131*, 15176-15187.

[90] Planas, N.; Christian, G.; Mas-Marzá, E.; Sala, X.; Fontrodona, X.; Maseras, F.; Llobet, A. *Chem. Eur*. J. **2010**.

II. OBJECTIVES

The interesting features of Ru^{IV}=O complexes as catalysts for oxidative transformations presented in Chapter I together with the increasing need to develop an efficient water oxidation catalyst to be used in an overall water splitting cell for the photo-production of H_2 were the basic ideas combined when proposing the goals of this PhD thesis. These objectives can be divided into 4 main topics:

a) Synthesis and characterization of new di- and tetranuclear ruthenium complexes containing Hbpp modified bridging ligands. Analysis of their catalytic activity towards water oxidation and study of their deactivation pathway.
b) Covalent anchoring of the dinuclear ruthenium complexes onto TiO_2 rutile nanopowder. Evaluation of the new materials obtained as solid state catalysts for water oxidation employing Ce(IV) as chemical oxidant.
c) Upon the demonstration of the feasibility of the TiO_2 heterogenized system; Anchoring of the dinuclear ruthenium complexes onto conducting FTO-TiO_2 films. Evaluation of these new modified electrodes as electro-activated water oxidation catalysts.
d) Synthesis of new hemilabile ligands capable to assist redox catalysis by means of N/O linkage isomerism. Synthesis and characterization of their corresponding ruthenium complexes. Evaluations of their capacity of stabilizing high oxidation states and avoid deactivation pathways.

III. RESULTS AND DISCUSSION

III.1. Ruthenium-Hbpp based complexes capable to oxidize water. Deactivation pathway

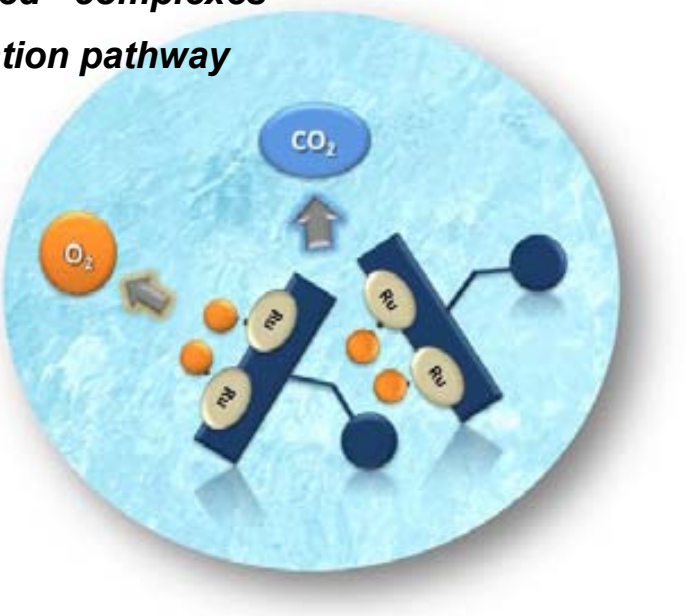

III.1.1. Abstract

This chapter summarizes the results included in the following papers and manuscripts:

- "Synthesis, Structure and Reactivity of New Tetranuclear Ru-Hbpp Based Water Oxidation Catalysts" Laia Francàs, Xavier Sala, Eduardo Escudero-Adán, Jordi Benet-Buchholz, Lluís Escriche and Antoni Llobet. *Inorganic Chemistry* **2011**, 50, 2771-2781.
- "A Ru-Hbpp-Based Water-Oxidation Catalyst Anchored on Rutile TiO_2" Laia Francàs, Xavier Sala, Jordi Benet-Buchholz, Lluís Escriche, and Antoni Llobet. *ChemSusChem* **2009**, 2, 321-329.
- "Ru-Hbpp-Based Water-oxidation Catalysts anchored on FTO/TiO_2" Laia Francàs, Xavier Sala, Jordi Benet-Buchholz, Lluís Escriche and Antoni Llobet. IN PREPARATION

All the above-mentioned works deal with dinuclear or tetranuclear ruthenium complexes that contain a Hbpp or Hbpp modified ligand together with terpyridine or phosphonate terpyridine as ancillary ligands (Chart 1). The complexes containing free phosphonic and carboxylic groups have been supported onto FTO-TiO_2 films and/or rutile TiO_2 solid surfaces. The activity towards water oxidation (WO) of TiO_2-supported and non-supported molecular complexes has been evaluated using Cerium(IV) as oxidant. The WO activity of the catalysts supported onto conducting FTO-TiO_2 films has been tested by means of electrochemical activation.

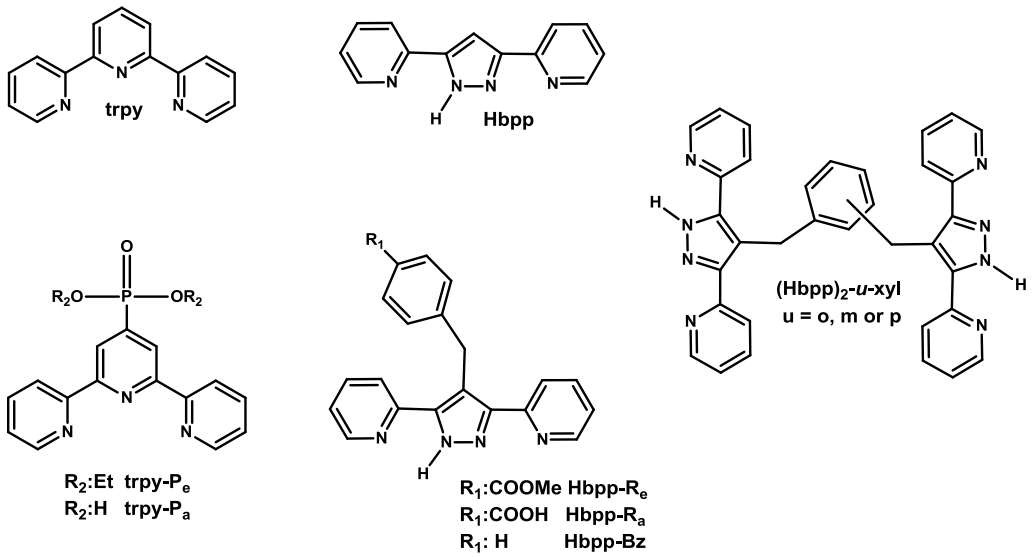

Chart 1. The Ligands.

III.1.2. Ligand synthesis

The synthetic strategy to prepare the new Hbpp modified ligands is depicted in Scheme 1 and involves the nucleophilic attack of the β-diketonate precursor to an halobenzyl derivative, followed by reaction with hydrazine to generate the heterocyclic pyrazolate ring. For the Hbpp-Bz and Hbpp-R_e ligands the halo derivatives used were benzyl bromide and bromomethylbenzoate whereas for the tetranucleating ligands $(Hbpp)_2$-*u*-xyl (u = p, m or o) it was the corresponding p, m or o 1,4-bis(halomethyl)benzene (halo = chloro or bromo). The ligands preparation proceeds with moderate to good yields, despite the synthesis of the modified diketone Lk_2-*o*-Xyl. For the later, as shown in Scheme 2, two competitive reactions take place.[1] The first one (1) corresponds to the desired two consecutives nucleophilic attacks from two different deprotonated diketones to the dihaloderivate. The second one (2) occurs when, after the first nucleophilic attack, an acid-base equilibrium takes place between the haloderivate and the diketone (3). That allows an intramolecular nucleophilic attack that generates a cyclic sub-product, which can be isolated during the working-up procedure.

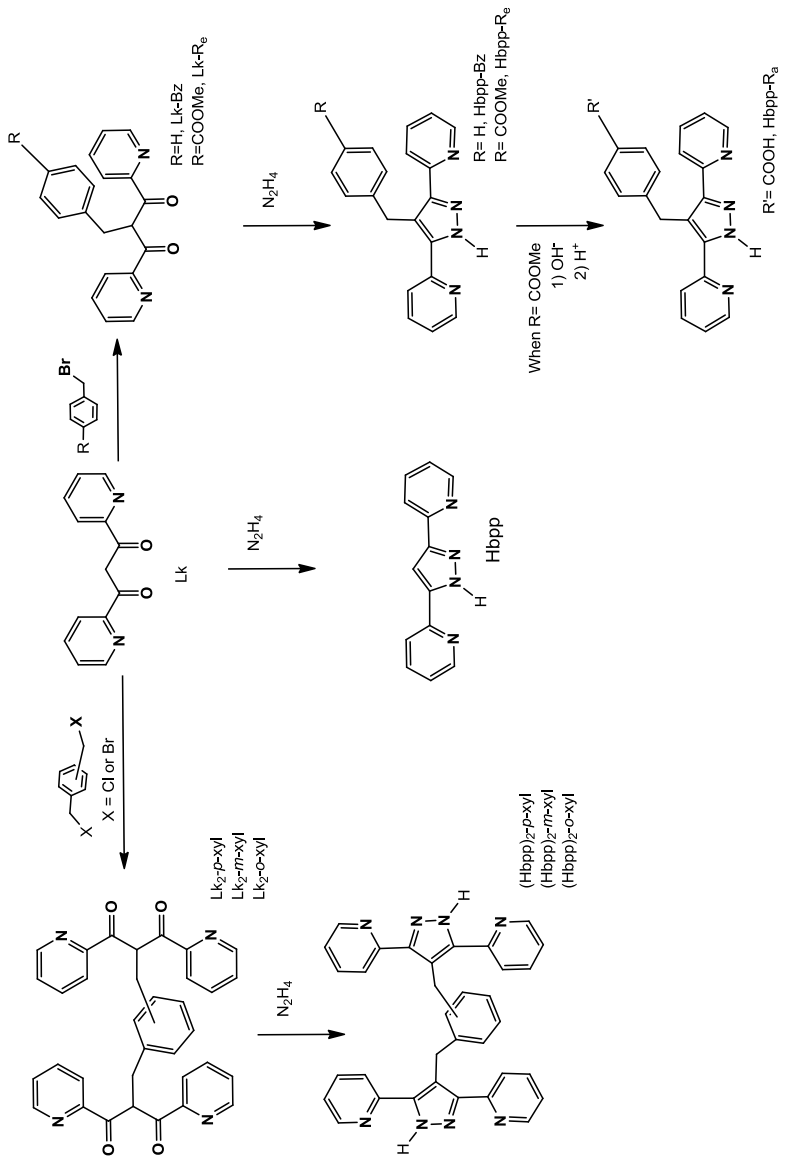

Scheme 1. Synthetic strategy to obtain the Hbpp modified ligands.

Basic hydrolysis of the **Hbpp-R_e** ligand generates the corresponding carboxylic **Hbpp-R_a** form in nearly quantitative yields (Scheme 1).

All the new ligands were characterized by elemental analysis and NMR spectroscopic technique(see the Experimental Sections of papers B, C and D).

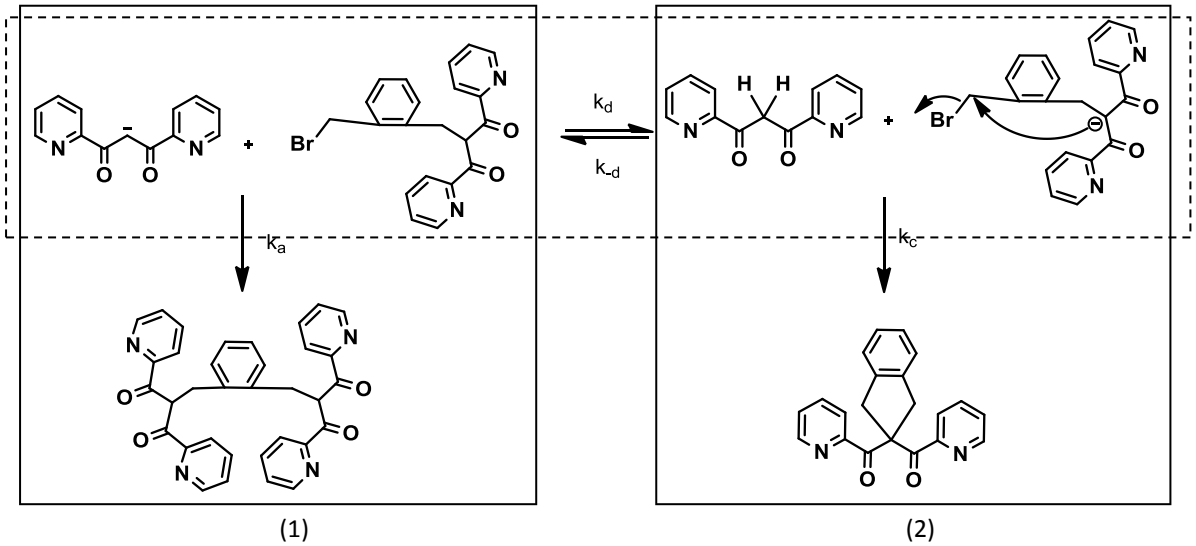

Scheme 2. Synthesis of Lk_2-*o*-Xyl and the identified side reaction.

III.1.3. Synthesis of the Ru Complexes

For the preparation of the complexes $\{[Ru^{II}_2(Y)(T)_2]_x(\mu\text{-}L)\}^{2x+}$ (see Table 1) the Ru(III) compounds $[RuCl_3(T)]$ (T= trpy, trpy-P_e) were used as precursors. To synthesize $[RuCl_3(trpy)]$ the procedure described in the literature was used.[2] A similar method was employed in the preparation of $[RuCl_3(trpy\text{-}P_e)]$, consisting on the direct reaction between $RuCl_3{\cdot}3H_2O$ and trpy-P_e in dry methanol under nitrogen atmosphere. The synthetic strategy followed to prepare the dinuclear chloro-bridged complexes involved the direct reaction of $[RuCl_3(T)]$ with the bpp^- ligand in the presence of NEt_3 as reducing agent followed by the overnight irradiation of the reaction mixture with a tungsten lamp (Scheme 3).

Under excess of acetate and in presence of stoichiometric amounts of Ag(I) the chloro bridging ligand can be easily replaced by a bridging acetate that, later on and under acidic conditions, is replaced by aqua ligands (Scheme 3).

Table 1. Complex numbering for $\{[Ru^{II}_2(Y)(T)_2]_x(\mu\text{-}L)\}^{2x+}$.

$\{[Ru^{II}_2(Y)(T)_2]_x(\mu\text{-}L)\}^{2x+}$						
			Y			
T	μ-L	x	μ-Cl	μ-Ac	$(H_2O)_2$	μ-Br
trpy	Hbpp-Bz	1	**1^{2+}**	**8^{2+}**	**14^{3+}**	-
	Hbpp-R_e	1	**2^{2+}**	**9^{2+}**	**15^{3+}**	-
	Hbpp-R_a	1	**3^{2+}**	-	**16^{3+}**	
	$(Hbpp)_2$-*p*-Xyl	2	**4^{4+}**	**10^{4+}**	**17^{6+}**	-
	$(Hbpp)_2$-*m*-Xyl	2	**5^{4+}**	**11^{4+}**	**18^{6+}**	-
	$(Hbpp)_2$-*o*-Xyl	2	**6^{4+}**	**12^{4+}**	**19^{6+}**	-
trpy-P_e	Hbpp	1	**7^{2+}**	**13^{2+}**	**20^{3+}**	-
trpy-P_a	Hbpp	1	-	-	**22^{3+}**	**21**

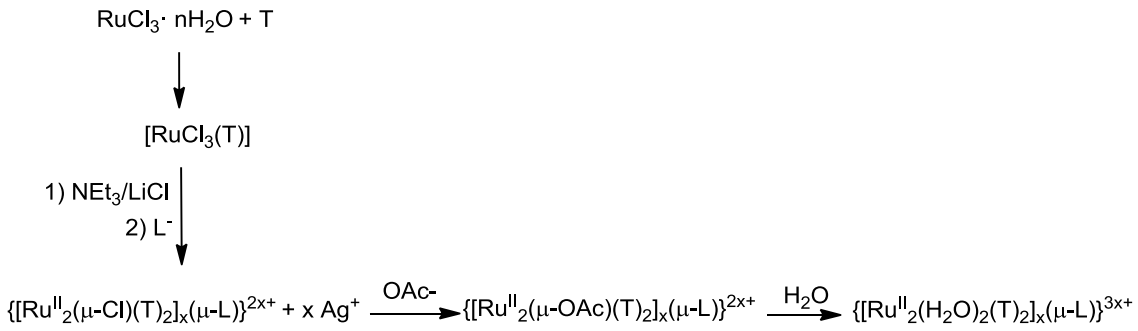

Scheme 3. Synthesis of the $\{[Ru^{II}_2(T)_2(Y)]_x(\mu\text{-}L)\}^{2x+}$ complexes (T=trpy , trpy-P_e or trpy-P_a, L= Hbpp modified ligand).

The formation of the aqua complexes is further corroborated by NMR, which shows the shift of the signals corresponding to the methyl group of the acetate ligand (from 0.45 ppm when coordinated to 1.95 ppm on its free form) after treatment of the starting acetato-bridge compound in acid media (see Figure 1 where these effect if shown for complexes **14^{3+}** and **8^{2+}**).

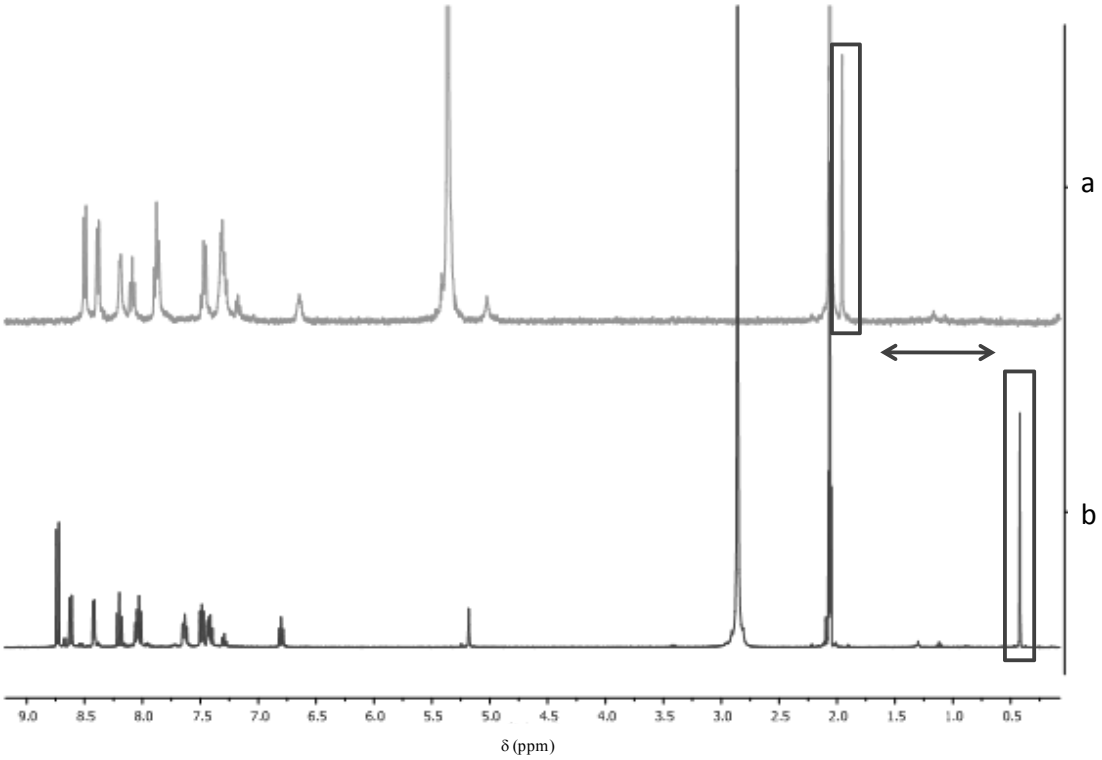

Figure 1: ^{1}H NMR spectra (400 MHz, 298 K) of complexes: (a) **14**$^{3+}$ (Acetone-d_6/D_2O/CF_3COOD), (b) **8**$^{2+}$ (Acetone-d_6).

The Ru(II) complexes with ligands containing acidic groups (like the carboxilate substituted Hbpp, Hbpp-R_a, or the phosphonate containing terpyridine trpy-P_a) are specially relevant in this work as precursors for preparing heterogeneous catalysts. Their syntheses have been attempted using the ester derivates of these ligands (Hbpp-R_e and trpy-P_e) in order to: (a) avoid the formation of coordination isomers coming from the potential coordination of the acid group to the metal centre and (b) increase their solubility in organic solvents (that simplifying the work up procedures). The last synthetic step consists on the hydrolysis of the ester groups, which in all cases has been achieved leaving unaffected the first coordination sphere of the Ru(II) complexes.

In the case of the Hbbp-R_e ligand, the basic treatment of complex **2**$^{2+}$ hydrolyzes the ester group, which allows the isolation of complex **3**$^{2+}$ and, after solving it in acid media, the aqua derivate **16**$^{3+}$ can be obtained (Scheme 4a). The later can also be obtained through the acetato bridged synthetic intermediate Ru-(OAc)-Ru, **9**$^{2+}$, by a

consecutive sequence of acidic and basic treatments (see Experimental Section of paper C).

The hydrolysis of the phosphonate group in complex $\mathbf{7^{2+}}$ to obtain the phosphoric acid derivate trpy-P_a is carried out under inert conditions. The reaction proceeds via the substitution of the ethyl group by TMSBr, followed by the methanol treatment of the obtained TMS-derivative to obtain the desired phosphoric acid group (Scheme 4b). During the hydrolysis process the chloro bridge is replaced by a bromo bridging group. The final complex precipitates in its neutral form (with only one oxygen of the phosphonate group protonated) as evidenced by the crystal structure, the mass spectra, and the redox titration of this compound (SI of paper D). The treatment of this complex in acidic media allows obtaining the corresponding aqua derivate $\mathbf{22^{3+}}$.

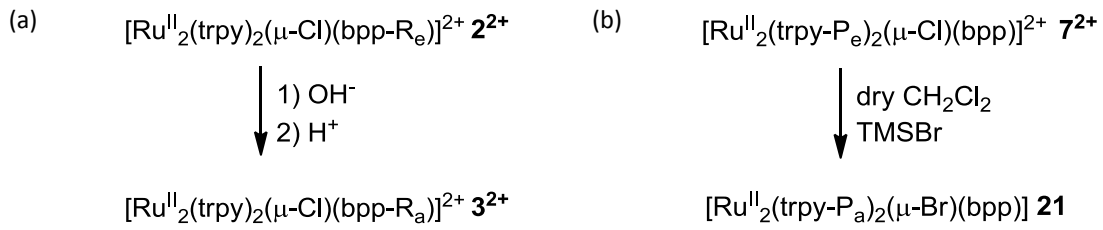

Scheme 4. The two different hydrolysis routes used in this work (a) for the carboxilate derivate, (b) for the phosphonate derivate.

All the Ru complexes prepared in the present work were characterized by elemental analysis and spectroscopic (UV-vis, MS, NMR) and electrochemical techniques.

III.1.4. Characterization of Ru Complexes

III.1.4.1. X-Ray Structures

Suitable crystals for X-ray diffraction analysis were obtained for complexes: $\mathbf{1}^{2+}$, $\mathbf{2}^{2+}$, $\mathbf{8}^{2+}$, $\mathbf{11}^{4+}$ and **21**. In all the five complexes the Ru metal centers adopts a pseudo-octahedral coordination geometry with three positions occupied by the meridional trpy ligand, two by the tetradentate Hbpp-related ligand and the final either by a bridging Cl or Br ligand or by an oxygen atom of the acetato bridge. In all cases bond distances and angles are unremarkable and thus similar to previous complexes already described in the literature.[3] An interesting feature that can be observed in the dinuclear complexes $\mathbf{1}^{2+}$ and $\mathbf{8}^{2+}$ (Figures 2a and 2b) is the different relative spatial disposition of the trpy ligands, which cause a C_{2V} and C_2 symmetry, respectivelly. Whereas in the Cl-bridged complex they are situated orthogonally facing one another, in the acetato-bridged complex they are placed above and below the equatorial plane defined by the two pyridines and the pyrazolate group of the Hbpp-modified ligand. This is a consequence of the geometrical and steric demands imposed by the acetato ligand and the rigidity of the bpp^- framework. The same distortion is also observed in the tetranuclear complex $\mathbf{11}^{4+}$, where the two dinuclear subunits are linked by the *m*-xylyl entity (Figure 2c).

The X-ray structures for complexes $\mathbf{2}^{2+}$ and **21** evidences that the additional carboxylate and phosphonate moieties are not involved in the first ruthenium coordination sphere.

For complex **21** the additional phosphoric moiety causes a distortion in the planarity of the terpyridine ligands and in the angle between them (being here of 47 ^{o} in comparison with the 66 ^{o} found for the complex with the chloro bridge and the non-modified terpyridines).[4] This angle decrease could be caused by the hydrogen bonding of a methanol molecule with the two phosphoric groups of the complex (Figure 2d).

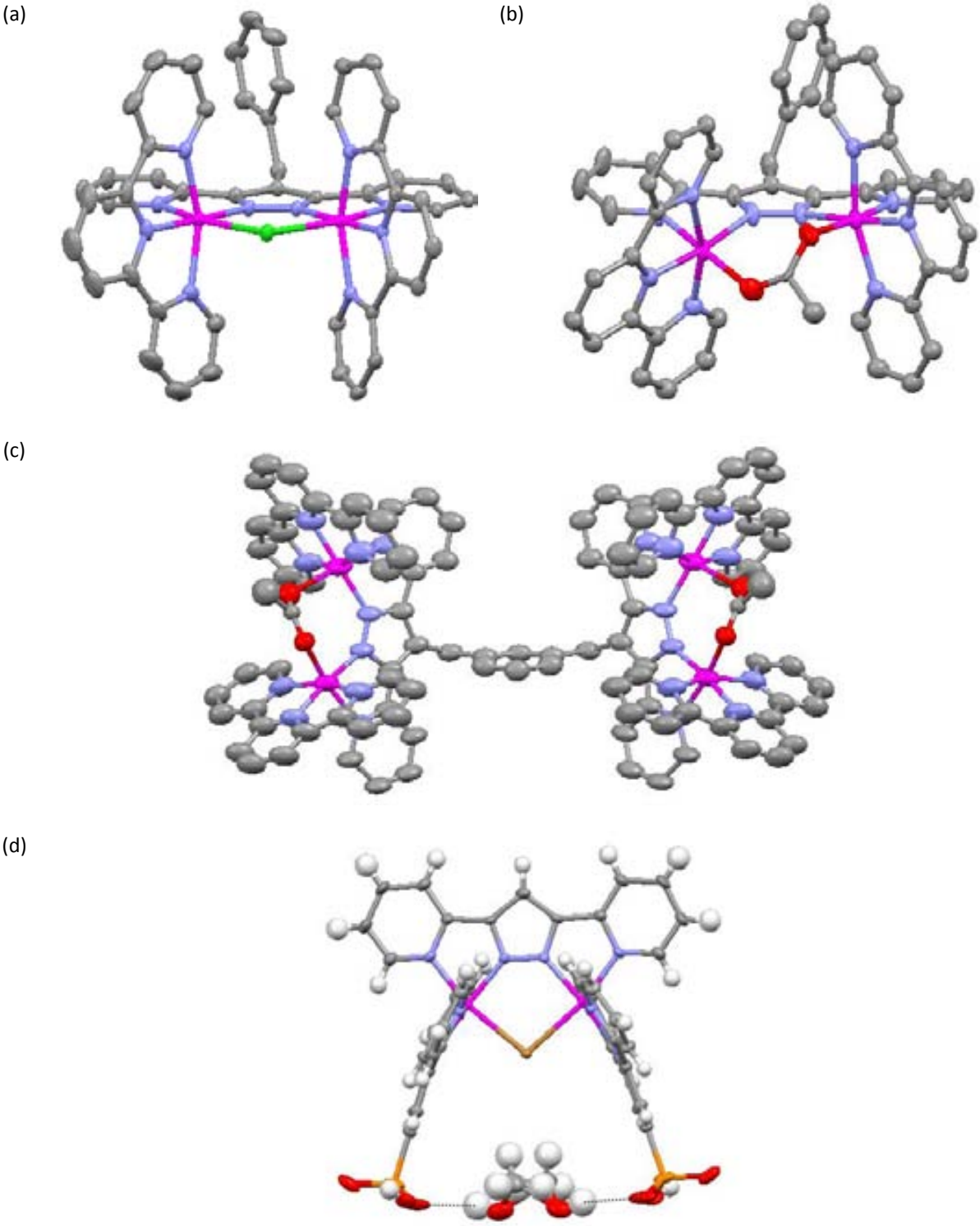

Figure 2. Mercury™ ellipsoid plot (50% probability) for the cationic part of complexes (a) $\mathbf{1}^{2+}$, (b) $\mathbf{9}^{2+}$, (c) $\mathbf{11}^{4+}$ and (d) **21**. Color codes: Ru, pink; Cl, green; N, blue; O, red; Br, brown; H, white. In (a), (b) and (c) Hydrogen atoms are not shown.

III.1.4.2. NMR spectroscopy

Both 1D and 2D NMR spectroscopy have proved to be powerful tools in order to structurally characterize in solution all the complexes prepared in this work. All the resonances observed in the NMR spectra can be unambiguously assigned based on their integrals, symmetry and multiplicity. The chloro bridged dinuclear complexes $\mathbf{1}^{2+}$, $\mathbf{2}^{2+}$, $\mathbf{3}^{2+}$ and $\mathbf{7}^{2+}$ display in solution a C_{2v} symmetry with one symmetry plane containing the bpp^- part of the bpp-modified ligand as well as the two Ru centers, the Cl bridging ligand and the central N of the trpy moieties. This plane bisects the trpy ligands and is perpendicular to a second symmetry plane that bisects the bpp-modified ligand and interconvert the two trpy ligands. The acetato bridged complexes $\mathbf{8}^{2+}$, $\mathbf{9}^{2+}$ and $\mathbf{13}^{2+}$ have C_2 symmetry since in order to accommodate the acetato bridging ligand the pseudo-octahedral geometry of the Ru center has to be further distorted. As mentioned above this result in one Ru center moving above the equatorial plane together with its trpy ligand whereas the other metal center does the opposite movement. In solution and at room temperature these three complexes present dynamic behaviour with the two Ru centers moving simultaneously very fast below and above the equatorial plane. As a result, the NMR the resonances can be assigned as if these complexes had C_{2v} symmetry. Consequently, the external pyridyls of the trpy ligand appear as magnetically equivalent at room temperature.[5]

In complexes $\mathbf{7}^{2+}$ and $\mathbf{13}^{2+}$, the CH_2 of the ethyl chain in the phosphonate ester groups presents a diasteriotopic behaviour, which is caused by their restricted rotation. For this reason, these two methylene protons show different chemical shifts (at 4.240 and 4.268 ppm in the chloro bridged complex, and 4.297 and 4.320 ppm in the acetato bridged complex), and the coupling between them, with the CH_3 and the phosphorous atom make them to appear as two ddq. The chemical shift, the multiplicity and the value of the coupling constants have been confirmed by using simulations with the gNMR[6] software (Figure 3). In complex **21,** the NMR spectrum is important to point out the absence of aliphatic proton signals, which means that the hydrolysis has been completely carried out. The chemical shift observed in the $^{31}P\ \{^1H\}$ NMR spectra was the expected for this kind of phosphorous derivative.[7]

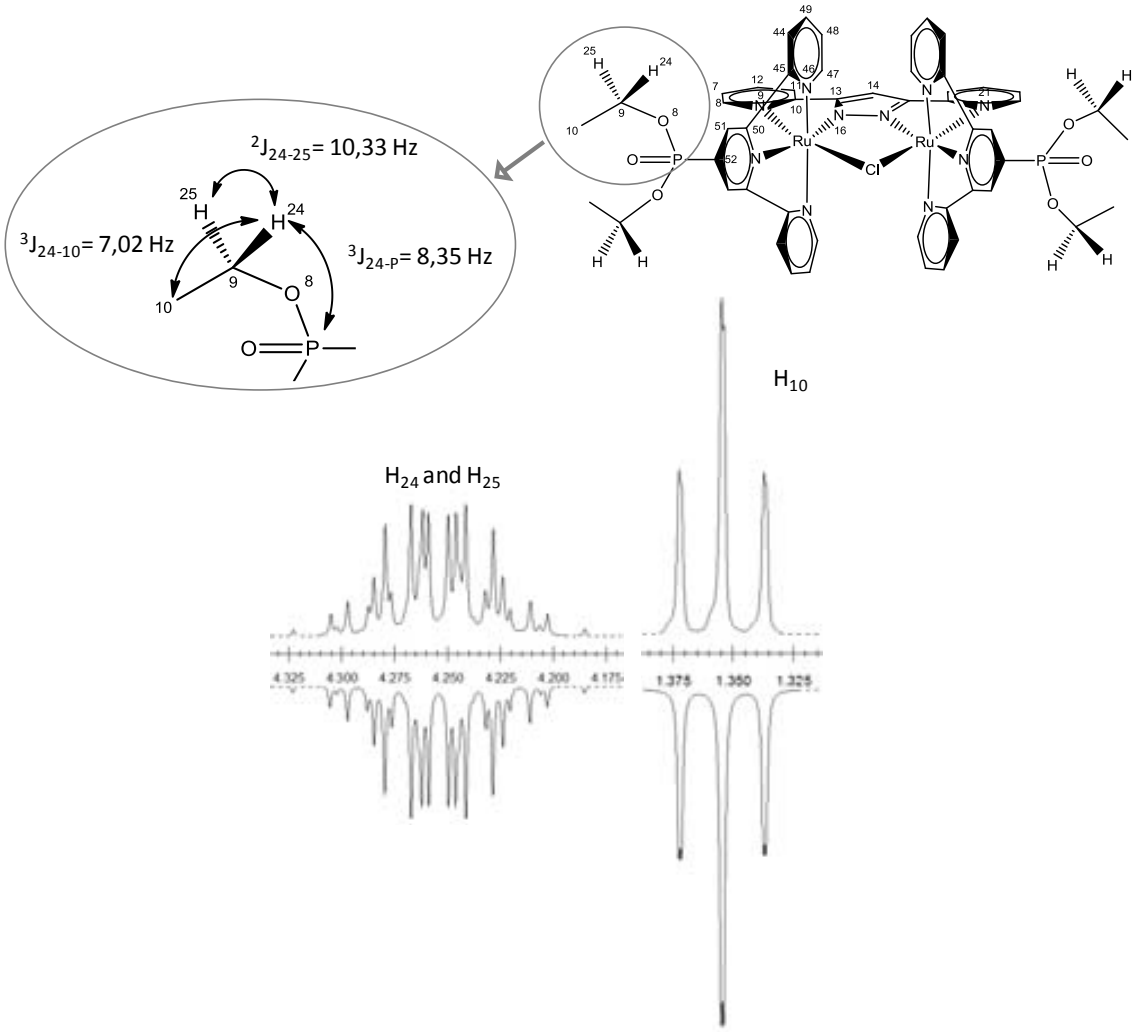

Figure 3. (top) Drawn structure with atom labeling scheme and (bottom) comparison of the experimental and the simulated spectrum of the ethyl fragment for complex $\mathbf{7}^{2+}$.

The NMR spectra for the tetranuclear complexes $\mathbf{4}^{4+}$-$\mathbf{6}^{4+}$, $\mathbf{10\text{-}12}^{4+}$ and $\mathbf{17}^{6+}$-$\mathbf{19}^{6+}$ are very similar to that recorded for their dinuclear counterparts, except for the resonances of the bridging xylyl linker (Figure 4). In other words, the two dinuclear sites of the tetranuclear complexes are undistinguishable by NMR. This is a consequence of the presence of a C_2 axis that runs through the aromatic linker and interconverts each dinucleating unit together with the presence of a local C_2 (or pseudo C_2 in the case of the acetate and aqua complexes) that interconverts each trpy ligand of each dinuclear site (Figure 5).

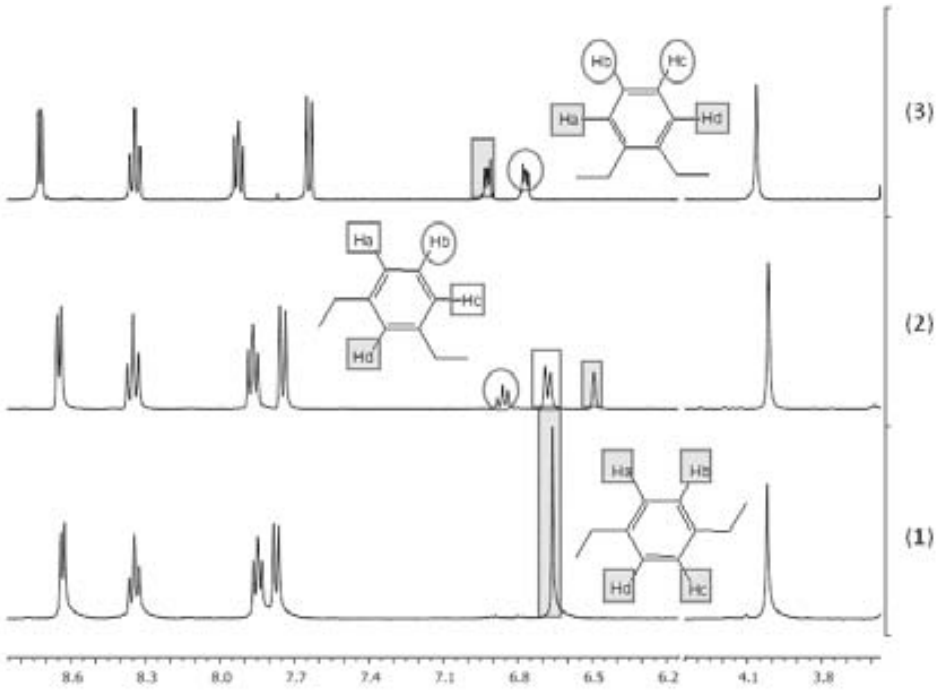

Figure 4. Aromatic zone ^{1}H NMR spectra of the ligands (1) $(Hbpp)_2$-*p*-Xyl, (2) $(Hbpp)_2$-*m*-Xyl, (3) $(Hbpp)_2$-*o*-Xyl in D_2O with a drop of CF_3COOD. The non-symmetry of the ring protons can be observed.

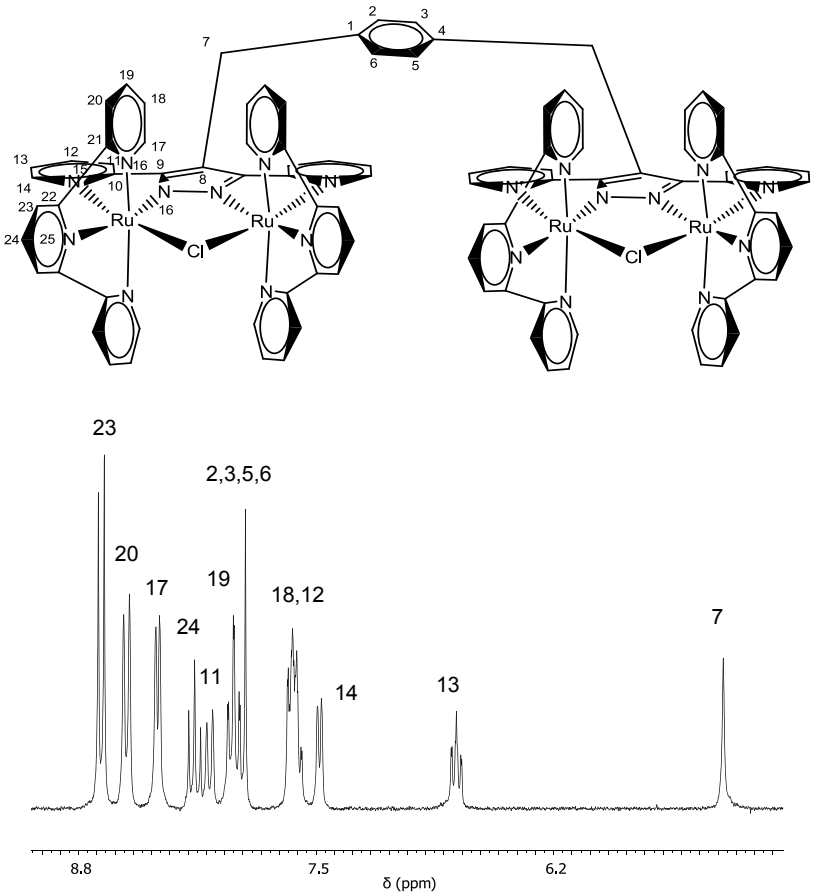

Figure 5. Drawn structure with atom labeling scheme and ^{1}H-NMR (acetone-d_6) of complex $\mathbf{4}^{4+}$.

III.1.4.3. UV-Vis Spectroscopy

The UV-Vis spectral features in solution for all the complexes with the corresponding solvents used are listed in the experimental section of papers B, C and D. As a general trend, three regions can be distinguished for all the spectra: one between 200 and 350 nm, in which very intense bands are observed due to intraligand π-π* transitions;[8] another one between 350 and 550 nm, in which there are mainly broad unsymmetrical Ru(dπ)-trpy/bpp(π*) metal-to-ligand charge transfer (MLCT) bands;[9] and finally the last region above 550 nm in which d-d transitions are observed. From an electronic point of view, the main difference between the spectra of these families of complexes comes from the presence of the different monodentate or bidentate bridging labile ligands. Figure 6 shows the UV-vis spectra of complexes **4**$^{4+}$, **10**$^{4+}$ and **17**$^{6+}$, as an example, to observe the different behaviour when μ-Cl, μ-Ac or 2 H_2O molecules occupy this labile position. A red shift of the MLCT bands is observed for complex **10**$^{4+}$. There are also differences induced by the presence of the phophonate groups directly attached to the trpy ligands. It can be observed that phosphonate-trpy containing complexes show the MLTC bands displaced 15 nm to higher wavelengths with respect to their non-phosphonated counterparts.

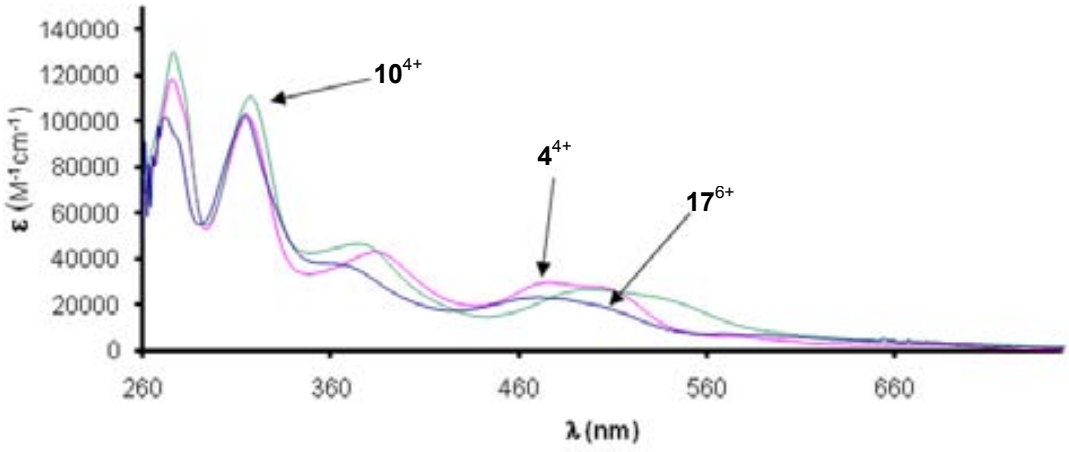

Figure 6. UV-vis spectra of 8 μM samples of complexes **7**$^{4+}$(pink) and **10**$^{4+}$ (green) in CH_2Cl_2 and of 5 μM **13**$^{6+}$ (blue) at pH = 1.0 in 0.1 M triflic acid solution.

III.1.4.4. Electrochemical properties

Cyclic voltammetry experiments were carried out to explain the electrochemical properties of the whole set of complexes. The results are shown in Table 2.

Table 2. Redox properties for the complexes described in the present work ($E_{1/2}$ in V and ΔE in mV) and for related Ru-Hbpp complexes for comparative purposes. Chloro and acetato bridged complexes are recorded using CH_2Cl_2 as solvent whereas the aqua complexes are reported at pH = 1.0 in 0.1 M triflic acid aqueous solution.

	III,II-II,II		III,III-III,II			IV,III-III,III		III,III-III,II		III,II-II,II	
	$E_{1/2}$	ΔE	$E_{1/2}$	ΔE		$E_{1/2}$	ΔE	$E_{1/2}$	ΔE	$E_{1/2}$	ΔE
$[Ru^{II}_2(\mu\text{-Cl})(bpp)(trpy)_2]^{2+}$	0.71	76	1.12	83	$[Ru^{II}_2(H_2O)_2(bpp)(trpy)_2]^{3+}$	0.88	110	0.65	64	0.59	64
$\mathbf{1}^{2+}$	0.78	84	1.23	78	$\mathbf{14}^{3+}$	0.90	84	0.65	64	0.56	60
$\mathbf{2}^{2+}$	0.79	52	1.19	58	$\mathbf{16}^{3+}$	0.98	88	0.66	70	0.61	74
$\mathbf{4}^{4+}$	0.76	82	1.12	123	$\mathbf{17}^{6+}$	0.90	100	0.68	54	0.56	50
$\mathbf{5}^{4+}$	0.77	82	1.13	71	$\mathbf{18}^{6+}$	0.94	86	0.65	60	0.59	72
$\mathbf{6}^{4+}$	0.74	63	1.11	85	$\mathbf{19}^{6+}$	0.94	65	0.65	55	0.59	57
$\mathbf{7}^{2+}$	0.84	41	1.19	53	$\mathbf{20}^{3+}$	0.95	90	0.70	86	0.66	31
FTO-TiO_2-$\mathbf{3}^{+}$	0.73	88	1.20	92	FTO-TiO_2-$\mathbf{16}^{2+}$	1.14	70	0.93	50	0.61	70
FTO-TiO_2-**21**	0.76	250	1.19	210	FTO-TiO_2- $\mathbf{22}^{2+}$	0.97	87	0.63	94	0.60	40
$[Ru^{II}_2(\mu\text{-AcO})(bpp)(trpy)_2]^{2+}$	0.73	86	1.05	86							
$\mathbf{8}^{2+}$	0.79	96	1.15	102							
$\mathbf{9}^{2+}$	0.78	93	1.13	90							
$\mathbf{10}^{4+}$	0.76	76	1.07	87							
$\mathbf{11}^{4+}$	0.72	67	1.01	104							
$\mathbf{12}^{4+}$	0.73	72	1.03	96							
$\mathbf{13}^{2+}$	0.85	31	1.12	45							
$[RuCl_3(trpy\text{-}P_e)]$	0.16	57									
$[RuCl_3(trpy)]$	0.03	50									

The voltammograms of complex $[RuCl_3(trpy\text{-}P_e)]$ shows only one reversible wave at 0.16 V, which is associated to the oxidation of Ru(II) to Ru(III). The comparison of this complex with $[RuCl_3trpy]$, shows that the $[RuCl_3(trpy\text{-}P_e)]$ presents a 120 mV shift to higher potentials. This displacement can also be found in the first wave of complexes $\mathbf{7}^{2+}$ and $\mathbf{13}^{2+}$.

For the μ-Cl^- and μ-AcO^- complexes that do not contain aqua groups, the voltammograms in organic solvents show two chemically reversible and electrochemically quasi-reversible redox waves. As an example, Figure 7a shows the CV of complex $\mathbf{10}^{4+}$ in CH_2Cl_2 displaying two faradaic redox processes. The first one at 0.76 V is assigned to the formation of the mixed-valence species for each subunit (III-II + 1 e^- -> II-II) that occurs at exactly the same potential and thus manifests the independent behaviour of each dimeric subunit,

$\{[Ru^{III}Ru^{II}(trpy)_2(\mu\text{-}Cl)]_2(\mu\text{-}(bpp)_2\text{-}p\text{-}xyl)\}^{6+} + 2\ e^- \rightarrow$

$\{[Ru^{II}Ru^{II}(trpy)_2(\mu\text{-}Cl)]_2(\mu\text{-}(bpp)_2\text{-}p\text{-}xyl)\}^{4+}$ (1)

A second redox process is observed at 1.07 V and involves the removal of a second electron associated with the III-III + $1e^-$ -> III,II transition, as indicated in the equation below,

$\{[Ru^{III}Ru^{III}(trpy)_2(\mu\text{-}Cl)]_2(\mu\text{-}bpp)_2\text{-}p\text{-}xyl)\}^{8+} + 2\ e^- \rightarrow$

$\{[Ru^{III}Ru^{II}(trpy)_2(\mu\text{-}Cl)]_2(\mu\text{-}bpp)_2\text{-}p\text{-}xyl)\}^{6+}$ (2)

The 310 mV difference is indicative of a relatively strong electronic coupling between the metal centers through the bridging ligands of each subunit.

As can be observed in Table 2, dinuclear complexes $\mathbf{1^{2+}}$-$\mathbf{2^{2+}}$ and $\mathbf{8^{2+}}$-$\mathbf{9^{2+}}$ containing bpp-modified ligands show significantly higher redox potentials than their bpp^- counterparts, as expected due to the electron withdrawing nature of the additional benzylic units. This electronic effect is manifested in both redox processes but to a much larger extend in their second oxidation. For the Ru(III-II/II-II) couple the potentials increase roughly 60-70 mV whereas for the second one Ru(III-III/III-II) the potentials increase by 100-110 mV. For the Cl^- ($\mathbf{4^{4+}}$-$\mathbf{6^{4+}}$) and AcO^- ($\mathbf{10^{4+}}$-$\mathbf{12^{4+}}$) tetranuclear complexes the effect of the benzyl group to the first couple is also observed although somewhat attenuated (Table 2). In sharp contrast for the second redox couple the tetranuclear Cl^- complexes ($\mathbf{4^{4+}}$-$\mathbf{6^{4+}}$) are practically not affected whereas for the AcO^- ones ($\mathbf{10^{4+}}$-$\mathbf{12^{4+}}$) the potentials are lower (Table 2). These observations manifests how subtle ligand variations can strongly influence the electronic nature of the species and put forward the difficulty of predicting electronic effects in species resulting from multiple electron transfer processes.

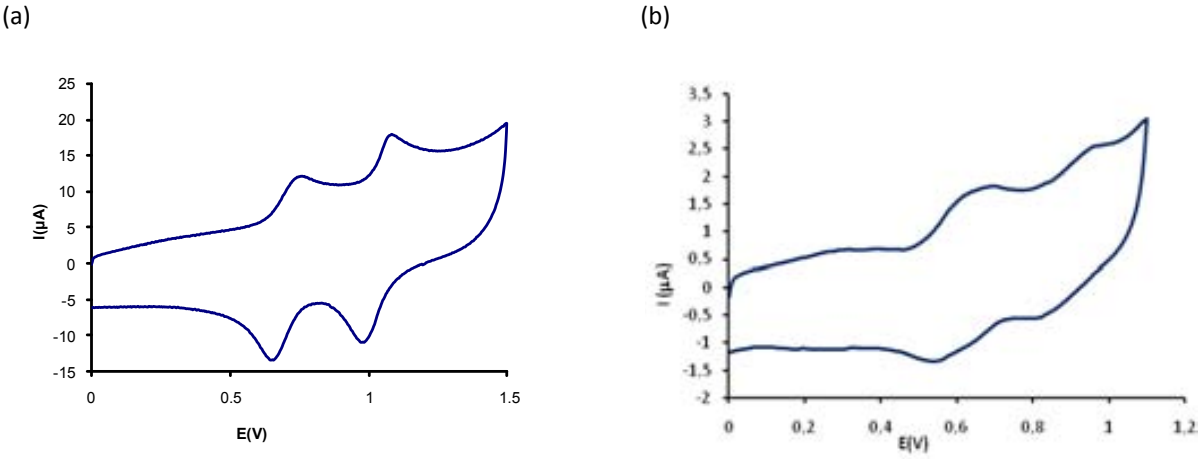

Figure 7. Cyclic Voltammograms for: (a) acetato bridged complex $\mathbf{10}^{4+}$ in 0.1M *n*-Bu_4NPF_6 in CH_2Cl_2 at 300 mV/s scan rate. (b) Aqua complex $\mathbf{17}^{6+}$ at pH = 1.0 in 0.1 M triflic acid aqueous solution at 100 mV/s scan rate. In both cases a glassy carbon electrode is used as the working electrode and the potential is measured vs. SSCE.

The electrochemistry of the aqua complexes $\mathbf{14}^{3+}$-$\mathbf{16}^{3+}$, $\mathbf{20}^{3+}$, $\mathbf{22}^{3+}$ and $\mathbf{17}^{6+}$-$\mathbf{19}^{6+}$ containing two or four aqua groups was performed at pH = 1.0 in 0.1 M aqueous triflic acid solutions. The redox features observed were radically different from the previously commented in organic solvents due to the proton coupled electron transfer (PCET) nature of the electrochemical processes. The simultaneous removal of electrons and protons causes the generation of hydroxo and oxo ligands which promotes an easy access to higher oxidation states, a fact which can be justified by the σ- and π-donor nature of the oxido group to Ru. The three redox processes observed in the CV are assigned by comparison with the parent Ru-Hbpp analogue under the same conditions.[4] In general the redox potentials of complexes $\mathbf{14}$-$\mathbf{15}^{3+}$ and $\mathbf{17}^{6+}$-$\mathbf{19}^{6+}$ are a few mV lower than those of $[Ru_2(H_2O)_2(bpp)(trpy)_2]^{3+}$, as can be observed in Table 2, again due to the electron withdrawing nature of the benzyl group.

As an example, for complex $\mathbf{17}^{6+}$ at pH = 1 (Figure 7b), three redox processes are clearly observed which are assigned to the following reactions (for clarity purposes only the groups potentially undergoing PT or ET are written, thus for instance $[Ru^{II}(H_2O)\text{-}Ru^{II}(H_2O)]_2^{6+}$ corresponds to complex $\mathbf{17}^{6+}$):

$$[Ru^{III}(OH)\text{-}Ru^{II}(H_2O)]_2^{6+} + 2e^- \rightarrow [Ru^{II}(OH)\text{-}Ru^{II}(H_2O)]_2^{4+} \quad E_{1/2} = 0.33\ V \quad (3)$$

$$[Ru^{III}(OH)\text{-}Ru^{III}(OH)]_2^{6+} + 2e^- + 2H^+ \rightarrow [Ru^{III}(OH)\text{-}Ru^{II}(H_2O)]_2^{6+} \quad E_{1/2} = 0.45\ V \quad (4)$$

$$[Ru^{IV}(OH)\text{-}Ru^{III}(OH)]_2^{8+} + 2e^- \rightarrow [Ru^{III}(OH)\text{-}Ru^{III}(OH)]_2^{6+} \quad E_{1/2} = 0.60\ V \quad (5)$$

The next redox process, which is not observed in the voltammogram, generates the dioxo species $Ru^{IV}(O)\text{-}Ru^{IV}(O)$ that are proposed as responsible for the generation of molecular oxygen. As was also the case in the NMR spectra, here the redox behaviour of the two dimeric subunits of the tetranuclear complexes is indistinguishable due to the negligible electronic coupling between them.

Studies on the dependence of the electrochemical properties with respect to pH (from 1.0 to 12.0) of the aqua complexes **14**$^{3+}$ and **17**$^{6+}$ have been done performing cyclic voltammetry experiments in buffered aqueous solutions. The resultant Pourbaix diagram for complex **17**$^{6+}$ (Figure 8) shows the different stability zones of the corresponding species with a different degree of protonation and/or oxidation state. These Pourbaix diagrams agree with the fact that the electrochemical properties of these complexes are only slightly modified with respect to the $[Ru_2(H_2O)_2(bpp)(trpy)_2]^{3+}$ complex by the effect of the withdrawing nature of the benzyl group.[4]

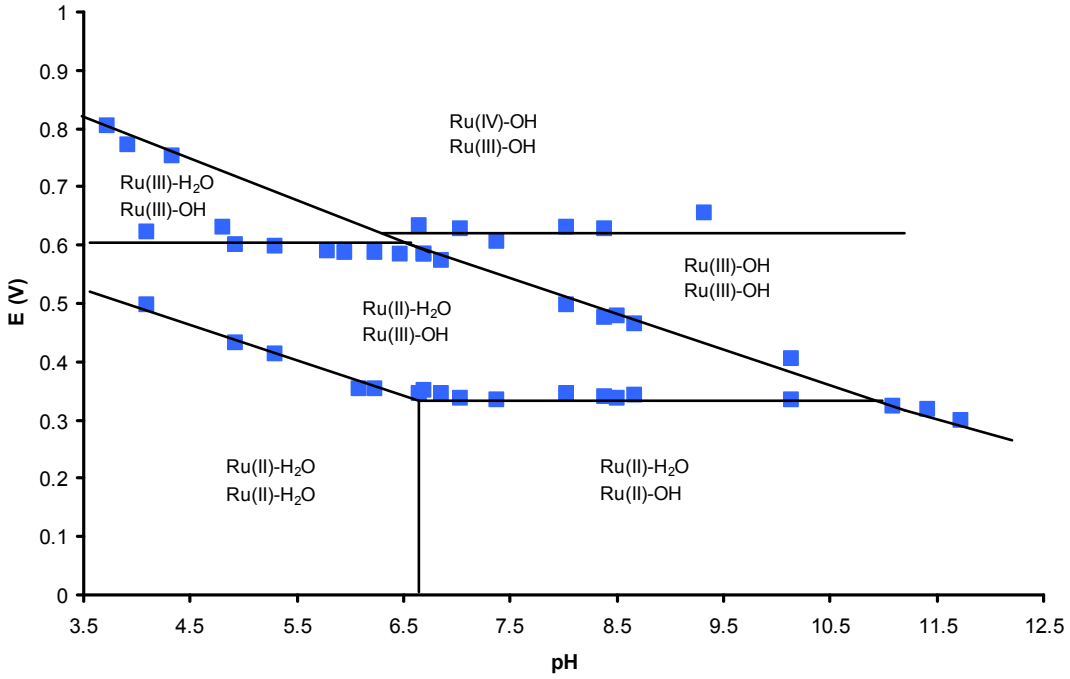

Figure 8. Pourbaix diagram for the aqua complex **17**$^{6+}$ showing the zones of thermodynamic stability of the different species as function of pH and $E_{1/2}$. The oxidation state of the Ru metal and the degree of protonation of the initial aqua group are indicated; for instance the label [Ru(II)-H_2O Ru(III)-OH] is used for $\{[Ru^{II}Ru^{III}(H_2O)(OH)(trpy)_2]_2[(\mu\text{-}bpp)_2\text{-}p\text{-}xyl]\}^{6+}$.

III.1.5. Attachment of the Ru Complexes onto TiO_2 Rutile and FTO-TiO_2 Films

The attachment onto TiO_2 surfaces has been carried out with the carboxylate and phosphonate-modified complexes $\mathbf{3}^{2+}$ and **21**, respectively. Two different TiO_2 supports were used: TiO_2 rutile nanopowder, to perform water oxidation using Ce(IV) as oxidant, and FTO-TiO_2 conducting films to test the electrocatalytic water oxidation. Complex $\mathbf{3}^{2+}$ has been anchored onto both supports, whereas complex **21** has only been supported onto FTO-TiO_2 films.

Furthermore, also the free ligand Hbpp-R_a has been anchored onto TiO_2 to test its stability. Adding the TiO_2 rutile nanopowder into a MeCN solution of the ligand and stirring the mixture at room temperature this process can be carried out. After a few hours the ligand is completely anchored on the support, as shown by the disappearance of the ligand from the solution (NMR checking). The mixture is then centrifuged and the remaining solid filtered and washed several times with MeCN to obtain finally the TiO_2-bpp-R_a hybrid material. Both the free ligand Hbpp-R_a in homogeneous phase and the anchored derivative, TiO_2-bpp-R_a, were shown to be totally stable under oxidative conditions (in the presence of Ce(IV) in a pH = 1 triflic acid solution). Furthermore, in the latter case, no ligand leaching was observed under these conditions indicating the high stability of the TiO_2–OOR bond.

The attachment of the Ru complex onto TiO_2-rutile was also carried out in MeCN by introducing typically a 250 mg sample of TiO_2 in a 4 mL solution containing 2.7 mg (2.0 μmols) of $\mathbf{3}^{2+}$. In just 5 minutes the solution completely decolorized indicating the total anchoring of the complex in the TiO_2 thus generating TiO_2-$\mathbf{3}^{+}$. This new material was thoroughly washed with clean CH_2Cl_2 and then air dried at room temperature. The solid obtained is then added into 1.5 mL of a 0.1 M triflic acid solution and stirred at room temperature for 24 h, producing the substitution of the chloro bridging ligand by two aqua groups and generating the water oxidation catalyst TiO_2-$\mathbf{16}^{2+}$, as indicated in Scheme 5a.

The attachment of the catalysts on transparent and conducting FTO-TiO_2 films was carried out by soaking the conducting electrodes in methanolic solutions of the desired compounds (Figure 9 and Scheme 5). The solvent was changed from acetonitrile to methanol to improve the process avoiding the possible substitution of the chloro bridge for two acetronitrile molecules. However the new process takes longer times

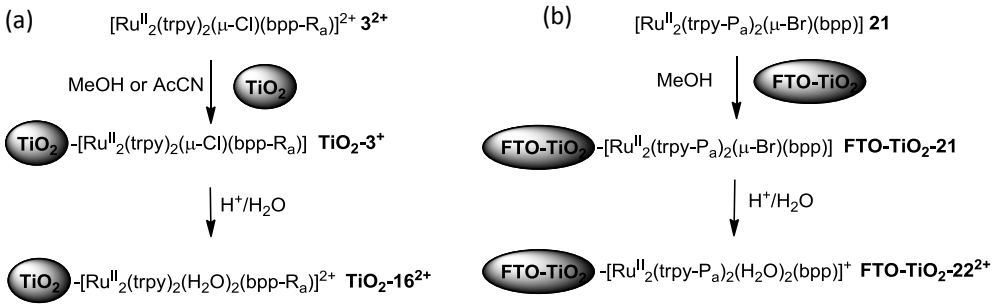

Scheme 5. Anchoring strategy (a) for complex **3^{2+}** on rutile-TiO_2 and (b) for complex **21** on FTO-TiO_2.

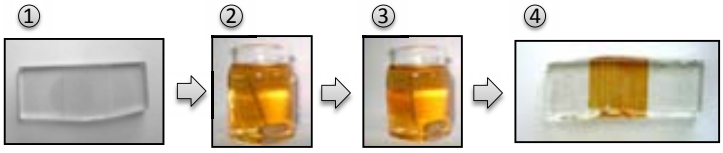

Figure 9. Pictures during the catalyst anchoring process: ① Initial FTO-TiO_2 film, FTO-TiO_2 film soaked in a methanolic solution of complex **3^{2+}** ② at time 0, ③ after 24 h, and ④ the FTO-TiO_2-**3$^+$** at the end of the anchoring process.

This anchoring process has been studied as function of the initial complex concentration. The results show a strong linear dependence between the initial concentration, the initial attachment rate and the final amount of anchored complex (Figure 10). The quantification of the anchored mmol of catalyst was calculated by applying the Lambert-Beer law to the UV-vis spectra of the solution before and after the anchoring process (Figure 11a). Finally, the substitution of the bridging ligands for aqua molecules is achieved by soaking the films in a 0.1 M triflic acid aqueous solution at pH=1 during 24 h (Scheme 5b).

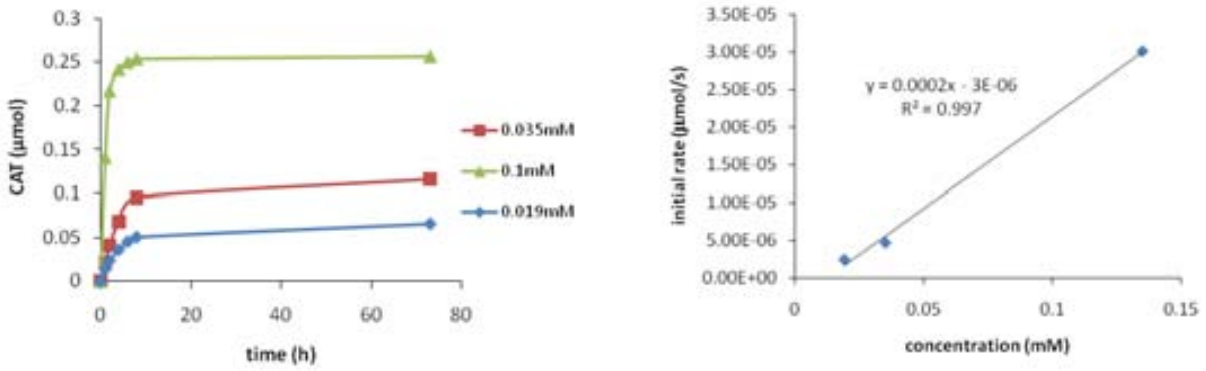

Figure 10. (a). Evolution of the anchoring process at three different concentrations of complex **21** (b) Dependence of the initial anchoring rate depending on the concentration of the initial solution for complex **21**.

The anchored species have been spectroscopically and electrochemically characterized. In the UV-Vis spectra, a band appearing at 460 nm, attributed to a MLCT, confirms the attachment of the complex onto the FTO-TiO_2 surface (Figure 11b). The electrochemical experiments also corroborate that the complexes are anchored onto the solid surface. The supported species FTO-TiO_2-**3**$^{+}$ and FTO-TiO_2-**21** present the same redox processes than their analogous free complexes, but at lower redox potentials (Figure 12) and (Table 2).

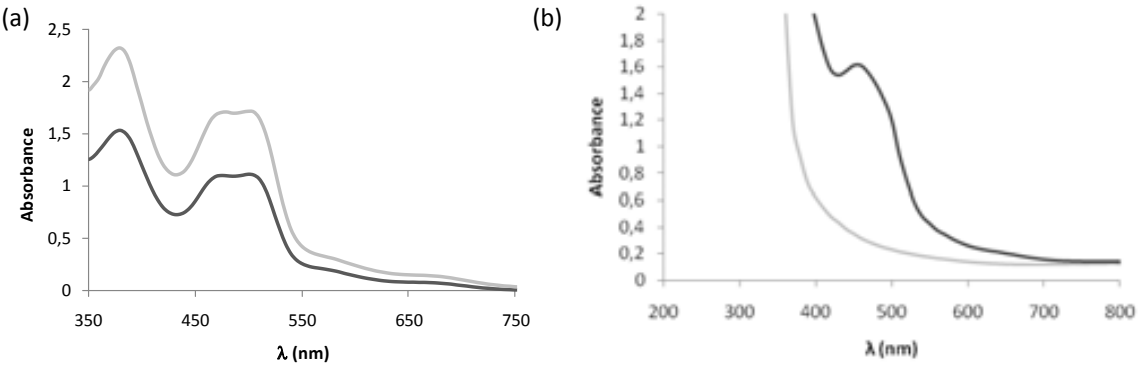

Figure 11. UV-vis spectra of (a) the solution and (b) the FTO-TiO_2 film, before (light grey) and after (dark grey) the anchoring process of complex **21**.

These experiments confirm that after 24 hours the chloro bridge substitution by two H_2O molecules on the surface supported complex has been accomplished (Figure 12).

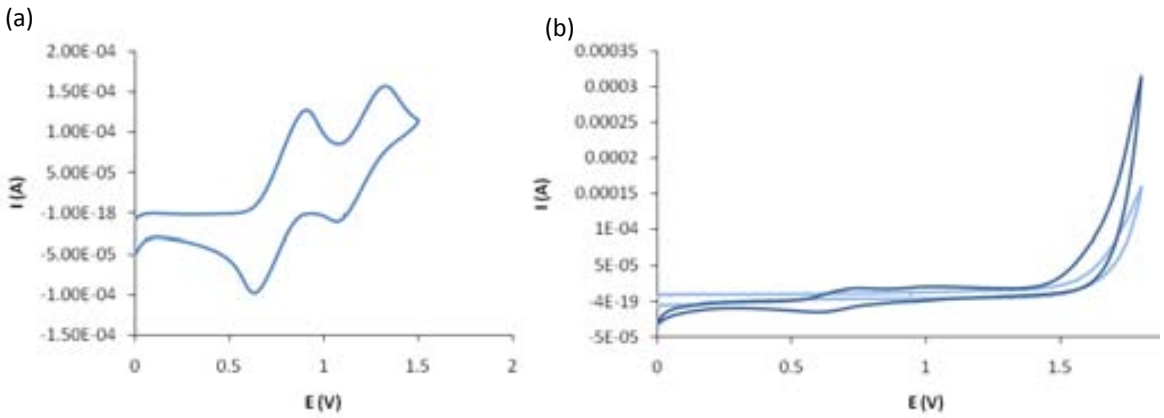

Figure 12. Cyclic voltammograms: (a) FTO-TiO_2-**21** in CH_2Cl_2, scanning anodically at a scan rate of 100 mV/s, (b) FTO-TiO_2-$\mathbf{22}^{2+}$ at pH=1 in 0.1M triflic acid scanning anodically at a scan rate of 50 mV/s, dark blue, the FTO-TiO_2 blank, light blue.

Electrochemically, the FTO-TiO_2-$\mathbf{22}^{2+}$ films show quite different behaviour than its homogeneous counterpart, complex $\mathbf{20}^{3+}$ (Figure 13a). The most relevant difference corresponds to the electrocatalytic water oxidation wave, that is clearly observed for complex $\mathbf{20}^{3+}$ with an onset potential of 1.3 V, but not present at this potential in the CV of the anchored FTO-TiO_2-$\mathbf{22}^{2+}$ complex (Figure 13a). That can also be noted by comparing the blank's (FTO-TiO_2) and FTO-TiO_2-$\mathbf{22}^{2+}$ CVs, where a very small shift of the electrocatalytic wave can be observed (Figure 12b). Electrochemical studies of the anchored complex FTO-TiO_2-$\mathbf{16}^{2+}$ also show a displacement to upper potentials of the electrocatalytic WO wave (Figure 13b). These experimental evidences indicate that the anchoring process has modified the catalytic properties of these complexes.

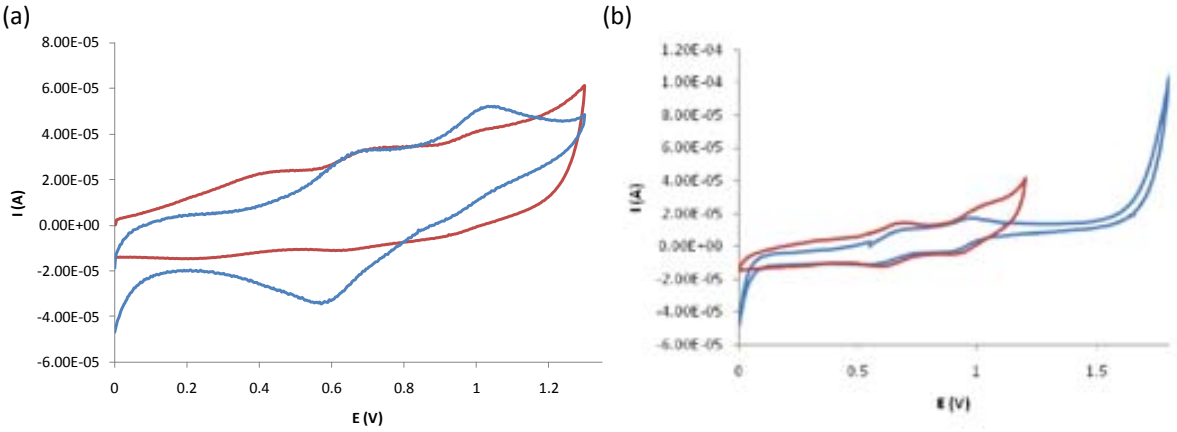

Figure 13. Cyclic voltammograms for: (a) complex $\mathbf{20}^{3+}$ (red) and the anchored complex FTO-TiO_2-$\mathbf{22}^{2+}$ (blue). (b) complex $\mathbf{16}^{3+}$(red) and the anchored complex FTO-TiO_2-$\mathbf{16}^{2+}$ (blue).

III.1.6. Water oxidation

All the complexes (homogeneous and heterogeneous) prepared and characterized above were tested as catalyst in the water oxidation reaction (6).

$H_2O \rightarrow O_2 + 4H^+ + 4e^-$ (6)

To perform this reaction the initial Ru-aqua groups (Ru(II)-H_2O) have to be oxidized to their Ru(IV)-O form, which are the catalytically active species. This activation can be done by two different ways:

1) Using a chemical oxidant, such as Ce(IV):

   $4Ce(IV) + H_2O\text{-}Ru(II)\text{-}Ru(II)\text{-}H_2O \rightarrow 4Ce(III) + O\text{-}Ru(IV)\text{-}Ru(IV)\text{-}O$ (7)

   In these cases the total amount of evolved gases in the reaction were monitored as a pressure increase by manometry and the nature of the formed gases was analyzed by means of online MS spectroscopy. In the latter technique the generated gases were continuously removed from the reaction vessel toward the MS chamber.

2) Generating the active Ru(IV) species by means of a controlled potential electrolysis (CPE). The oxygen evolution in these experiments was followed using a Clark electrode, which is selective for oxygen detection.

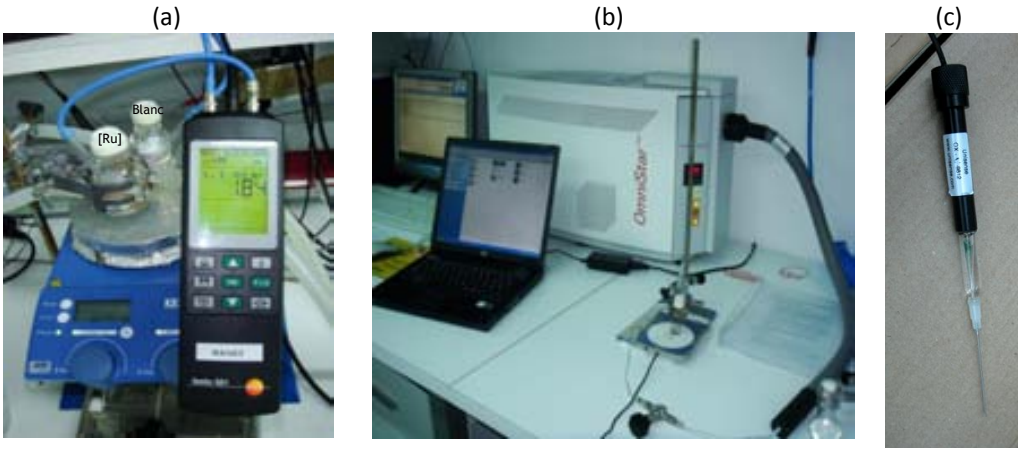

Figure 14. Techniques used to follow the water oxidation reaction. (a) Differential pressure manometer. (b) Mass Spectrometer. (c) Clark electrode.

III.1.6.1. Homogeneous complexes

The aqua complexes **14^{3+}**, **17^{6+}-19^{6+}** were tested as water oxidation catalysts in presence of a strong oxidant such as Ce(IV) in homogeneous phase, and the results obtained are shown in Table 3. As can observed, all the complexes tested in this work, generate a mixture of O_2 and CO_2 during the reaction time. This is in sharp contrast with $[Ru_2(H_2O)_2(trpy)_2(bpp)]^{3+}$, where no CO_2 is formed. Consequently, all the efficiencies of the complexes reported here on are lower than that of $[Ru_2(H_2O)_2(trpy)_2(bpp)]^{3+}$.

Table 3. Catalytic oxidative performance of aqua complexes **14^{3+}**, **17^{6+}-19^{6+}**, and $[Ru_2(H_2O)_2(trpy)_2(bpp)]^{3+}$. All reactions were carried out in a total volume of 2 mL at pH = 1.0 in 0.1 M triflic acid. Ce(IV) was used as oxidant. [a] Ratio Cat/Ce(IV), 1/100. [b] Ratio Cat/Ce(IV), 1/200.[c]Eff.= Efficiency.

Entry	Complex	[Cat]	TN/O_2	TN/CO_2	$[O_2]/[CO_2]$	TN/Total	Eff.[c]
1	$[Ru_2(H_2O)_2(trpy)_2(bpp)]^{3+}$, [a]	1.0	18	-	-		72.0
2	**14^{3+}**, [a]	1.0	5.8	5.8	1.0	11.7	29.2
3	**17^{6+}**, [b]	1.0	10.1	5.1	2.0	15.2	33.5
4		0.5	14.8	5.8	2.5	20.7	46.3
5	**18^{6+}**, [b]	1.0	13.5	6.4	2.1	19.9	45.5
6		0.5	15.6	6.2	2.5	21.9	48.9
7	**19^{6+}**, [b]	1.0	13.9	6.9	2.0	20.8	46.7
8		0.5	18.4	6.1	3.0	24.5	36.0

As an example, Figure 15 shows the manometry and MS profiles obtained in entry 3 of Table 3. As the MS profile indicates, O_2 and CO_2 are generated together from the very beginning, thus pointing out that two competitive reactions are taking place. It can also be observed that the rate of O_2 formation is two times faster than the rate of CO_2 generation. From the combination of the O_2/CO_2 ratio ($r_{o\text{-}c}$) provided by the MS profile and the quantitative analysis obtained from manometry, we can conclude that in these conditions 20.4 μmol of O_2 and 10.2 μmol of CO_2 are generated, which represents a TN of 10.1 for O_2 and 5.1 for CO_2.

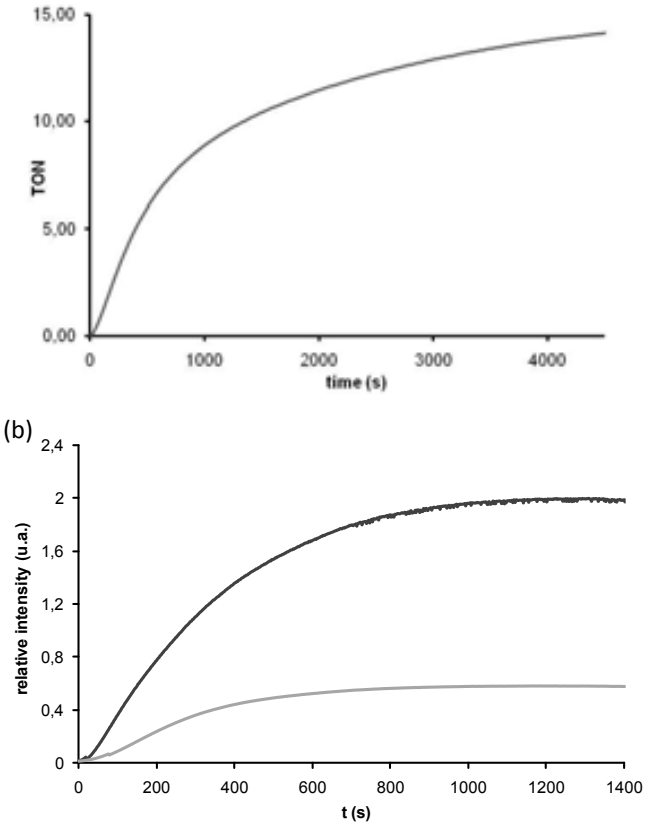

Figure 15. Gases generated during the catalysis as a function of time in the system: Cat (**17**$^{6+}$) 1 mM/Ce 200 mM/0.1 M triflic acid with a total volume of 2 mL at 25.0 °C. (a) Manometry profile, (b) Online mass spectrometry profile for **17**$^{6+}$. O_2 dark grey; CO_2 light grey.

An interesting effect is observed when the same system is diluted to a half as shown in entry 4 of Table 3. In this case the total TN (CO_2 + O_2) increases from 15.2 to 20.7 and the final O_2/CO_2 ratio (r_{o-c}) rises from 2.0 to 2.5. The same trend but at a different extent is also observed for the other two tetranuclear complexes as can be observed in entries 5-8 of Table 3. This phenomenon can be understood assuming that in the tetranuclear complexes the oxygen is intramolecularly formed in each electronically independent dinuclear subunit, as is the case for the parent Ru-Hbpp complex, $[Ru_2(H_2O)_2(trpy)_2(bpp)]^{3+}$.[5b] On the other hand, the origin of CO_2 is associated with a bimolecular reaction where an active Ru-O group of a neighboring catalyst molecule attacks the methylenic group of the xylylic bridging unit. This is the only possible pathway since Ce(IV) does not react with the free ligand at room temperature and the geometrical disposition of the Ru-O units prevents an intramolecular ligand oxidation. Therefore, dilution does not affect the intramolecular O_2 generation reaction but decreases the rate at which CO_2 is produced.

Another interesting aspect that can be glimpsed in Table 3 is the fact that for the *para* and *meta* derivatives r_{o-c} increases from roughly 2 to 2.5 when diluted to a half (entries 3-6, Table 3). However, for the *ortho* complex the same dilution boosts r_{o-c} from 2.0 to 3.0. This increase can be associated with the steric accessibility of the methylenic units of the xylylic groups as a function of the geometrical substitution.

Furthermore, the methylenic units are the most easily oxidizable groups of the molecule and thus can be assumed as the starting reaction of a chain of oxidative process which leads to the final decomposition of the ligand backbone. We associate the formation of CO_2 to the oxidation of the benzylic site since this is the easiest part of the molecule to be oxidized. However, once this site is oxidized the oxidative process can continue further and other parts of the complex can also be oxidized. Thus, for the *para* and *meta* isomers the accessibility of these CH_2 units to undergo a bimolecular oxidative reaction is relatively similar whereas it is significantly diminished for the *ortho* isomer (see Figure 16) This is also in agreement with the catalytic performance of the dinuclear complex **14**$^{3+}$ that has the lowest $r_{o\text{-}c}$ value ($r_{o\text{-}c}$ = 1, Table 3 entry 2). The steric hindrance in this case is the lowest and, consequently, this complex posses also the lowest efficiency.

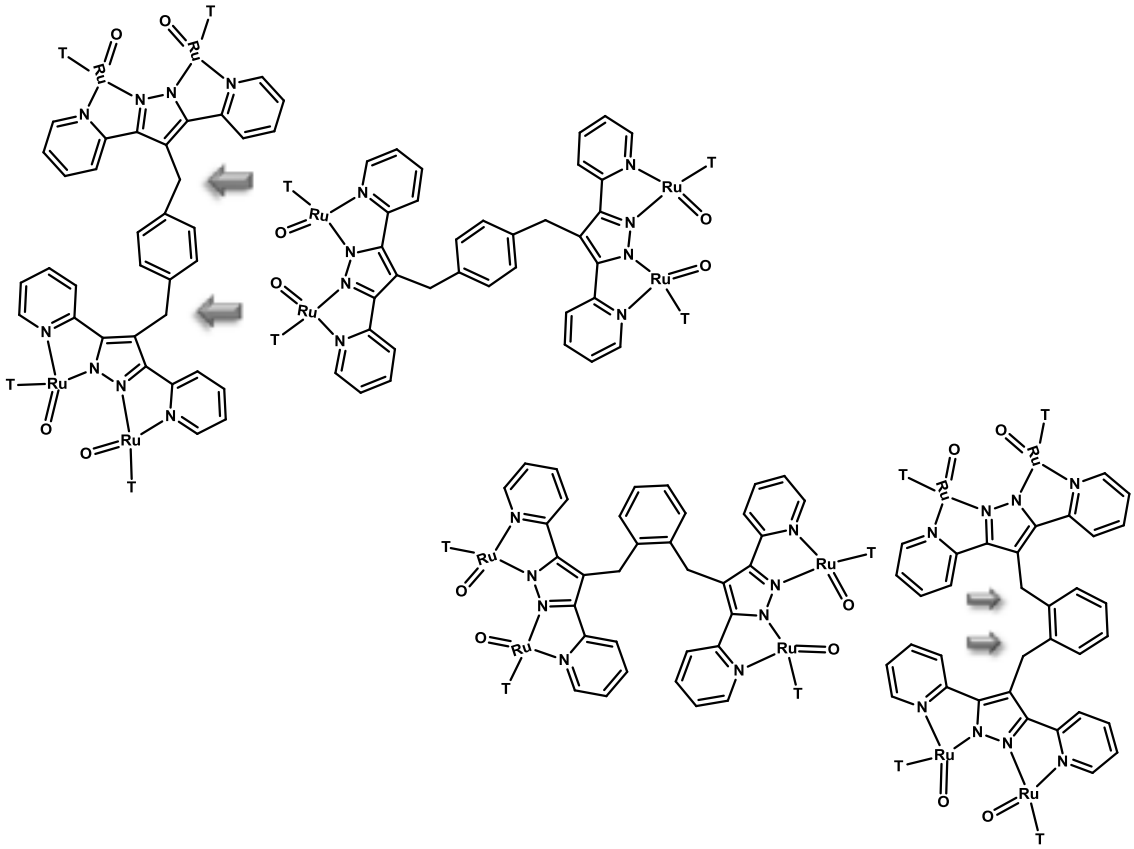

Figure 16. Schematic drawing of complexes **17**$^{6+}$ and **19**$^{6+}$. The arrow indicates the relative accessibility of the methylenic units for bimolecular oxidation. The trpy ligands are represented by a "T" for clarity purposes and their axial coordination is not shown.

III.1.6.2. Heterogeneous complexes with chemical activation

The heterogeneous TiO_2-**16**$^{2+}$ system has been used to catalytically oxidize water using Ce(IV) as sacrificial oxidant. The addition of 200 μmols of Ce(IV) to 2 mmol of the TiO_2-**16**$^{2+}$ hybrid material at pH=1 immediately generates molecular oxygen according to the following equation,

$$2\ H_2O\ +\ 4\ Ce(IV)\ \rightarrow\ O_2\ +\ 4\ H^+\ +\ 4\ Ce(III) \quad (8)$$

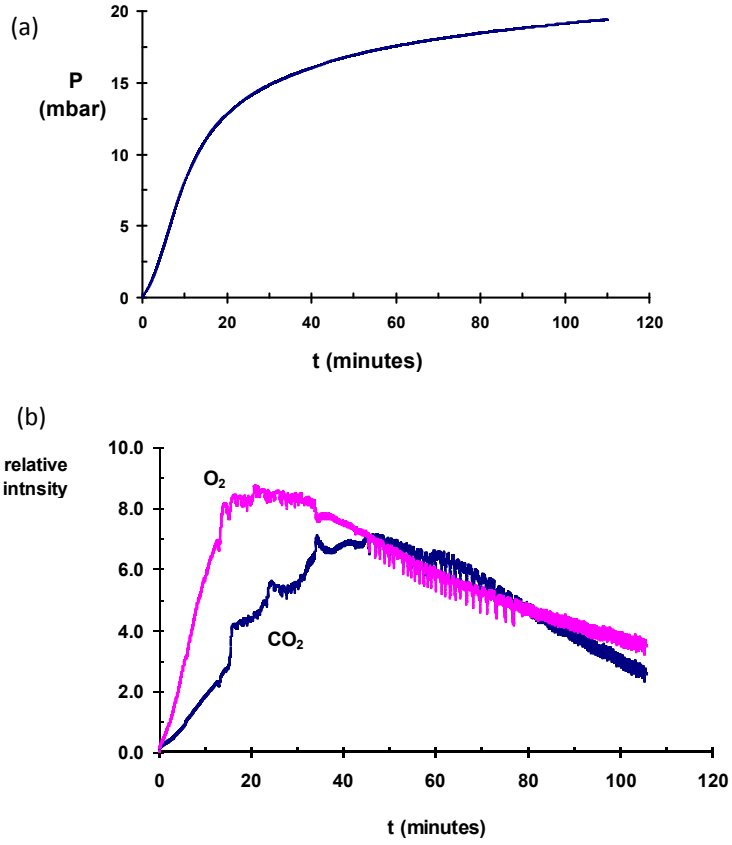

Figure 17. Monitoring of the catalytic gases generated upon oxidative treatment of **TiO_2-16**$^{2+}$ with Ce(IV) as a function of time: (a) manometry profile and (b) mass spectroscopy profile.

However, this oxygen evolution is accompanied by CO_2 generation, as shown in Figure 17. As it happens in the homogenous case, the combination of manometry and MS spectroscopy experiments allowed us to calculate the amounts of the gases formed that turns out to be roughly 7 μmols of O_2 (3.5 turnovers, TN) and 5.8 μmols of CO_2. It is interesting to observe from Figure 17b, that O_2 is formed at an initial rate that is 2.8 times higher than the initial rate of CO_2 formation. This fact implies that the first reaction is the formation of oxygen in an heterogeneous way and, later on, the active complex reacts with another anchored metal complex to form CO_2.

The generation of CO_2 can arise from both (a) the oxidation of the benzylic methylene group or (b) a decarboxylation event[10] with concomitant leaching of the metal catalyst into the solution. The evidence of the bimolecular process observed in the homogeneous complexes **4**$^{3+}$, **17**$^{6+}$-**19**$^{6+}$ (also with CO_2 generation), supports the former process. This ligand oxidation causes the leaching of the metal catalyst to the solution. This is clearly inferred by the fact that initially the TiO_2-**16**$^{2+}$ has a brownish colour and the solution is light yellow due to the presence of Ce(IV) but after 2 hours, when the reaction is completely finished, the solution appears brownish and the solid white (Figure 18). This brown solution has a similar UV-Vis trace than the homologous $[Ru_2(H_2O)_2(trpy)_2(bpp)]^{3+}$ complex when treated under similar conditions in the homogeneous phase but unfortunately, the exact nature of this deactivated/degraded complex remains still elusive. Blank experiments with only TiO_2 and TiO_2-(Hbpp-R_a) under similar oxidative/pH conditions gave neither O_2 nor CO_2 in agreement with the fact that ligand oxidation is caused by a bimolecular catalyst-catalyst interaction instead of a direct oxidation with Ce(IV).

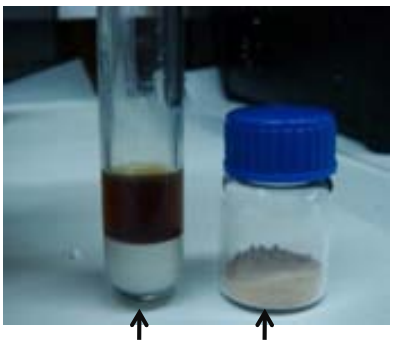

Figure 18. TiO_2-**16**$^{2+}$, before and after catalytic WO

III.1.6.3. Heterogeneous complexes with electrochemical activation

The anchored complexes FTO-TiO_2-**16**$^{2+}$ and FTO-TiO_2-**22**$^{2+}$ have been tested as water oxidation electrocatalysts. First of all, it is important to note that their electrochemical properties show that the water electrochemical wave is weaker and happens at a higher potential than their homogenous partners, which indicates that during the anchoring process most of the catalytic capacity is lost.

The catalytic reaction has been carried out in an electrochemical cell formed by two different compartments, the anodic one, where water oxidation takes place, and the cathodic one where proton reduction (Figure 19) happens.

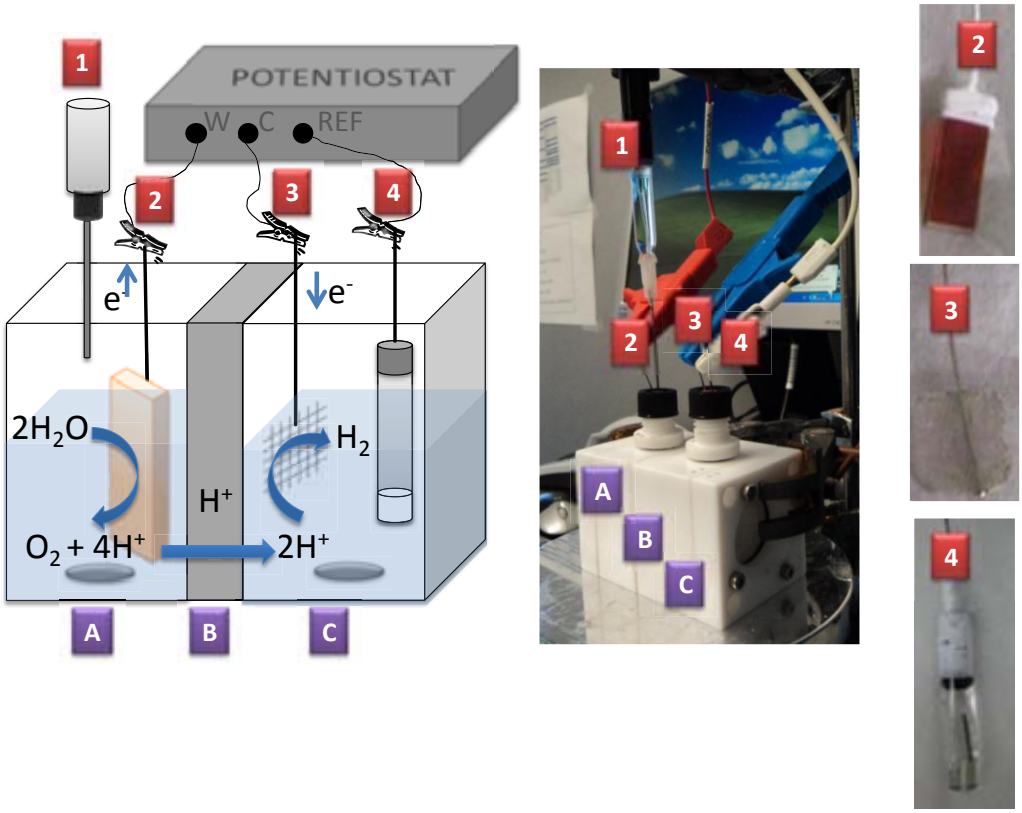

Figure 19. Electrochemical cell (left, schematic draw; right, real picture) formed by: Anodic compartment A; Cathodic compartment C; Proton permeable Naftion membrane B to the proton exchange; Clark electrode 1; Working electrode FTO-TiO_2-catalyst 2; Platinum counter-electrode 3; SSCE reference electrode 4.

When FTO-TiO_2-**16**$^{2+}$ was used as catalyst in the above mentioned electrochemical cell a 1.7 V potential was applied during 6 h. Online O_2 measurement of the headspace of the compartment containing the FTO-TiO_2-**16**$^{2+}$ electrode with a clack electrode prove (1 in Figure 19), revealed that no oxygen was released. The UV-vis analysis of the acidic solution in the anodic compartment of the cell at the end of the experiment presented absorption spectra corresponding to a species closely related to **16**$^{3+}$ as can be observed in Figure 20c. In Figures 20a and 20b the cyclic voltammograms of the electrode **FTO-TiO_2-16**$^{2+}$ before and after the CPE can be observed. Their comparison reveal an important decrease of dinuclear ruthenium compound anchored on the surface of electrode. Additionally, new redox active species were detected. All this data indicates that a major part of the current was employed in undesired processes such as leaching of the catalyst, catalyst decomposition reactions yielding new products and energy dissipation in the form of heat.

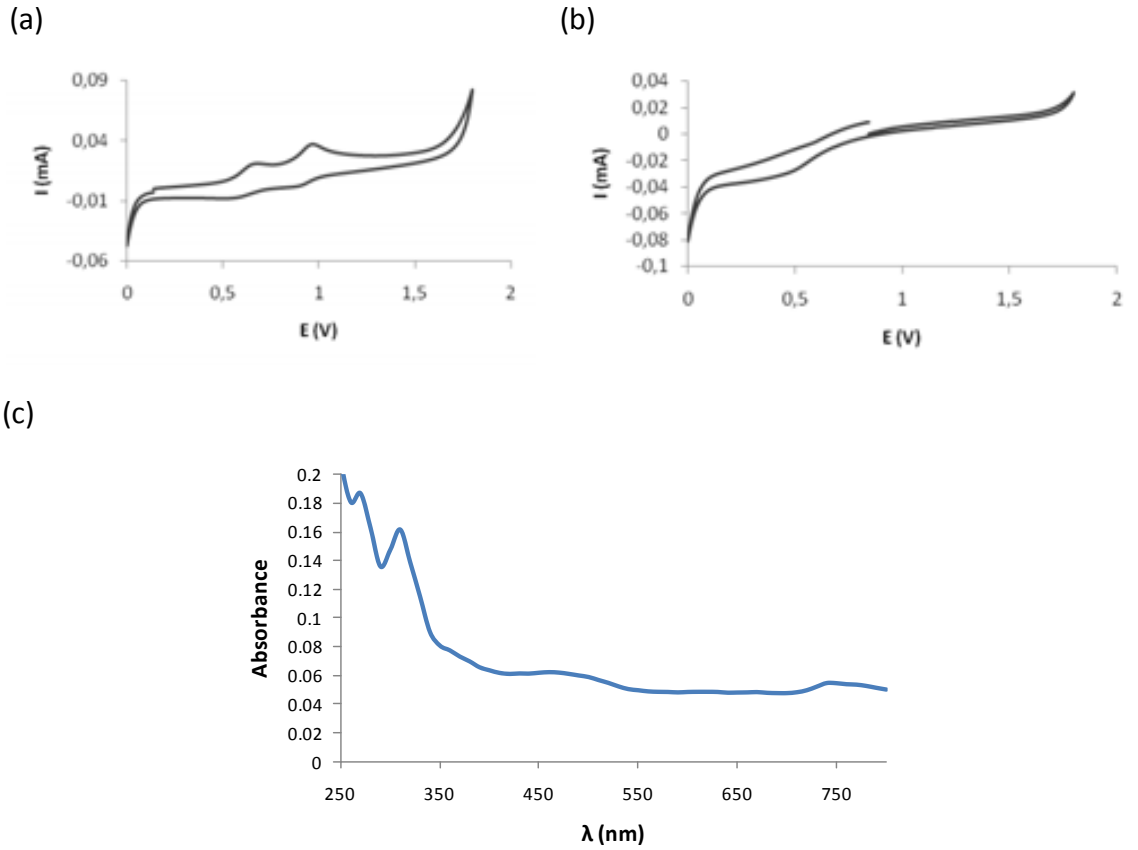

Figure 20. Cyclic voltamograms of FTO-TiO_2-**16**$^{2+}$ (a) before and (b) after the bulk electrolysis, and (c) the UV-Vis spectra of the solution after the CPE.

On the other hand, the results using FTO-TiO_2-**22**$^{2+}$ as electrode show that when a 1.6 V potential is applied during 6 h no oxygen is generated. However, in this case the leaching process was negligible as can be observed by comparing the CV before and after the electrolysis (Figures 21a and 21b). The major part of the current could be associated to the blank activity.

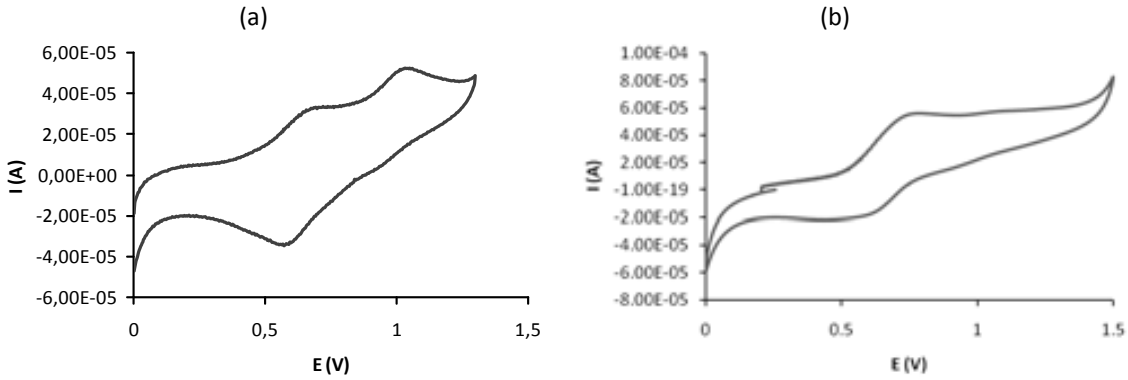

Figure 21. Cyclic voltammograms of FTO-TiO_2-**22**$^{2+}$ (a) before and (b) after CPE.

In order to understand the origin of the up shift in the electrocatalytic wave after anchoring compounds $\mathbf{6}^{3+}$ and $\mathbf{13}^{3+}$, three points should be considered: a) the aqueous phase composition, including potentially coordinating anions b) the interaction between the catalysts and semiconductor surface and c) the nature of the cavity formed upon anchoring.

As has been previously reported for other water oxidation catalysts in homogeneous phase, the anions present in solution could participate in an anation process.[11] Likewise, the coordination of oxygen atoms from TiO_2 to the Ru centers would block the active sites, which would cause the up shift of the electrocatalytic wave.

Alternatively, a hypothetic hydrophobic nature of the resulting cavity would explain the properties observed in the FTO-TiO_2-$\mathbf{22}^{2+}$ case (Figure 22a). Hence, a hydrophobic nature of the cavity would not favour the entrance of H_3O^+, and this could be a plausible explanation of the observed redox properties.

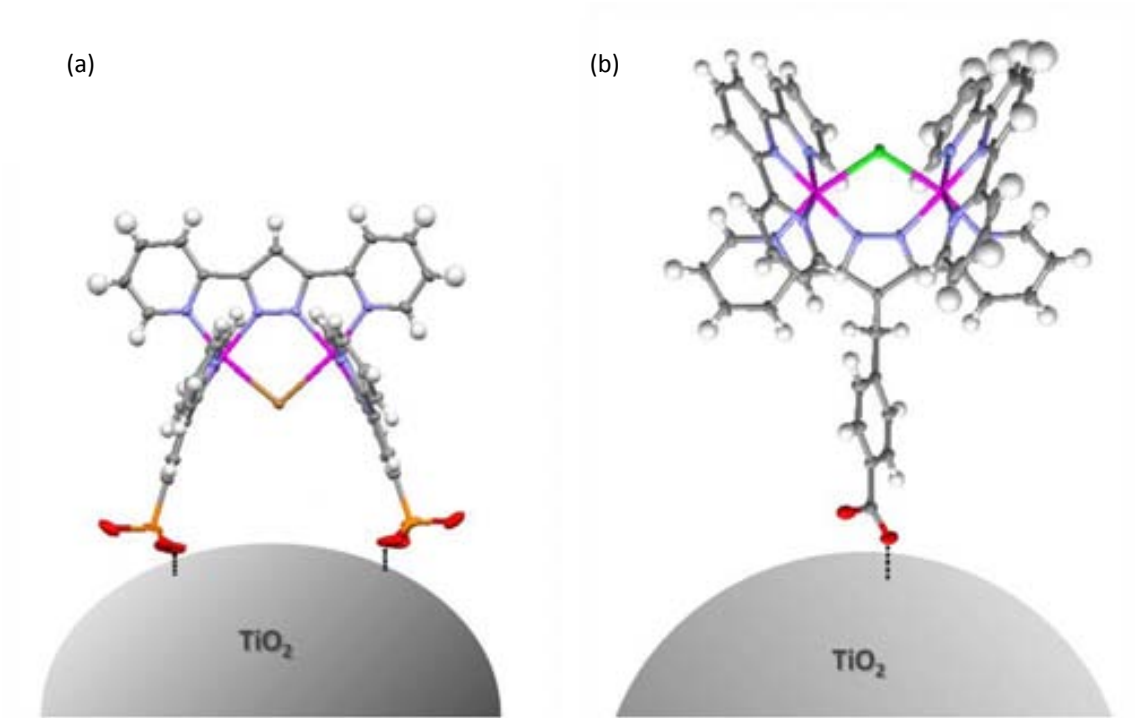

Figure 22. Schematic representation of the active site orientation in (a) FTO-TiO_2-$\mathbf{16}^{2+}$ and (b) FTO-TiO_2-$\mathbf{22}^{2+}$.

As can be observed in Figure 22b the active sites of the modified electrode FTO-TiO_2-**16**$^{2+}$ are oriented far from the TiO_2 surface. This disposition could prevent the formation of the above-mentioned hydrophobic cavity. This fact is in agreement with the nature of the electrocatalytic wave observed when the CV of this hybrid material is performed in ethanol, showing higher electrocatalytic current for FTO-TiO_2-**16**$^{2+}$ than for FTO-TiO_2-**22**$^{2+}$ (Figure 24). Nevertheless, the benzylic ligand moiety could confer enough flexibility to the anchored complex for allowing the interaction of the Ru active sites with the O atoms of the TiO_2. The latter, together with the observed oxidative catalyst degradation and subsequent leaching process commented above, could explain the lack of oxygen evolution during CPE also observed when employing this modified electrode. The interaction between the active sites and TiO_2, which is locking them, could be caused by the prolonged time needed for the new anchoring process, as well as, by the large amount of supported catalyst. Figure 23 shows the CV of FTO-TiO_2-**16**$^{2+}$, using the two different anchoring methods: the first one consists in soaking the FTO-TiO_2 films into acetonitrile complex solution during 24 h and the second one is performed by soaking the FTO-TiO_2 films into methanol complex solution during 48 h. As can be observed in the first case (Figure 23a) the CV is similar to its homogenous counterpart, instead of the second one (Figure 23b), which only presents two electrochemical waves.This could explain why the catalyst anchored onto TiO_2 rutile powder using the first method maintain its activity.

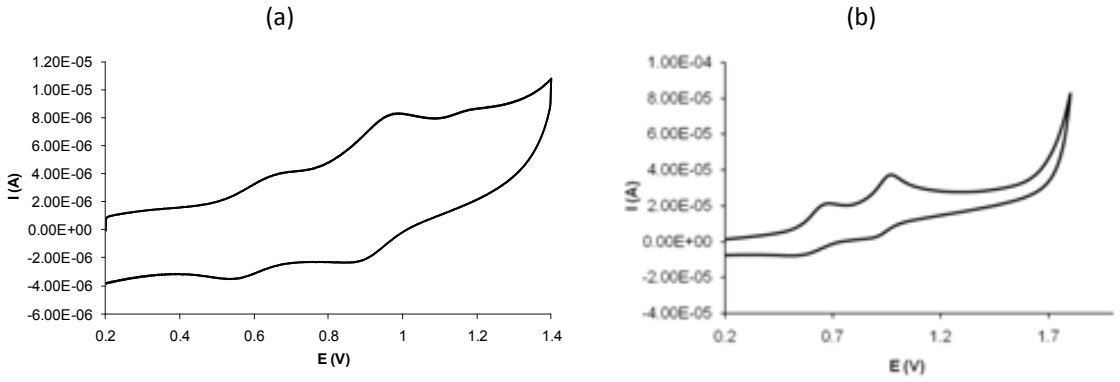

Figure 23. CV of FTO-TiO_2-**16**$^{2+}$ anchored using the process which consist in (a) soaking the FTO-TiO_2 films into acetonitrile complex solution during 24 h, and (b) soaking the FTO-TiO_2 films into methanol complex solution during 48 h.

III.1.7. Oxidation of Organic Substrates

As it has been stated previously, the water oxidation process is a very difficult process at kinetic and thermodynamic level that forces the use of powerful sacrificial oxidants and compromises the stability of the organic frameworks used in the architecture of the molecular catalysts. However, there are other catalytic processes related with the selective oxidation of organic subtracts which are also interesting and less demanding with respect to the stability of the ligand.[12] For this reason we have tested the ability of some of the most representative complexes described here to oxidize technologically relevant organic substrates.

In this context, complex **8**$^{2+}$ has been preliminary tested in *cis*-β-methyl styrene epoxidation catalysis in dichloroethane using $PhI(OAc)_2$ as oxidant and adding 5 μL of water. The results show that complex **8**$^{2+}$ is active performing 72 TN with and epoxid yield of 72 % (Figure 23 and Table 4), which indicates that could be an efficient catalyst for different organic oxidations.

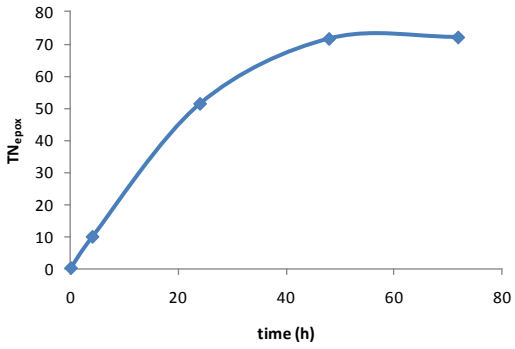

Figure 23. Catalytic profile of *cis*-β-methyl styrene epoxidation catalysis

Table 4.

Catalyst	**8**$^{2+}$
Solvent	CH_2ClCH_2Cl
Time(h)	72
Epoxid Yield	72%
Conversion	100%

Rel. CAT:SUBST:OX; 1:100:200 with additional 5.5 μL water. In a total volume of 2.5 mL

The anchored complexes FTO-TiO_2-**16**$^{2+}$ and FTO-TiO_2-**22**$^{2+}$ have been also tested towards an organic oxidation by performing the cyclic voltamogramm from 0 to 2 V in ethanol, which is acting as a substrate (Figure 24). Both complexes show an oxidative electrocatalytic wave which means that both can act as catalysts in organic oxidations. The FTO-TiO_2-**16**$^{2+}$ presents a more intense electrowave than FTO-TiO_2-**22**$^{2+}$, which is in agreement with the orientation of the active sites (Figure 22).

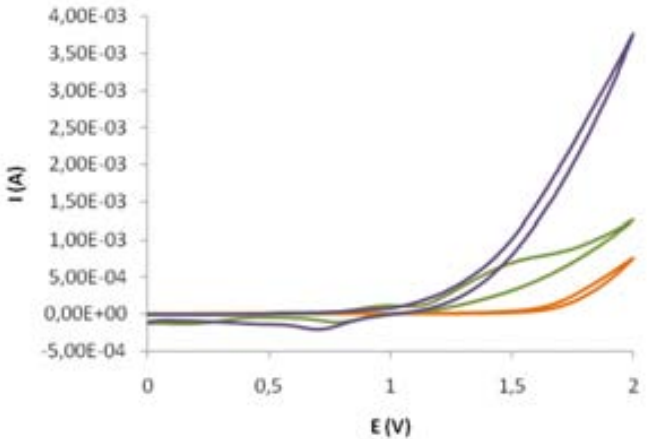

Figure 24. Cyclic voltammograms in EtOH scanning anodically at a scan rate of 20 mV/s: FTO-TiO_2 (orange) FTO-TiO_2-**22**$^{2+}$ (green); FTO-TiO_2-**16**$^{2+}$ (purple).

III.1.8. References

[1] Ridvan, L. *Tetrahedron* **1997**, *53*, 14793-14806.

[2] Sullivan, B.P.; Calvert, J.M.; Meyer, T. J. *Inorg.Chem.* **1980**, *19*, 1404.

[3] (a) Laurent, F.; Plantalech, E.; Donnadieu, B.; Jimenez, A.; Hernandez, F.; Martinez-Ripoll, M.; Biner, M.; Llobet, A. *Polyhedron.* **1999**, *18*, 3321 (b) Romero, I.; Rodriguez, M.; Llobet, A.; Collomb-Dunand-Sauthier, M.-N.; Deronzier, A.; Parella, T.; Soteckli-Evans, H. *J. Chem. Soc. Dalton Trans*. **2000**, 1689. (c) Sens, C.; Rodriguez, M.; Romero, I.; Llobet, A.; Parella, T.; Benet-Buchholz, J. *Inorg. Chem.* **2003**, *42*, 8385. (d) Sala, X.; Romero, I.; Rodriguez, M.; Llobet, A.; Gonzalez, G.; Martinez, M.; Benet-Buchholz, J. *Inorg. Chem.* **2004**, *43*, 5403. (e) Sala, X.; Plantalech, E.; Poater, A.; Rodriguez, M.; Romero, I.; Sola, M.; Llobet, A.; Jansat, S.; Gómez, M.; Stoeckli-Evans, H.; Benet-Buchholz, J. *Chem. Eur. J*. **2006**, *12*, 2798.

[4] Sens, C.; Romero, I.; Rodríguez, M.; Llobet, A.; Parella, T.; Benet-Buchholz, J. *J. Am. Chem. Soc.* **2004**, *126*, 7798-7799.

[5] (a) Planas, N.; Christian, G. J.; Mas-Marzà, E.; Sala, X.; Fontrodona, X.; Maseras, F.; Llobet, A. *Chem. Eur. J.* **2010**, *16*, 7965-7968. (b) Bozoglian, F.; Romain, S.; Ertem, M. Z.; Todorova, T. K.; Sens, C.; Mola, J.; Rodríguez, M.; Romero, I.; Benet-Buchholz, J.; Fontrodona, X.; Cramer, C. J.; Gagliardi, L.; Llobet, A. *J. Am. Chem. Soc.* **2009**, *131*, 15176-15187.

[6] P.H.M. Butzelaar, g NMR-version 4.0, IvorySoft, Cherwell Scientific Oxford, UK, **1997**.

[7] (a) Houarner-Rassin, C.; Chaignon, F.; She, C.; Stockwell, D.; Blart, E.; Buvat, P.; Lian, T.; Odobel, F. *J. Photochem. Photobiol. A: Chem.* **2007**, *192*, 56-65. (b) Gallagher, L. A.; Serron, S. A.; Wen, X.; Hornstein, B. J.; Dattelbaum, D. M.; Schoonover, J. R.; Meyer, T. J. *Inorg. Chem.* **2005**, *44*, 2089-2097.

[8] (a) Hu, Y.-Z.; Xiang, Q.; Thummel, R. P. *Inorg. Chem*. **2002**, *41*, 3423. (b) Brown, D.; Muranjan, S.; Jang, Y.; Thummel, R. *Org. Lett*. **2002**, *4*, 1253. (c) Wu, F.; Thummel, R. P. *Inorg. Chim. Acta* **2002**, *327*, 26. (d) Juris, A.; Prodi, L.; Harriman, A.; Ziessel, R.; Hissler, M.; El-Ghayoury, A.; Wu, F.; Riesgo, E. C.; Thummel, R. P. *Inorg. Chem*. **2000**, *39*, 3590. (e) Wu, F.; Riesgo, E. C.; Thummel, R. P.; Juris, A.; Hissler, M.; El-Ghayoury, A.; Ziessel, R. *Tet. Lett*. **1999**, *40*, 7311.

[9] (a) Rodríguez, M.; Romero, I.; Llobet, A.; Deronzier, A.; Biner, M.; Parella, T.; Stoeckli-Evans, H. *Inorg. Chem*. **2001**, 40, 4150. (b) Barkawi, K.; Llobet, A.; Meyer, T. J. *J. Am. Chem. Soc*. **1988**, 110, 7751. (c) *Llobet, A. Inorg. Chim. Acta.* **1994**, *221*, 125-131.

[10] Zhou, J.; Xi, W.; Hurst, J. K. *Inorg. Chem.* **1990**, *29*, 160.

[11] (a) Concepcion, J. J.; Jurss, J. W.; Templeton, J. L.; Meyer, T. J. *Proc. Natl. Acad. Sci.* **2008**, *105*, 17632-17635. (b) Liu, F.; Concepcion, J. J.; Jurss, J. W.; Cardolaccia, T.; Templeton, J. L.; Meyer, T. J. *Inorg. Chem.* **2008**, *47*, 1727-1752. (c) Ottenwaelder, X.; Rudd, D. J.; Corbett, M. C.; Hodgson, K. O.; Hedman, B.; Stack, T. D. P. *J. Am. Chem. Soc.* **2006**, *128*, 9268-9269.

[12] (a) Gagliardi, C. J.; Jurss, J. W.; Thorp, H. H.; Meyer, T. J. *Inorg. Chem.* **2011**, *50*, 2076-2078. (b) Drew, K.; Girishkumar, G.; Vinodgopal, K.; Kamat, P. V. *J. Phys. Chem. B.* **2005**, *109*, 11851-11857. (c) Gallagher, L. A.; Serron, S. A.; Wen, X.; Hornstein, B. J.; Dattelbaum, D. M.; Schoonover, J. R.; Meyer, T. J. *Inorg. Chem.* **2005**, *44*, 2089-2097. (d) Gallagher, L. A.; Meyer, T. J. *J. Am. Chem. Soc.* **2001**, *123*, 5308-5312.

III.2. Synthesis, Characterization and Linkage Isomerism in Mono- and Dinuclear Ruthenium Complexes Containing the New Pyrazole Based ligand Hpbl

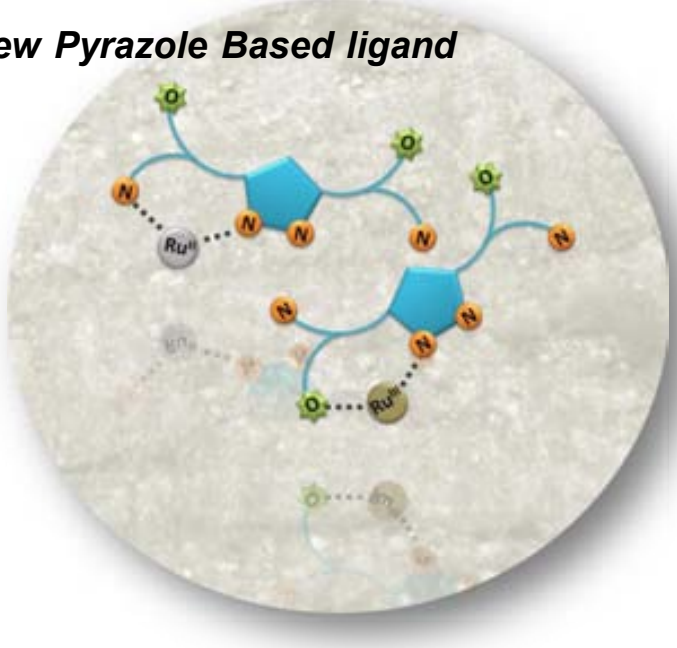

III.2.1. Abstract

The results summarized in this chapter are included in the unpublished work:

- "Synthesis, Characterization and Linkage Isomerism in Mono- and Dinuclear Ruthenium Complexes Containing the New Pyrazole Based ligand Hpbl" Laia Francàs, Daniel Moyano, Jordi Benet-Buchholz, Xavier Fontrodona, Lluís Escriche, Antoni Llobet and Xavier Sala. IN PREPARATION

In this chapter the synthesis and complexing abilities towards Ru of a new hemilabile bridging ligand Hpbl (Chart 1) are described. The aim of the work is to develop a new family of ruthenium complexes capable to perform linkage isomerism in order to stabilize (when necessary) the Ru high oxidation states. These systems should also avoid some of the deactivation pathways observed during the catalytic processes. The stabilization will be done via the linkage isomerism that allows the coordination of the oxygen to the metal center.

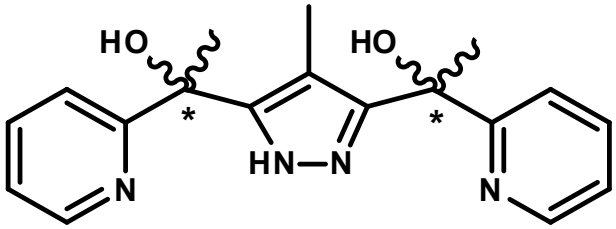

Chart 1

This N/O linkage isomerism is based on the fact that Ru(II) has more nitrogen than oxygen affinity, which allows the nitrogen coordination in the initial Ru(II) complex. However, when the metal centre is oxidized to Ru(III) the affinity changes and the oxygen coordination becomes more favoured than the nitrogen one.

III.2.2. Ligand synthesis

The synthetic strategy to prepare the new Hpbl ligand is depicted in Scheme 1.

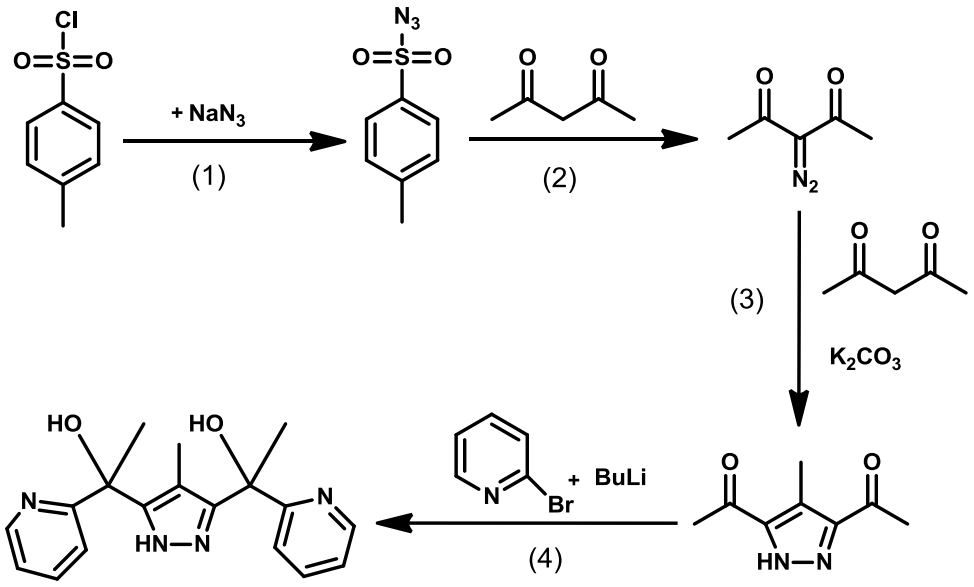

Scheme 1. Synthetic strategy to obtain the Hpbl ligand.

Steps (1) and (3) are carried out following the procedure described in the literature.[1] In step (2) the described synthesis[2] has been simplified by avoiding the final unneeded distillation. The last step (4), which allows the isolation of the final ligand, involves a double nucleophilic attack of a pyridine lithiate derivative to the two carbonyl groups of the diketopyrazole intermediate. That gives rise to a molecule with six donor atoms from two pyridines, two alcohols and one pirazole ring and containing two quiral centres (Scheme 2).

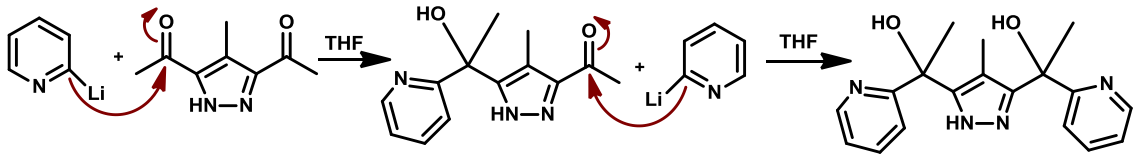

Scheme 2.

The reaction crude was purified by column chromatography over neutral silica and eluted with ethyl acetate. The last eluted fraction corresponds to the desired product, which was obtained as a mixture of two diasteromers in a 3:1 ratio (see

Figure 1 and the ^{1}H NMR spectrum in Figure 3), which cannot be separated. The new ligand was characterized by the usual spectroscopic and analytical techniques.

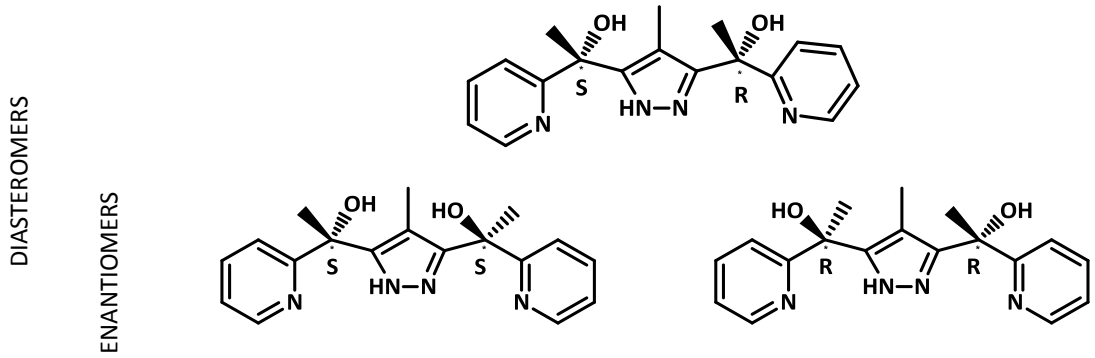

Figure 1. Drawing of the different isomers of Hpbl.

III.2.3. Synthesis of Ru Hpbl Complexes

Complexes **[1](PF$_6$)**, **2a^{2+}**, **[3a](PF$_6$)**, **[3b](PF$_6$)$_2$** and **[3c](PF$_6$)$_2$** were prepared following the synthetic routes represented in Scheme 3, using [RuCl$_3$(trpy)] as metal precursor. They were characterized by elemental analysis, electrochemical and spectroscopic techniques (UV-vis, MS, NMR).

The synthesis of the mononuclear chloro complex **[1](PF$_6$)** is performed by the direct reaction of equimolar amounts of Hpbl and [RuCl$_3$(trpy)] in the presence of NEt$_3$ as reducing agent, at 40 ^{0}C and stirring overnight. The complex is purified by column chromatography on alumina, eluting with CH$_2$Cl$_2$:MeOH (140:1) and MeOH. The last MeOH eluted fraction corresponds to complex **[1](PF$_6$)**. When this complex is treated under acidic conditions, the chloro ligand is replaced by an aqua ligand leading complex **2a^{2+},** as shown in Scheme 3. The preparation of this aqua complex (**2a^{2+}**) was also attempted in the presence of Ag(I) ions in order to remove the chloride ions from the media, allowing to isolate complex **[2a](PF$_6$)$_2$** as a solid salt. However, this synthetic route gave non-reproducible results, probably because of the coordination capacity of the silver metal to the free N atoms of Hpbl ligand. After complexation the ratio of the two diasteromers was maintained, but they could be separated by a preparative alumina TLC.

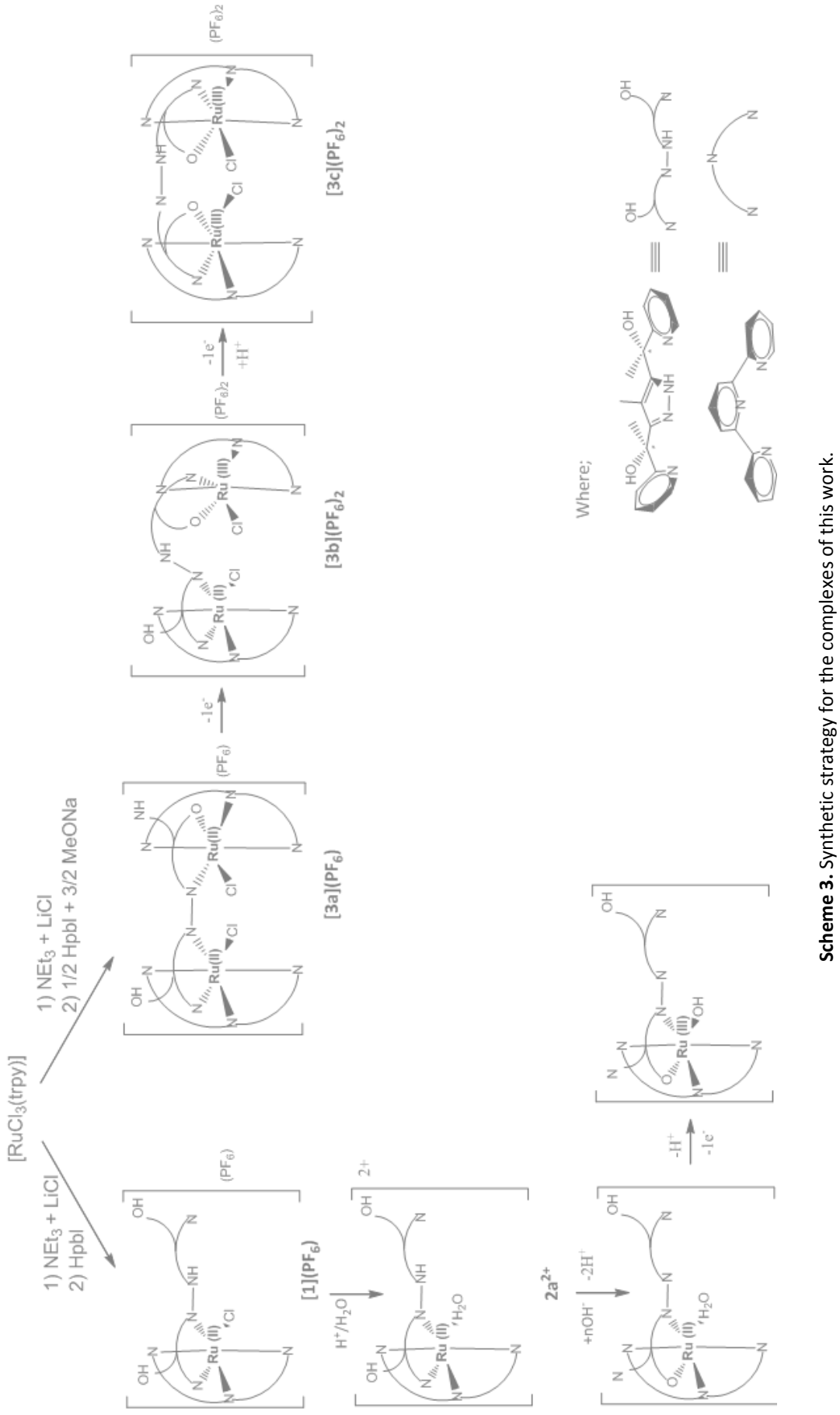

Scheme 3. Synthetic strategy for the complexes of this work.

The dinuclear complex **[3a](PF$_6$)** has been synthesized under nitrogen atmosphere using a 3:2:1 (MeONa:[RuCl$_3$(trpy)]:Hpbl) molar ratio. This reaction can be performed using two techniques: (1) Microwave reaction by carrying out five heating cycles using the conditions summarized in Table 1. (2) Refluxing the mixture during 24 h. The working-up procedure is the same for both methodologies and consists in dissolving the precipitate in hot CH_2Cl_2, cool it down and isolate the desired complex as the non-dissolved solid.

Table 1. Microwave condition reaction.

Temperature	80 ^{0}C
Equilibration time	5 min
Reaction time	10 min
Power	300 W
Stirring	Yes
Cooling	On

Complexes **3b**$^{2+}$ and **3c**$^{2+}$ can be obtained by oxidation involving the loss of one or two electrons, respectively.

III.2.4. Characterization

III.2.4.1. X-ray structures

The X-ray diffraction analysis was carried out for complexes **2b, [3b](PF$_6$)$_2$** and **[3c](PF$_6$)$_2$**. In the case of **2b** the low crystal quality only allows determining the connectivity of the metal centre. However, this information is too relevant to be excluded. Figure 2 shows a view of the molecular structure of complex **2b** and complex cations **3b**$^{2+}$ and **3c**$^{2+}$ were the counter anions and solvent molecules are omitted for clarity.

The crystal structure of the mononuclear complex **2b** has been obtained by slow evaporation from a mixture of acetone and a basic water solution with NaOH. As previously stated, the low quality of the crystals (R ≈ 20-30 %) prevents a deeper analysis of the structure. The presence and number of counter anions and solvent

molecules is not clear and the oxidation state of the Ru metal center cannot be assigned. This ambiguity can not be clarified by observing the Ru-N and Ru-O bond distances, which are usually similar at the Ru(II) and Ru(III) oxidation states. However, the electron densities in the metal and the coordinating atoms is enough to ensure that the ruthenium metal centre adopts a pseudo-octahedral coordination geometry with three positions occupied by the meridional trpy ligand, two by half of the tetradentate Hpbl ligand and the final one by and oxygen atom which, owing to the basic pH of the media, can be considered as belonging to an hydroxo group (if Ru(III) is the oxidation state) or H_2O (if it is a Ru(II) compound). The coordination to the Hpbl ligand occurs through the pyrazolic nitrogen and the oxygen atom of the alkoxo group. This crystal structure allows observing another possible coordination scenario for the Hpbl ligand in which the pyridine moiety is replaced by the alkoxo in the coordination to the metal centre, giving rise to a non-coordinated pyridine.

In the dinuclear complexes both ruthenium metal centres adopt a pseudo-octahedral coordination geometry with three positions occupied by the meridional trpy ligand, two by the tetradentate Hpbl ligand and the sixth position occupied by a chloro ligand.

For the complex cation $\mathbf{3b}^{2+}$ the two metal centres present different oxidation states (Ru(II) and Ru(III)) due to the partial oxidation occurring during the crystallization process. The Ru(III) metal centre is coordinated to the Hpbl bridging ligand through an alkoxo group and the pyridine nitrogen atom, forming a five membered chelate ring. On the other hand, the Ru(II) metal centre is coordinated to the Hpbl ligand *via* two nitrogen atoms, one from the pyridine moiety and another from the pyrazol scaffold, that allowing the formation of a six membered chelate ring. It is important to notice that the pyrazol ring has one non-coordinated nitrogen due to the Ru(III)-O coordination. An interesting fact is that the free alcohol moiety is making a hydrogen bond with an acetone molecule. The asymmetric unit contains one molecule of the complex, two PF_6^- anions, two acetone molecules and half molecule of water. One of the acetone molecules is disordered in two positions with a ratio of 53:47. The water molecule is also disordered (50:50) and is shared with a neighboring unit cell.

From the crystallographic analysis it can be concluded that an oxidation process involving two electrons could take place during the crystallization of **3a**$^{+}$, which give rise to the formation of complex **3c**$^{2+}$ with both metal centers in Ru(III) oxidation state. The complexation behaviour of the Hpbl ligand to the two Ru(III) centres in the complex cation **3c**$^{2+}$ is similar to that described for the Ru(III) metal center in the complex **3b**$^{2+}$. Therefore, in the X-ray structure a free pyrazol ring can be observed. The asymmetric unit contains one molecule of the cationic complex, two PF_6^- anions and two and a half molecules of water. The water molecules are partially disordered with and occupancy of 1:1:0.5.

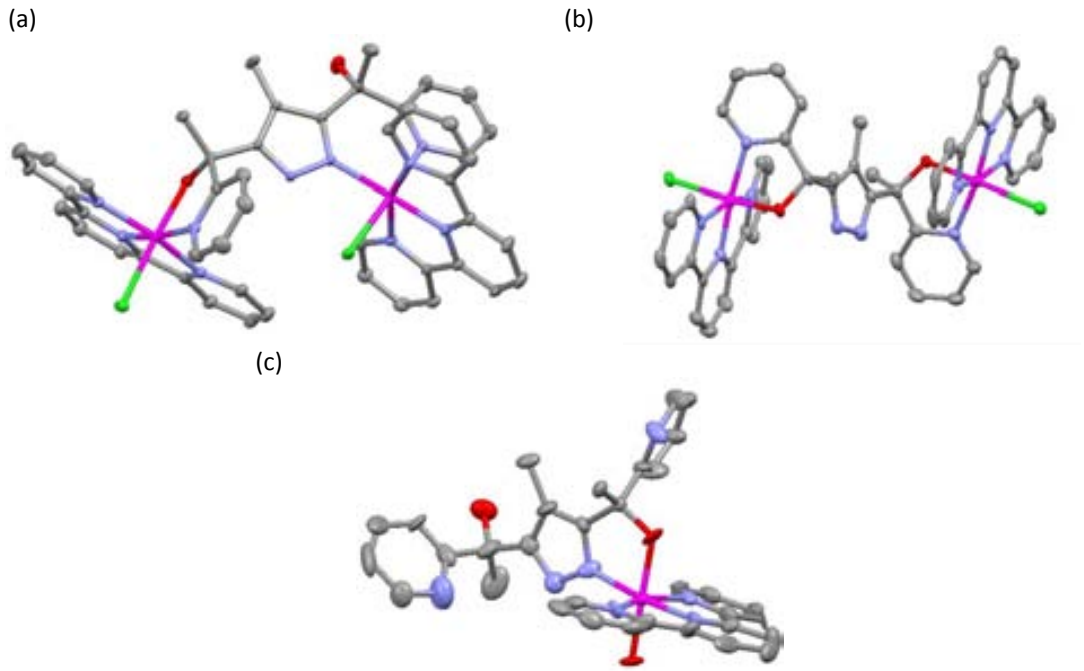

Figure 2. Mercury™ ellipsoid plot (50% probability) for the cationic part of complexes (a) **3b**$^{2+}$, (b) **3c**$^{2+}$ and (c) **2b**. Color codes: Ru, pink; Cl, green; N, blue; O, red; Hydrogen atoms are not shown.

The comparison of the X-ray structures of the two dinuclear complexes allows noticing the different orientation of the chloro ligands. While in complex **3b**$^{2+}$ they are the same direction, in complex **3c**$^{2+}$ they point to opposite directions. These different orientations could be relevant for their properties and catalytic behaviour.

III.2.4.2. NMR spectroscopy

Both 1D and 2D NMR spectroscopy allows to structurally characterizing all the complexes and the Hpbl ligand in solution. In all the NMR spectra a mixture of two

diastereomers can be observed in a ratio 3:1 (A:B) (Figure 3), which increases the number of signals and complicates the analysis of the spectra.

For the free ligand, all the resonances observed in the ^{1}H NMR spectrum can be unambiguously assigned based on their integrals, symmetry and multiplicity. In solution it presents a symmetry axis bisecting the pyrazol ring. For that reason in the NMR spectra we only observe resonances from one pyridine ring, one alcohol group and two methyl groups coming from the chiral centres and the central pyrazol ring. Furthermore, variable temperature (VT) ^{1}H NMR spectra were recorded in order to distinguish the resonances of both diastereomers, taking advantage of their different temperature dependence (Figure 3). This effect allows us to distinguish when the multiplicity of a signal is caused by couplings to other protons or by two different diasteromers. The most relevant change could be observed in the 7.35 ppm signal. This resonance could be associated to a triplet at RT but it splits to two doublets (one from each diastereomer) when the temperature is increased.

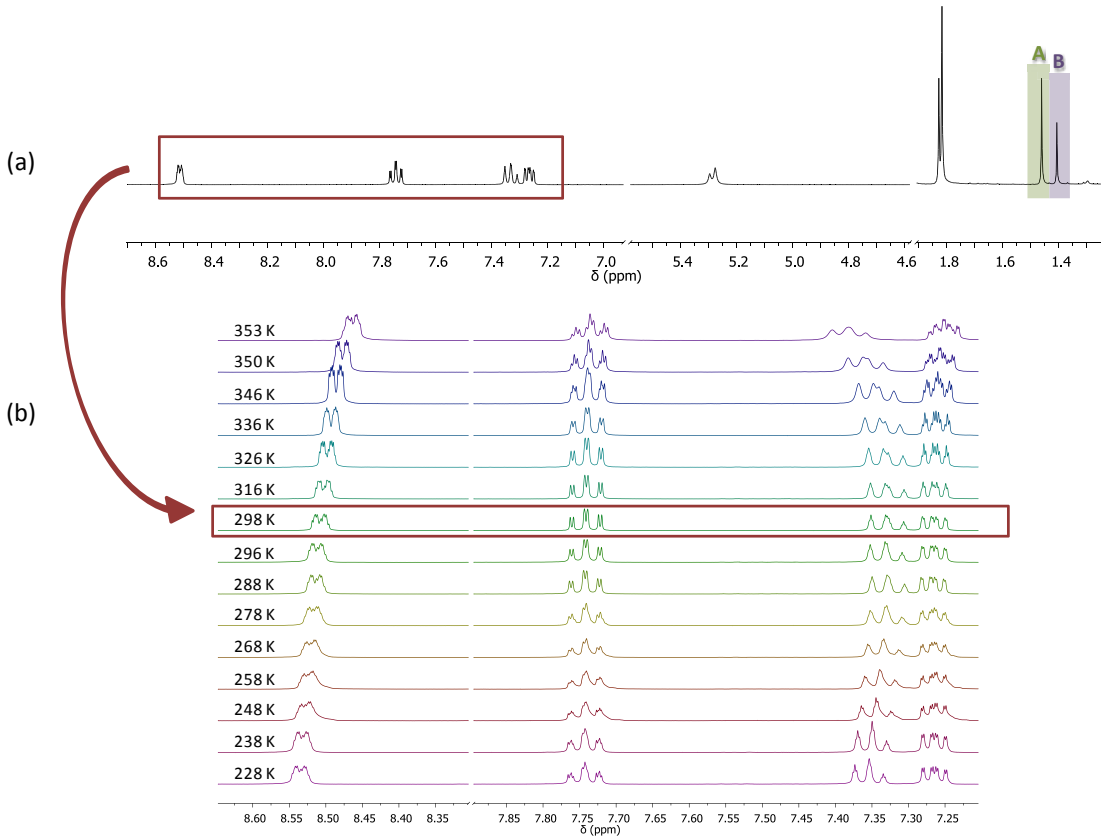

Figure 3. VT- ^{1}H NMR spectra for the ligand Hpbl: (a) The whole spectra highlighting the methyl groups of each diasteromer and (b) the aromatic part at different temperatures (400 MHz, acetonitrile-d_3).

The mononuclear character of complexes $\mathbf{1}^{+}$ and $\mathbf{2a}^{2+}$ induces a total non-symmetry to the molecule, giving a single signal for each proton, carbon or nitrogen in their respective spectra. In addition, all the signals are doubled due to the presence of two possible diasteromers. As previously stated, the relative amount of each diastereomer in the final complex $\mathbf{1}^{+}$ depends on the purification procedure followed during each single preparation. After some separation trials an enriched mixture in one diastereomer was obtained, which allowed us to distinguish the NMR resonances corresponding to each diastereomer. Nevertheless, the complete assignment is not possible for the external pyridylic groups of the trpy ligand, which remain indistinguishable (Figure 4). For the chloro complex $\mathbf{1}^{+}$ it is important to point out that both alcohol protons can be observed. Furthermore, the low and similar ppm range at which their appear suggest that they are both not coordinated to the ruthenium metal centre. In addition, the proton from the pyrazol ring can be observed at 13 ppm. The absence of a signal at around 9 ppm is a reason to conclude that the chloro atom is occupying an in-disposition (the equatorial chloro ligand is oriented toward the centre of the Hpbl ligand), instead of the out-disposition (where the chloro ligand would be orientated away from the centre of the bridging ligand). In the later case a significant downfield shift of the Hpbl proton resonances situated close to the chloro atom would be expected due to its de-shielding effect.

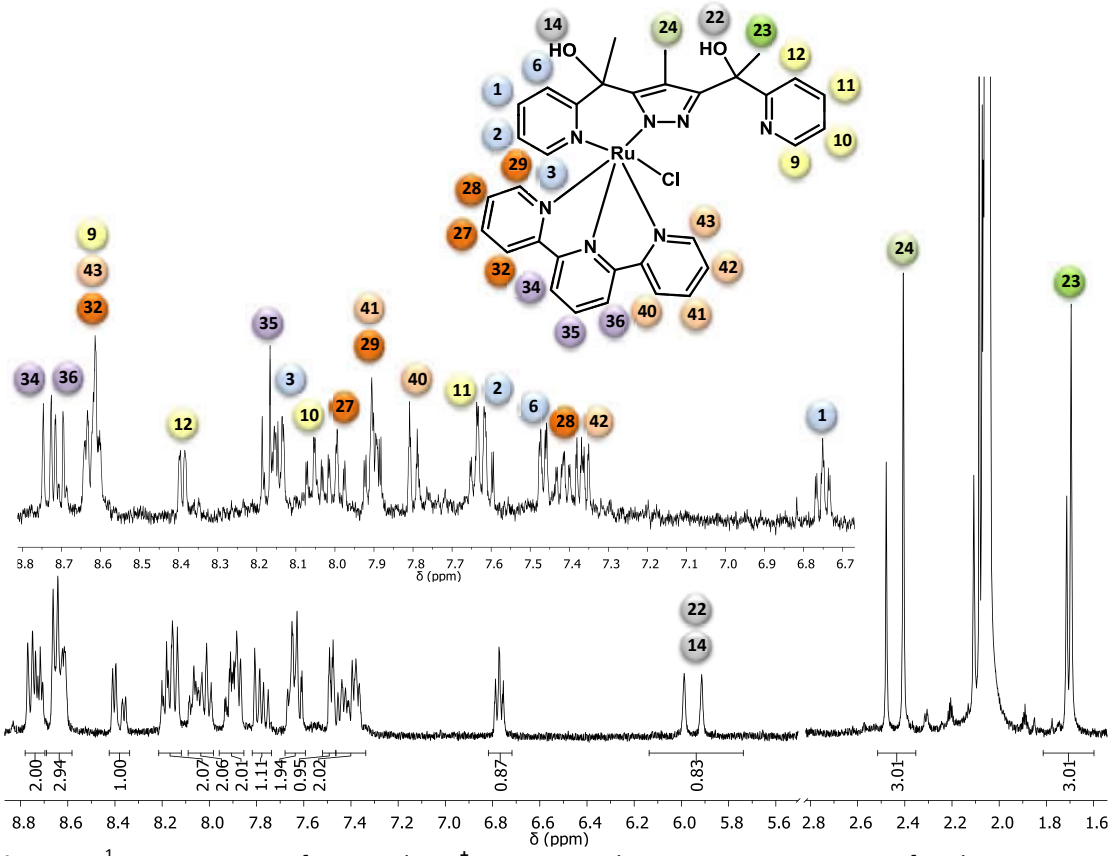

Figure 4. ^{1}H NMR spectra for complex **1**$^{+}$ in acetone-d_6. Inset: aromatic zone of a diastereomeric enriched mixture. Pink and orange highlighted trpy protons are indistinguishable.

The NMR study for the aqua complex **2a**$^{2+}$ has been carried out in an acetone-d_6 solution with a drop of D_2O with triflic acid. If we compare the ^{1}H NMR spectra of the chloro and the aquo complexes, the most shifted signals are the ones belonging to the non-coordinated pyridine due to its protonation in the acidic media used for record the NMR spectrum of the complex **2a**$^{2+}$.

As it has been commented in the introduction, the Ru aqua-complexes are affected by the raising pH in water solution and together with the polyprotic nature of the Hpbl ligand, makes necessary to gain further insight in these processes. Both 1D and 2D NMR spectra have been performed in acidic and basic media employing a mixture of acetone-d_6, D_2O and triflic acid or acetone-d_6, D_2O and NaOD, respectively. As ^{1}H NMR indicates, at basic pH, the number of involved species is higher than in acidic pH (Figure 5).

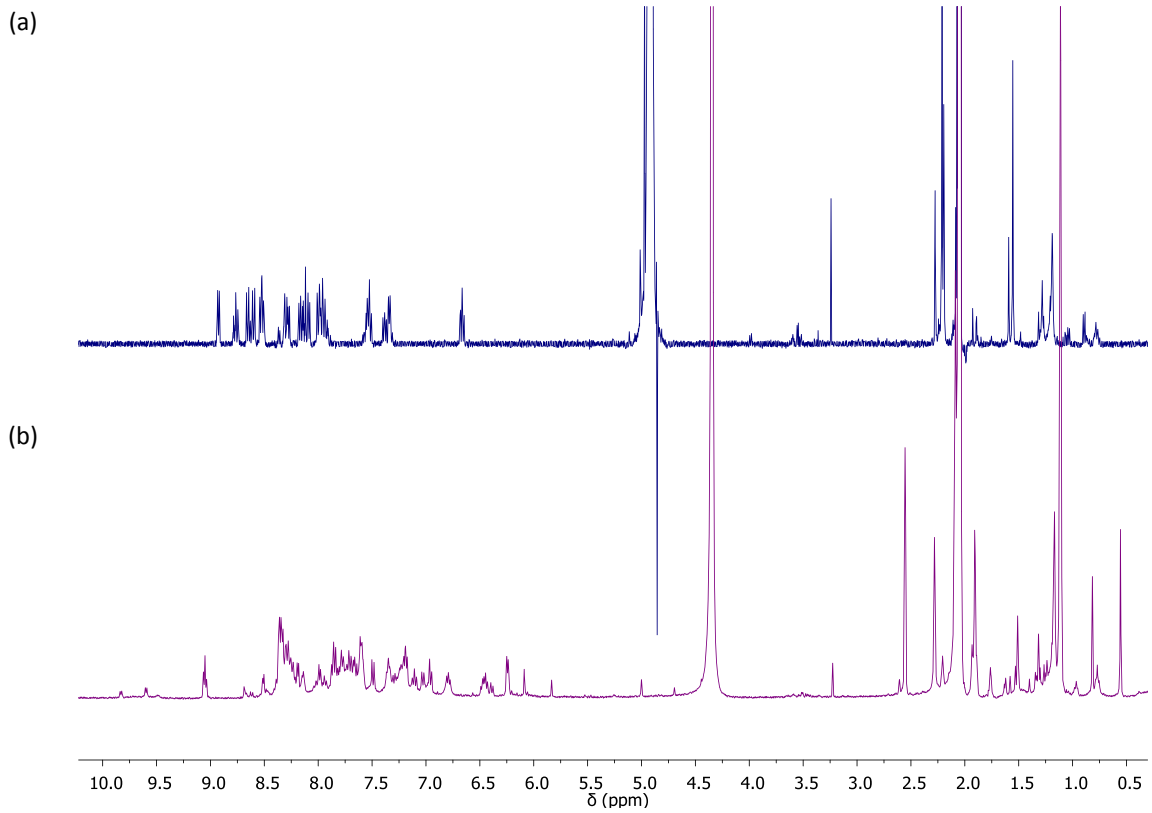

Figure 5. ^{1}H NMR for complex **2a**$^{2+}$ (a) in acidic medium employing D_2O, acetone-d_6 and CF_3SO_3D as solvent mixture and (b) in basic medium using D_2O, acetone-d_6 and NaOD.

DOSY NMR experiments have been performed in order to elucidate the size of the species involved at basic pH. They have allowed us to confirm the similar size of these species according to their almost identical diffusion rate. The addition of the well known $[Ru(H_2O)(bpea)(trpy)]^{2+}$ complex as internal standard confirms the mononuclear nature of the overall set of complexes, all of them showing similar diffusion rates (Figure 6). Therefore, the presence of dinuclear species coming from the oxo bridging of two mononuclear complexes can be discarded.[3]

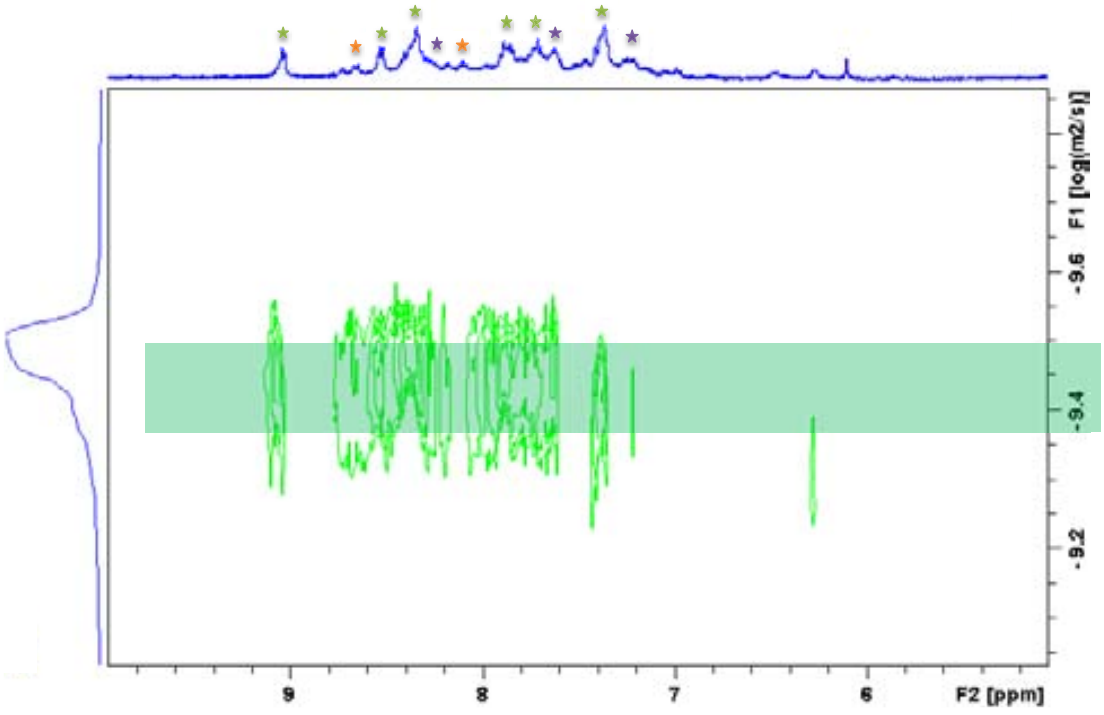

★ *complex* $\mathbf{2}^{2+}$ *and* $[RuH_2O(bpea)(trpy)]^{2+}$ *signal,* ★ $[RuH_2O(bpea)(trpy)]^{2+}$ *signal and* ★ *complex* $\mathbf{2}^{2+}$ *signal.*

Figure 6. DOSY NMR spectrum for complex $\mathbf{2a}^{2+}$ in D_2O, acetone-d_6 and NaOD using the mononuclear complex $[RuH_2O(bpea)(trpy)]^{2+}$ as internal reference.

The performance of HMBC-N NMR experiment helped us to study the nitrogen coordination to the metal centre.[4] The mononuclear nature of complex $\mathbf{1}^{+}$ is in agreement with the loose of symmetry observed in the HMBC-N spectrum when comparing with the highly symmetric spectrum of the free ligand (Figure 7).

(a) (b)

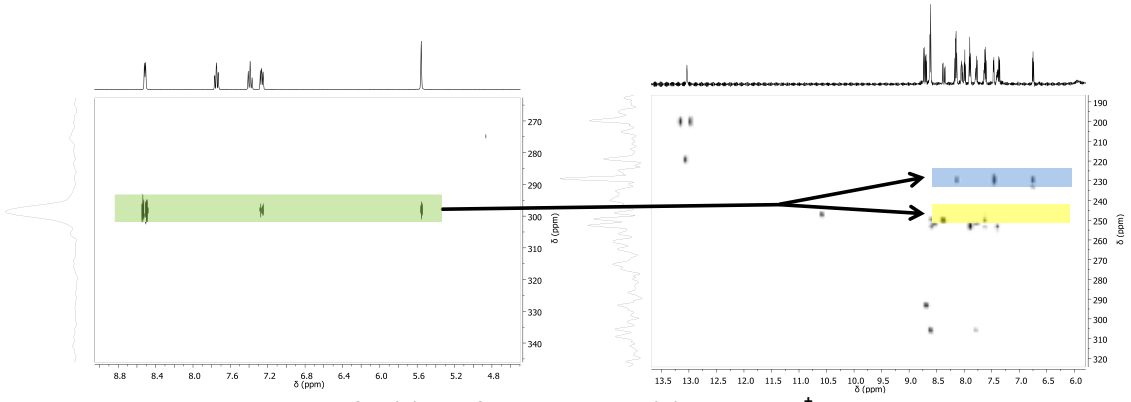

Figure 7. HMBC-N NMR spectra for (a) the free ligand and (b) complex $\mathbf{1}^{+}$ in acetone-d_6, the blue box indicates the coordinated nitrogen and the yellow box the non-coordinated one.

The ^{1}H NMR spectrum of complex **3a**$^{+}$ shows the entire signals as broad bands, which prevents their assignment and evidences the presence of dynamic processes. Variable temperature ^{1}H NMR experiences have been run in order to study this dynamic behaviour. However, despite the shape of the signals is temperature-dependent at the studied range, the ^{1}H NMR spectra has not been enough improved to be assigned. (Figure 8)

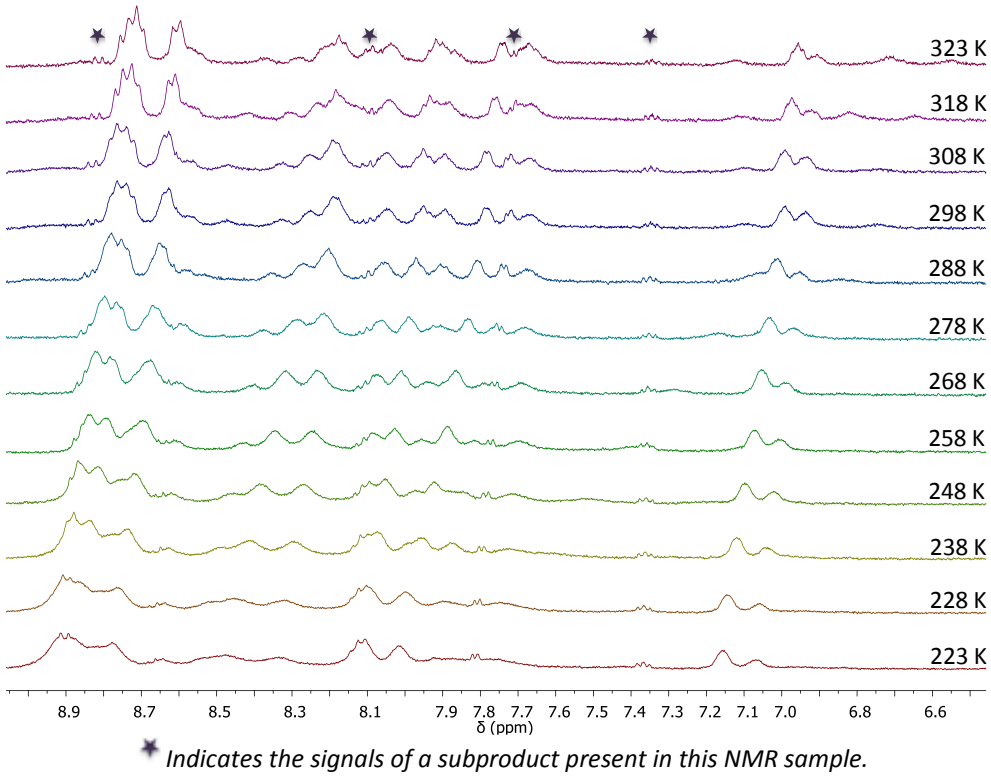

Figure 8. ^{1}H NMR spectra for the aromatic part of the Hpbl ligand at different temperatures (400 MHz, acetone-d_6).

III.2.4.3. UV-Vis spectroscopy

The UV-Vis spectral features in solution for complexes **1**$^{+}$ and **2a**$^{2+}$, which are listed in the experimental section of the manuscript (ANNEX II, paper E), agree with the published for similar complexes.[5] The spectra can be divided in three different regions: one between 200 and 350 nm, in which very intense bands are observed due to intraligand π-π* transitions;[6] another one between 350 and 560 nm, in which mainly broad unsymmetrical Ru(dπ)-trpy/Hpbl(π*) metal-to-ligand charge transfer (MLCT) bands are observed;[7] and finally the last region above 560 nm in which d-d transitions

appear. As shown in Figure 9, the band displacement for the broad unsymmetrical Ru(dπ)-trpy/Hpbl(π*) MLCT bands is different for each complex. The hypsochromic shift observed for complex **2a**$^{2+}$ confirms the coordination of the aqua ligand that relatively stabilize the dπ(Ru) levels and therefore gives rise to more energetic electronic transitions.

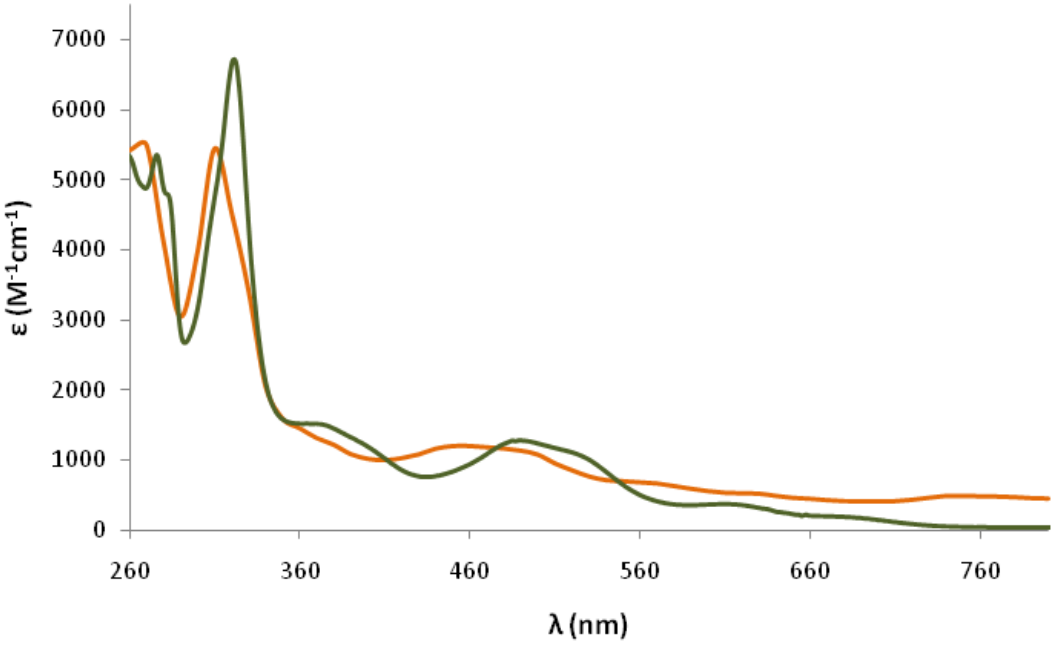

Figure 9. UV-Vis spectra for complex **1**$^{+}$ (green) and **2a**$^{2+}$ (orange).

A redox titration of complex **2a**$^{2+}$ with Ce(IV) has been carried out in order to spectroscopically characterize their different oxidation states. As shown in Figure 10 three isosbestics points indicating a neat interconvertion between only two single species are observed. As can be appreciated, in general, as the oxidation state increases the intensity of the absorptions decreases, except for the newly generated band at 400 nm. As general trend the absorption changes at the visible region correspond to a hypsochromic shift of the spectra.

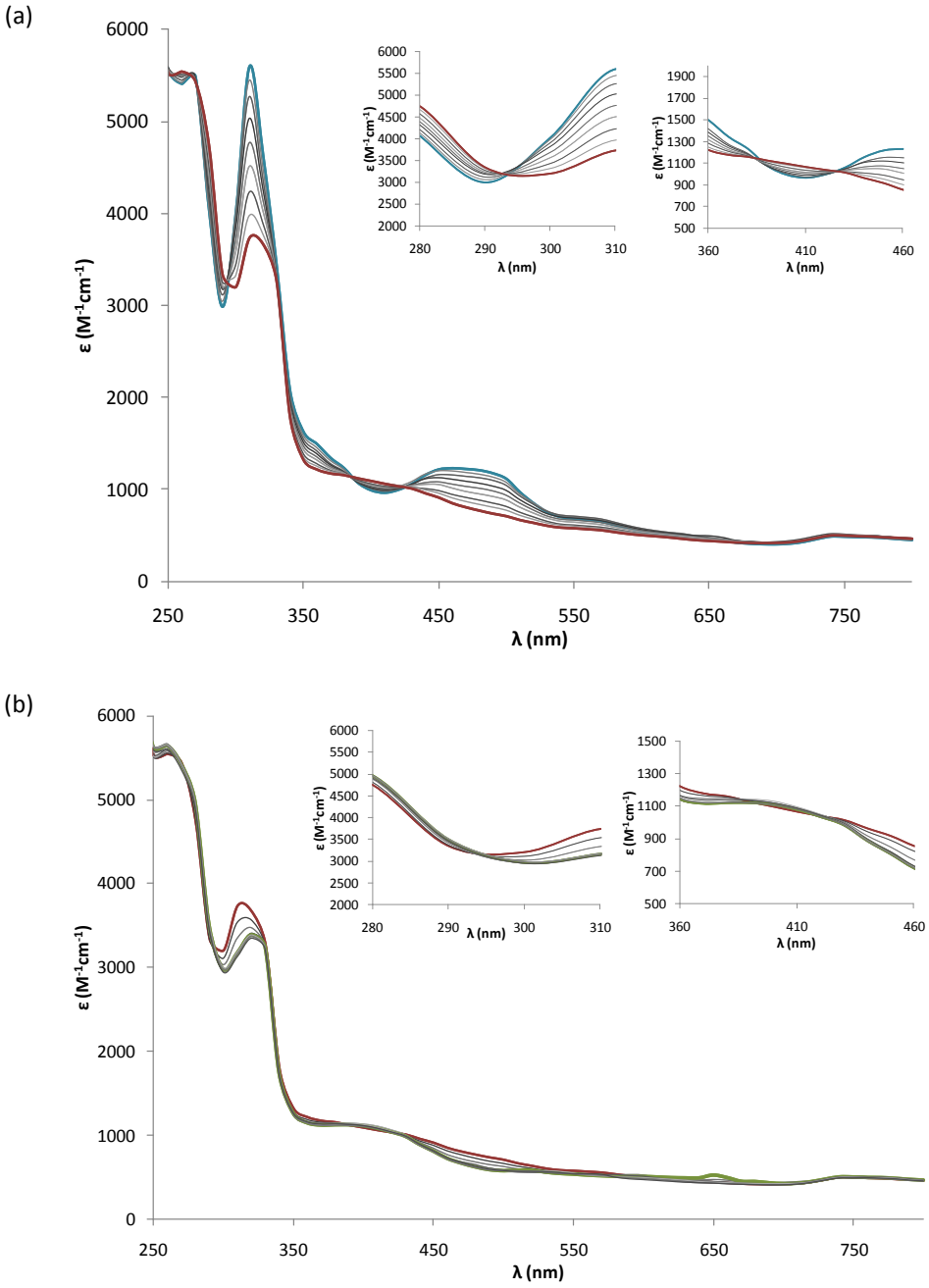

Figure 10. Titration of complex **2a**$^{2+}$ with Ce(IV) monitored by UV-Vis spectroscopy. UV-Vis spectra colour code: Ru(II) in blue, Ru(III) in red and Ru(IV) in green. This titration was performed by 10 µL sequential additions of a 0.6 mM $Ce(NH_4)_2(NO_3)_6$ solution into 0.5 mL of 0.1 mM complex **[1](PF$_6$)** solution. Both solutions are prepared in 0.1 M CF_3COOH aqueous solution. Inset: zoom of the isosbestics points zone. (a) From Ru(II) to Ru(III); (b) From Ru(III) to Ru (IV).

III.2.4.4. Electrochemical properties

The redox properties of complexes **1**$^{+}$, **2a**$^{2+}$ and **3a**$^{+}$ have been studied by cyclic voltammetry experiments (CV). Complex **1**$^{+}$ dissolved in 0.1 M n-Bu_4NPF_6 solution of dichloromethane displays one electrochemically quasi-reversible redox wave (Figure 11). The redox process takes place at 0.840 V and it is assigned to the formation of the corresponding Ru(III) complex,

$$[Ru^{II}Cl(Hpbl)(trpy)]^{+} - 1\ e^{-} \rightarrow [Ru^{III}Cl(Hpbl)(trpy)]^{2+} \quad (1)$$

As shown in Figure 11, no linkage isomerism has been observed within the CV time scale, even when running the experiments at low scan rates (50 mV/s, 20 ^{o}C).

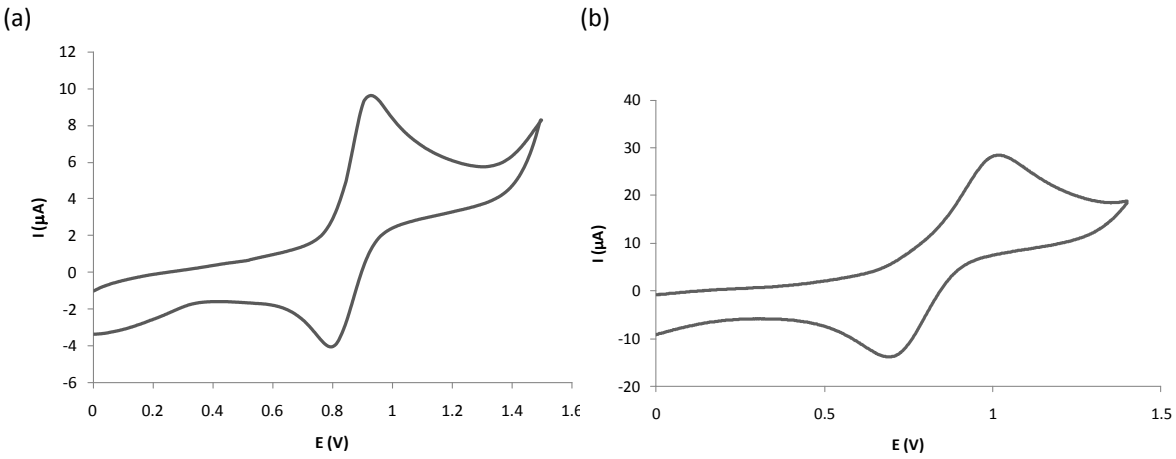

Figure 11. CV of complex **1**$^{+}$ in CH_2Cl_2 using 0.1 M of TBAH as electrolyte and at a scan rate of (a) 50 mV/s and (b) 1000 mV/s.

In sharp contrast, when complex **1**$^{+}$ is dissolved in a 0.1 M CF_3COOH (pH=1) aqueous solution, the aqua complex **2a**$^{2+}$ is generated, which shows a very different behaviour. As can be observed in Figure 12b, at high scan rate, the CV of **2a**$^{2+}$ presents two different processes. The first more intense one (A) appears at $E_{1/2}$= 0.725 V and is associated to the first Ru(III)/Ru(II) oxidation (2). The second and weaker one (B) appears at $E_{1/2}$= 0.932 V, corresponding to the Ru(IV)/Ru(III) oxidation step (3)

$$[Ru^{II}H_2O(Hpbl)(trpy)]^{2+} - 1\ e^{-} \rightarrow [Ru^{III}H_2O(Hpbl)(trpy)]^{3+} \quad (2)$$

$$[Ru^{III}H_2O(Hpbl)(trpy)]^{3+} - 1\ e^{-} \rightarrow [Ru^{IV}OH(Hpbl)(trpy)]^{3+} \quad (3)$$

Scanning up to 1.5 V (Figure 12c) we can observe a third irreversible wave (D) associated with the next oxidation step (4). This process is the responsible of oxygen evolution (Eq. (5) and (6)) and is typical for the aqua mononuclear ruthenium complexes.

$$[Ru^{IV}OH(Hpbl)(trpy)]^{3+} - 1\ e^{-} \rightarrow [Ru^{V}O(Hpbl)(trpy)]^{3+} \qquad (4)$$

$$[Ru^{V}O(Hpbl)(trpy)]^{3+} + H_2O \rightarrow [Ru^{III}OOH(Hpbl)(trpy)]^{3+} \qquad (5)$$

$$[Ru^{III}OOH(Hpbl)(trpy)]^{3+} \rightarrow [Ru^{II}H_2O(Hpbl)(trpy)]^{2+} + O_2 \qquad (6)$$

The observation of the second oxidation process (3) at lower potentials than in complex $\mathbf{1}^{+}$ can be attributed to the presence of aqua groups as ligands, which are capable to carry out PCET processes.[8] This means that protons and electrons can be removed simultaneously from the complex preventing the build-up of high Coulombic charges. The high potentials at which the second oxidation process takes place for complex $\mathbf{1}^{+}$ prevents its observation within the solvent window.

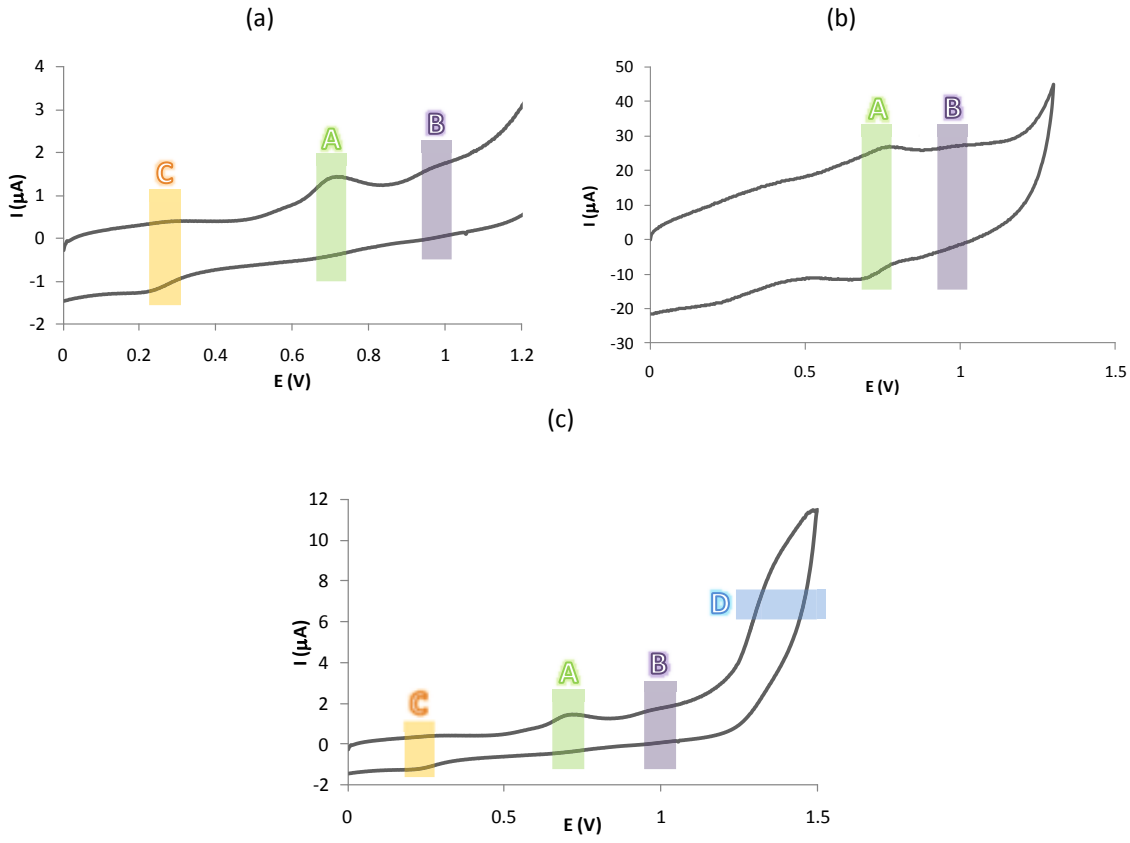

Figure 12. CV of complex $\mathbf{2a}^{2+}$ in 0.1 M a CF_3COOH aqueous solution at pH=1 using a scan rate of (a) 20 mV/s, (b) 1000 mV/s, (c) 20 mV/s and scanning from 0 to 1.5 V.

As expected for complex **2a**$^{2+}$, the oxidation state increase on the metal centre favours the change in the coordinating behaviour of the Hpbl ligand and that can be clearly observed through the electrochemical experiments. The existence of a linkage isomerism when cycling between the different oxidation states comes out from the comparison of the cyclic voltammograms at fast (Figure 12b) and slow (Figure 12a) scan rates. At fast scan rate and scanning anodically we observe two quasi-reversible electrochemical waves (A and B). However, at slow scan rates a quasi-irreversible anodic wave (A) and a quasi-irreversible cathodic wave (C) separated by about 0.5 V are observed. The latter confirms that the electrochemical process is associated to a chemical reaction. From now on, the nomenclature assigned to the different isomers will be as is indicated in Schemes 4 and 5, for mononuclear complexes, and in Scheme 6 for the dinuclear ones. The thermodynamic cycle of this process is represented in Scheme 4. When the oxidation state of the metal centre is II, Ru(II) is coordinated to five nitrogen atoms (**Ru-N$_5$**), three from the terpyridine ligand, and two from the Hpbl ligand. However, when the oxidation state III is reached, the coordination environment changes to a **Ru-ON$_4$**, where an oxygen atom form the neighbouring alkoxo group has replaced the one Hpbl nitrogen atom.

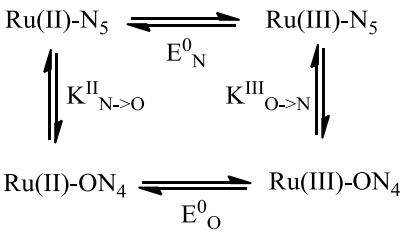

Scheme 4. Thermodynamic cycle corresponding to the linkage isomerisation process occurring by the electrochemical oxidation of complex **2a**$^{2+}$.

This phenomenon has been further corroborated scanning cathodically from 0.9 V. The dependence of the [ic1]/[ia1] and [ic2]/[ia2] ratios on the scan rate (Figure 13 and Figure 14) is consistent with the involvement of chemical reactions coupled to electrochemical processes as represented in Scheme 4.

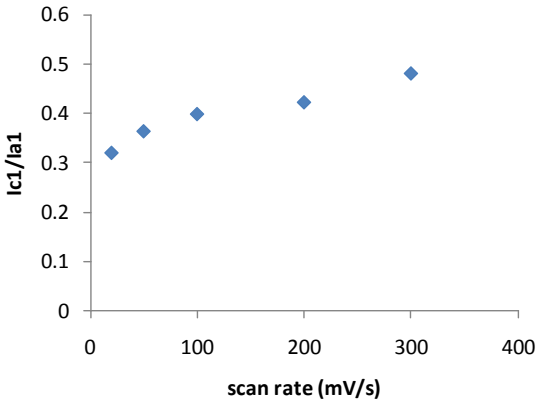

Figure 13. Dependence of ic1/ia1 on the scan rate, graphical representation.

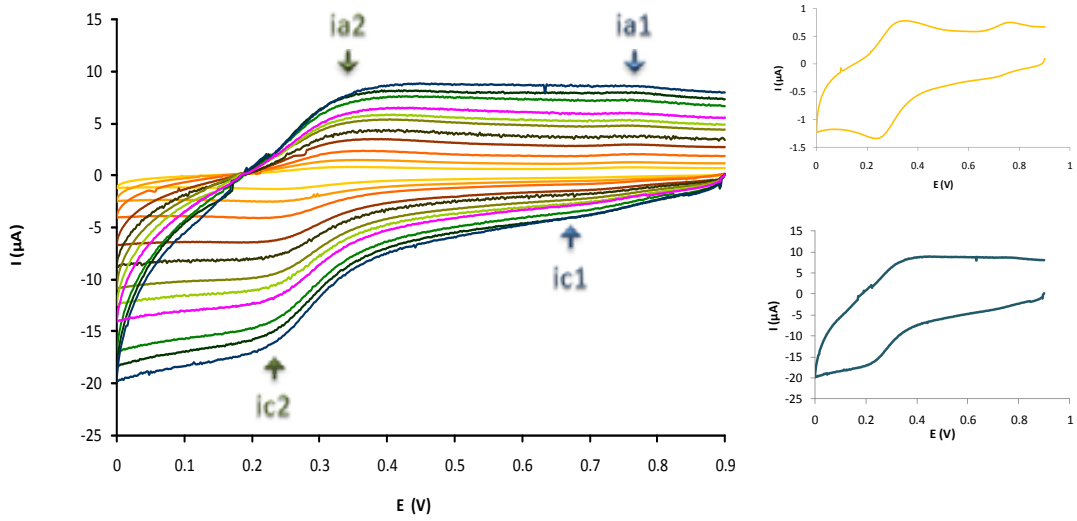

Figure 14. Cyclic voltammograms of complex **2a**$^{2+}$ in 0.1 M CF_3COOH aqueous solution at pH=1 scanning cathodically, starting at 0.9 V and applying an equilibration time of 3 min. Scan rates of 20, 50, 100, 200, 300, 400, 500, 600, 700, 800, 900 and 1000 mV/s. Inset: (top) CV at scan rate of 20 mV/s, (bottom) CV at scan rate of 1000 mV/s.

From the cyclic voltammetry experiments of complex **2a**$^{2+}$ at pH=1 we can estimate the equilibrium constant for the Ru(III)-O/Ru(II)-N pair ($K^{III}_{O\rightarrow N}$). From the extrapolation to $v\rightarrow\infty$ in the plot of [ic1]/[ic2] vs. v^{-1}, the value of $K^{III}_{O\rightarrow N}$ can be calculated, which in this case gives a value of $K^{III}_{O\rightarrow N}$= 0.235. The equilibrium constant, $K^{II}_{O\rightarrow N,}$ was calculated from the thermodynamic cycle shown in Scheme 4, where the value of the equilibrium constant $K^{III}_{O\rightarrow N}$ is that previously calculated and E^o are the $E_{1/2}$ potentials experimentally found for each process. In agreement to the Hess' Law, the next equation (7) can be build:

$$\Delta G^0_O=\Delta G^0(K^{II}_{N->O}) + \Delta G^0(K^{III}_{O->N}) + \Delta G^0_N \quad (7)$$

$$\Delta G^0 = -RT\ln K \quad (8)$$

$$\Delta G^0 = -nFE^0 \quad (9)$$

Considering the equations (7), (8), (9) and the constant values of R = 8.314 $J \cdot K^{-1} \cdot mol^{-1}$ and F = 96485 $C \cdot mol^{-1}$, the calculated equilibrium constant turns to be $K^{II}_{O \rightarrow N} = 6.70 \cdot 10^6$.

Due to the exceedingly high stability of the O-bonded isomer, the kinetic constants (Table 2) could only be obtained by simulation with the DigiSim software[9].

Table 2. Thermodynamic and kinetic parameters for the linkage isomerisation of **2a**$^{2+}$, determined by scan rate dependent CV see Figure 14.

$E_{1/2}$, N (V)	0.73
$E_{1/2}$, O (V)	0.27
$K^{II}_{O->N}$	$6.7 \cdot 10^6$
$K^{III}_{N->O}$	8.8737
$k^{II}_{O->N}$ (s^{-1})	0.0005
$k^{II}_{N->O}$ (s^{-1})	$7.463 \cdot 10^{-11}$
$k^{III}_{O->N}$ (s^{-1})	0.03381
$k^{III}_{N->O}$ (s^{-1})	0.3

The analysis of these values allow us to conclude that the involved linkage isomerism processes are slow, and the relative value of the equilibrium constants are in agreement with the Pearson's theory. This theory reflects the different coordinating affinity of Ru(II) and Ru(III) to nitrogen and oxygen atoms, respectively. Therefore, when the metal centre is in oxidation state (II), a relatively soft ion, it has more affinity to the likewise softer nitrogen atom than for the harder oxygen one, a tendency that is reversed once the ruthenium oxidation state increase to (III).

To deepen the electrochemical study of the system, the thermodynamic stability areas of complex **2a**$^{2+}$ with respect to pH and redox potential have been evaluated and the resulting Pourbaix diagrams for all the observed isomers are shown in Figures 15, 16 and 18. To perform this study only the electronic transition from Ru(II)

to Ru(III) has been considered due to the high complexity of the system. Three different species have been detected in the studied pH range. The first one corresponds to the initial isomer **Ru(III/II)-N_5**, which has five nitrogen atoms coordinated to the Ru metal centre (Figure 15).

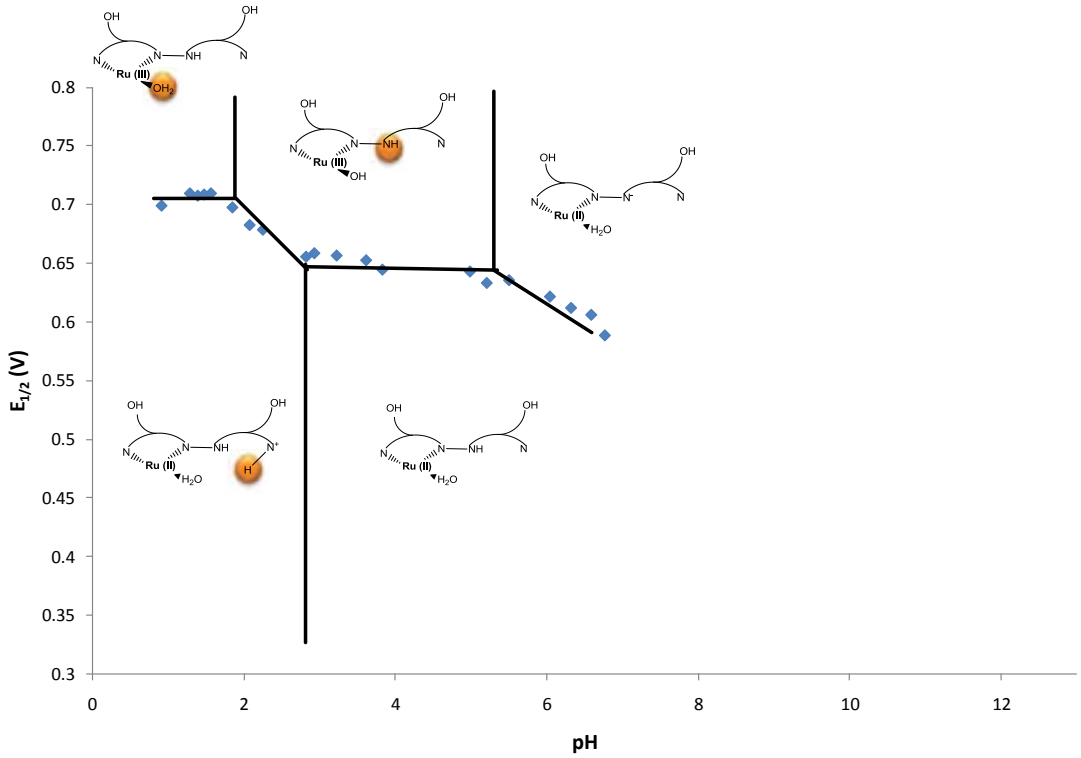

Figure 15. Pourbaix diagram for the **Ru-N_5** isomer of complex **2a**$^{2+}$. The zones of stability of the different species are indicated by the oxidation state of the Ru metal and the degree of protonation of the aqua and Hpbl groups. The terpyridine ligand is not drawn for clarity. The proton affected in each process is indicated in orange.

At low pH the **Ru(III/II)-N_5** isomer prevails but its concentration decrease as the pH increases and a second isomer appears. This second isomer is obtained by replacing a pyridine group by a vicinal alkoxide oxygen atom (Scheme 5a) and maintaining the rest of the coordination environment unaltered. (Figure 16).

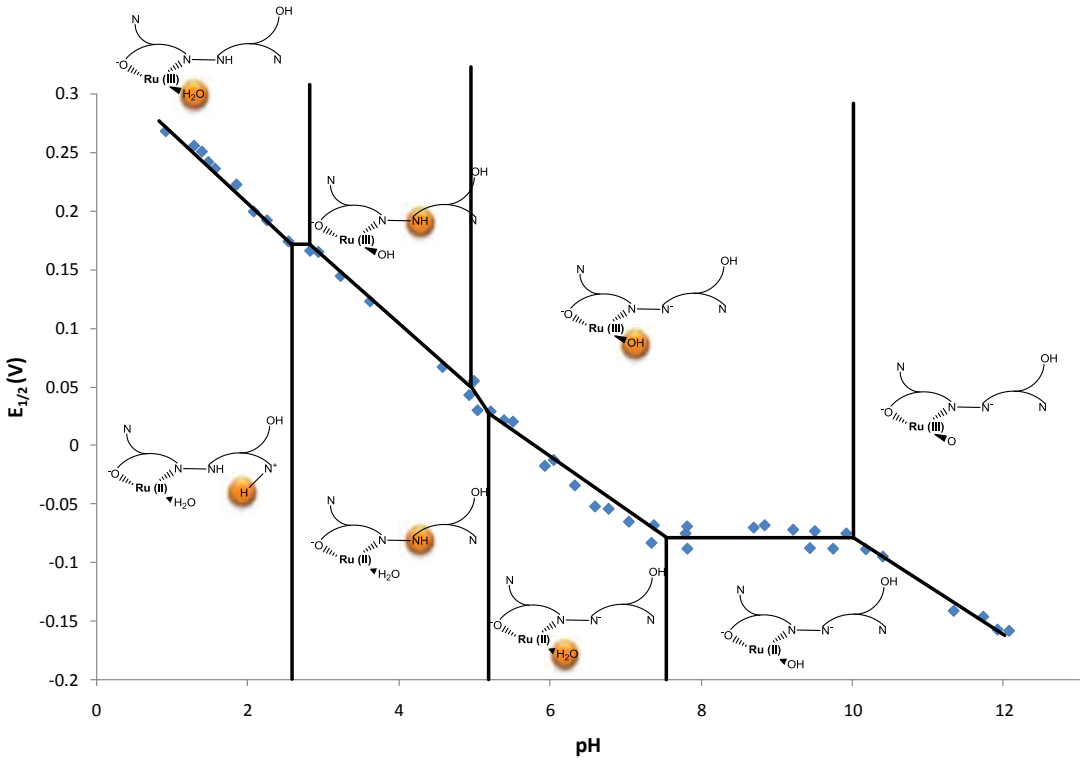

Figure 16. Pourbaix diagram for isomer **Ru-ON$_4$(Pz)** of complex **2a^{2+}**. The zones of stability of the different species are indicated by the oxidation state of the Ru metal and the degree of protonation of the aqua group and the Hpbl ligand. The terpyridine ligand is not drawn for clarity. The proton affected in each transformation is indicated in orange.

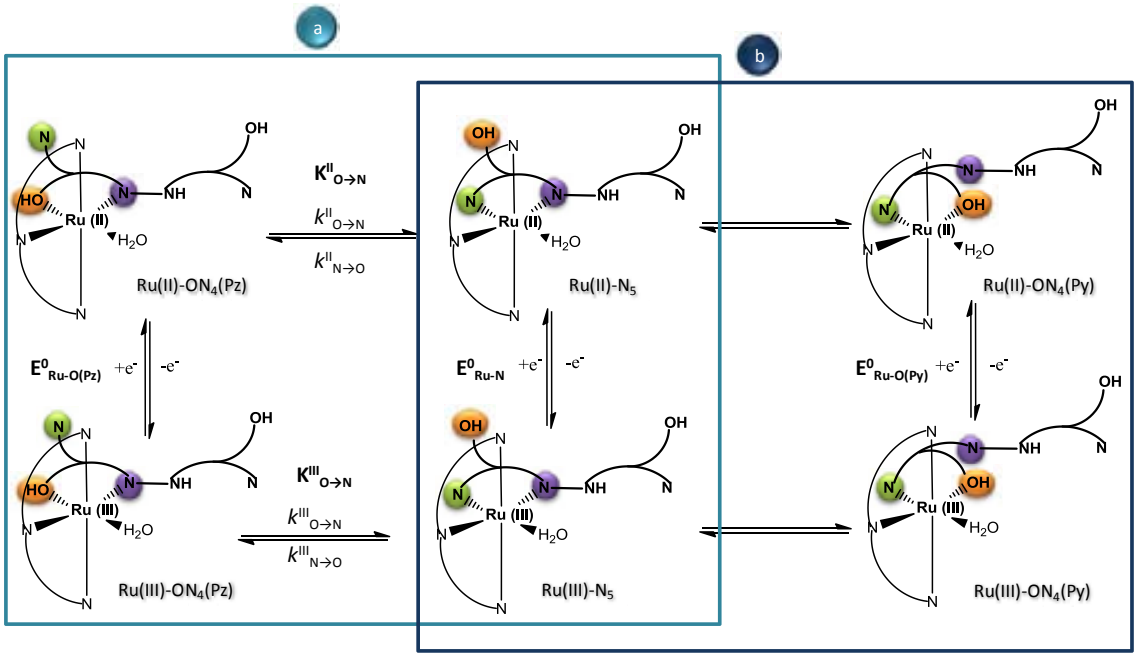

Scheme 5. Thermodynamic cycle for the linkage isomerisation process that takes places during the electrochemical oxidation of complex **2a^{2+}** at acidic pH (from 1 to 7) (a), and at basic pH (from 7 to 12) (a) and (b).

These two species coexist until pH=7 is reached; then a new species appears in the CV with a redox potential in between those of the **Ru(III/II)-N_5** and **Ru(III/II)-ON_4(Pz)** isomers (Figure 17).

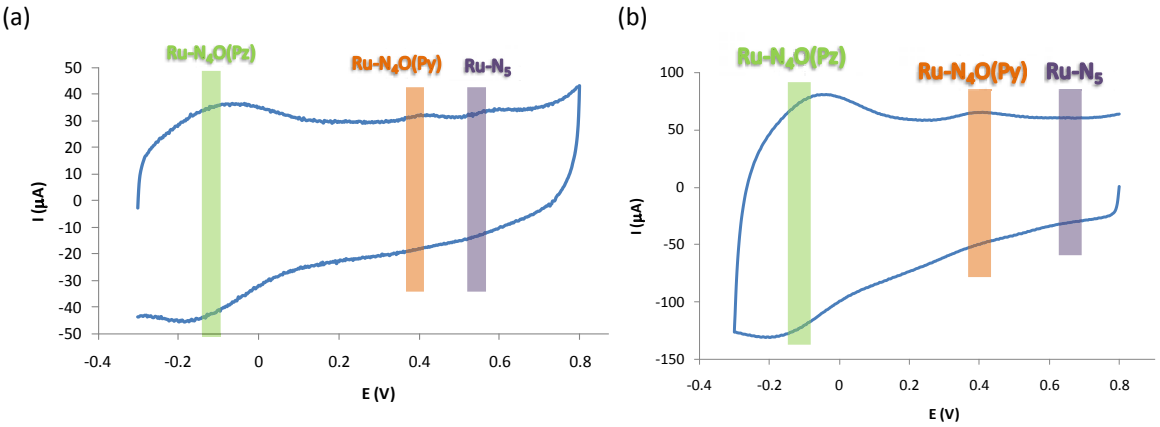

Figure 17. Cyclic voltammogram of complex **2a**$^{2+}$ in aqueous pH=8 buffer at a scan rate of 900 mV/s (a) scanning anodically (b) scanning cathodically with 3 minutes of equilibration time. The oxidation transitions are indicated by a green band for isomer **Ru-ON_4(Pz)**, an orange band for **Ru-ON_4(Py)** and a purple band for **Ru-N_5**.

We propose that this new isomer is another Ru-ON_4 species coming from the linkage isomerism between the pyrazolic nitrogen and the alkoxide oxygen atoms (Scheme 5b). This new isomer has three coordinated nitrogens from the terpyridine ligand and the other nitrogen from the pyridine of Hpbl, **Ru(III/II)-ON_4(py)** (Figure 18).This proposal is in agreement with its $E_{1/2}$, the results of DOSY NMR experiments (which discard the presence of dinuclear species) and the evidence of different N-decoordination patterns provided by the crystal structures (Figure 2). The presence of this **Ru(III/II)-ON_4(py)** isomer becomes more important as pH increase (Figure 19).

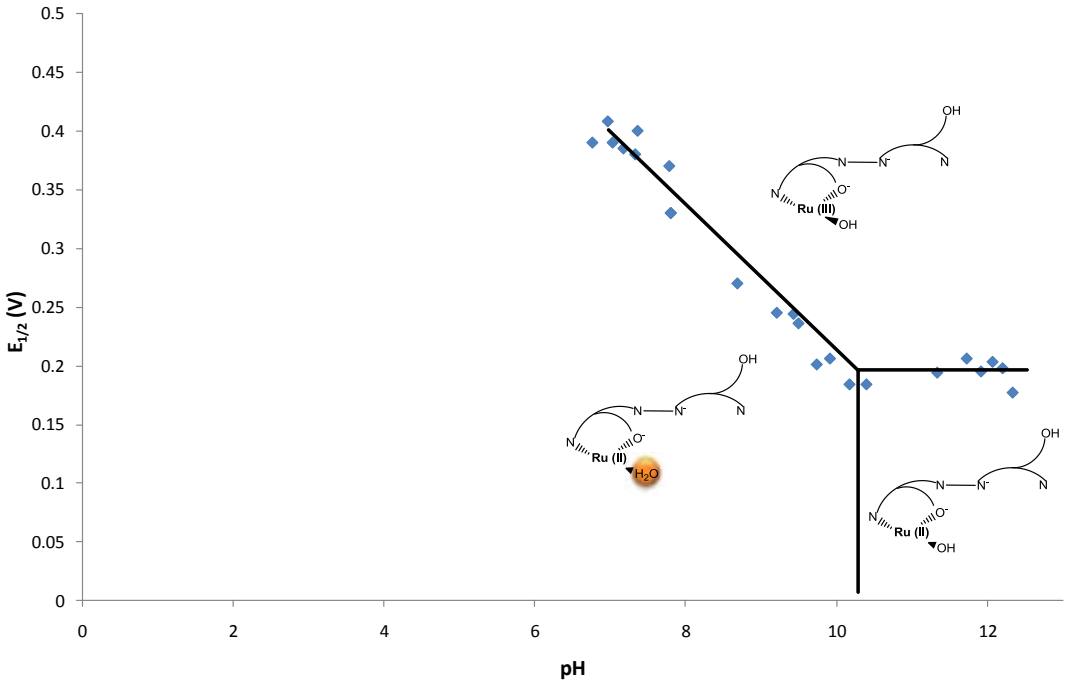

Figure 18. Pourbaix diagram for the **Ru-ON$_4$(Py)** isomer of complex **2a**$^{2+}$. The zones of stability of the different species are indicated by the oxidation state of the Ru metal and the degree of protonation of the aqua and Hpbl groups. The terpyridine ligand is not drawn for clarity. The proton affected by each process is indicated in orange.

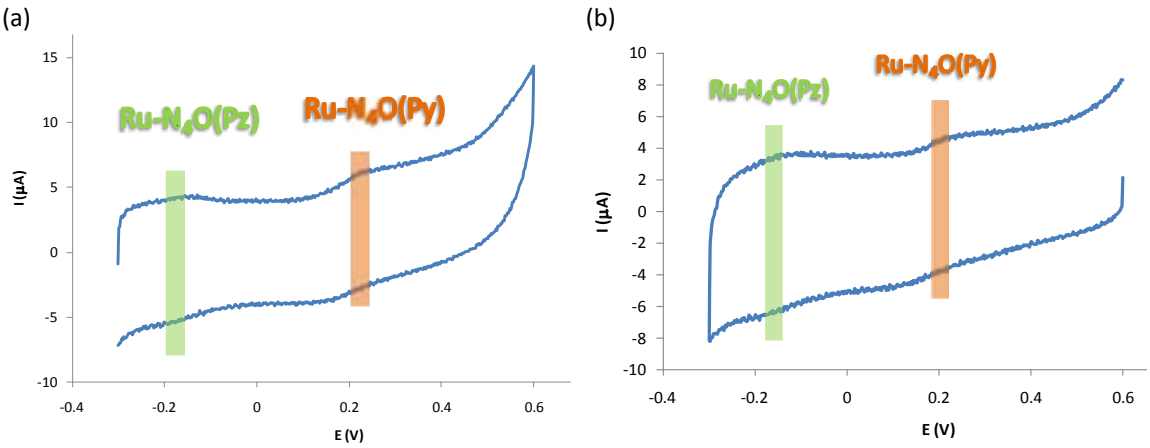

Figure 19. Cyclic voltammogram of complex **2a**$^{2+}$ in an aqueous pH=12 buffer solution at a scan rate of 100 mV/s (a) scanning anodically (b) scanning cathodically with 3 minutes of equilibration time. The oxidation transitions are indicated by a green band for the **Ru-ON$_4$(Pz)** isomer and by and orange band for the **Ru-ON$_4$(Py)** one.

Most of the pKa values, extrapolated from the Pourbaix diagrams, are similar to the ones described in the literature for similar polypyridylic ruthenium complexes.[5] The estimated pKa value for the Ru(II)-H_2O/Ru(II)-OH (pKa≈8) and Ru(III)-OH/Ru(III)-O

(pKa≈10) for the **Ru(III/II)-ON$_4$(Pz)** isomer (Figure 16) are much lower than the expected ones (pKa≈10 and pKa≈12, respectivelly). This decrease could be caused by the stabilization of the Ru(III)-O species though massive hydrogen bonding from OH^- and/or H_2O molecules, that including the alkoxo moiety. An example of such a hydrogen bonds bridging both entities is displayed in Figure 20.

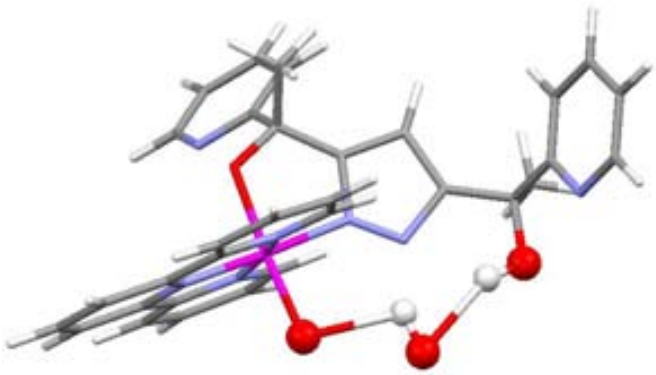

Figure 20. Mercury draw of the calculated structure of **[Ru^{III}-ON$_4$(Pz)-OH ·OH].** Hydrogen bonding between the Ru-OH and the alcohol group of the Hpbl ligand.

The electrochemical study of the dinuclear species **3a$^+$** in CH_2Cl_2 by cyclic voltammetry indicates the presence of three waves whose intensity depends on the scan rate and the starting redox potential (Figure 21). Scanning anodically (Figures 21a, and 21b) two waves with very different behaviour can be observed. The first one (A) at $E_{1/2}$=0.048 V corresponds to a quasi-reversible redox process with an [ic]/[ia] ratio independent of scan rate (10). This wave belongs to the N_5-Ru(II)—**Ru(III/II)-ON$_4$(Pz)** part of complex **3a$^+$** and does not present linkage isomerism linkage at the CV time scale.

N_5-Ru(II)—**Ru(II)-ON$_4$(Pz)** -1e$^-$ -> N_5-Ru(II)—**Ru(III)-ON$_4$(Pz)** (10)

On the other hand, the [ic]/[ia] ratio of the second wave (B), which is strongly scan rate dependent, belongs to the **N$_5$-Ru(III/II)**—Ru(III)-ON$_4$(Pz) part of complex **3a$^+$** and presents linkage isomerism as a response to an electrochemical stimuli (Figure 21 and equations (11) and (12)).

N$_5$-Ru(II)—Ru(III)-ON$_4$(Pz) -1e$^-$ -> **N$_5$-Ru(III)**—Ru(III)-ON$_4$(Pz) (11)

N$_5$-Ru(III)—Ru(III)-ON$_4$(Pz) -> **(Py)N$_4$O-Ru(III)**—Ru(III)-ON$_4$(Pz) (12)

As can be observed in Figure 21a the isomer generated after the linkage isomerism of the **N_5-Ru(III/II)**—Ru(III)-ON_4(Pz) subunit presents a slightly different redox potential (C) than that of N_5-Ru(II)—**Ru(III)-ON_4(Pz)** (B). This can only be rationalized by assuming the generation of a **(Py)N_4O-Ru(III)**—Ru(III)-ON_4(Pz) subunit upon oxidation and linkage isomerism where now the pyridine, instead of the pyrazole of the Hpbl ligand, is coordinated to the metal centre (12). This is in fact in agreement with the observed Ru(III) coordination environment in the crystal structure of **$3b^{2+}$ N_5-Ru(II)—Ru(III)-ON_4(Py)** (Figure 2a), where the oxidized metal centre is coordinated by the pyridylic nitrogen atom. Another isomer is generated when both metal centres are oxidized to Ru(III) resulting in the replacement of the pyrazolic nitrogen by the pyridylic one (13).

(Py)N_4O-Ru(III)—**Ru(III)-ON_4(Pz)** -> (Py)N_4O-Ru(III)—**Ru(III)-ON_4(Py)** (13)

Confirmation for the presence of this new isomer comes from two different points; (a) the X-ray structure of **$3c^{2+}$** (Figure 2b) showing a **(Py)N_4O-Ru(III)—Ru(III)-ON_4(Py)** arrangement of the metal centres and (b) the displacement of wave (B) to the same redox potential of wave (C) when scanning cathodically with a 3 min. equilibration time (Figure 21c). Therefore, despite this new coordination environment is favoured for Ru(III), its formation is slow and the species can only be observed after long time standing at the Ru(III) redox potential (Scheme 6).

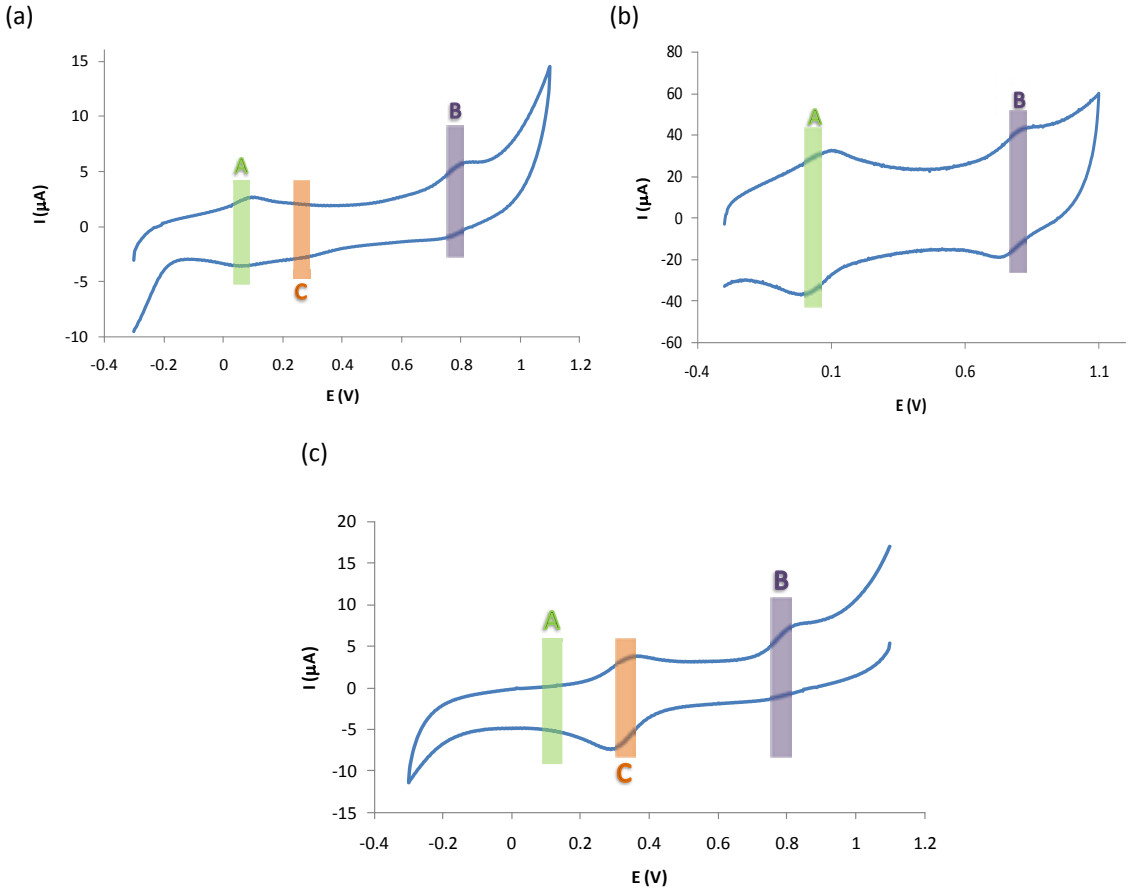

Figure 21. Cyclic voltammograms of complex **3a**$^{+}$ in CH_2Cl_2 using 0.1 M of TABH as electrolyte at a scan rate of (a) 40 mV/s and (b) 700 mV/s scanning anodically and (c) at 50 mV/s scanning cathodically.

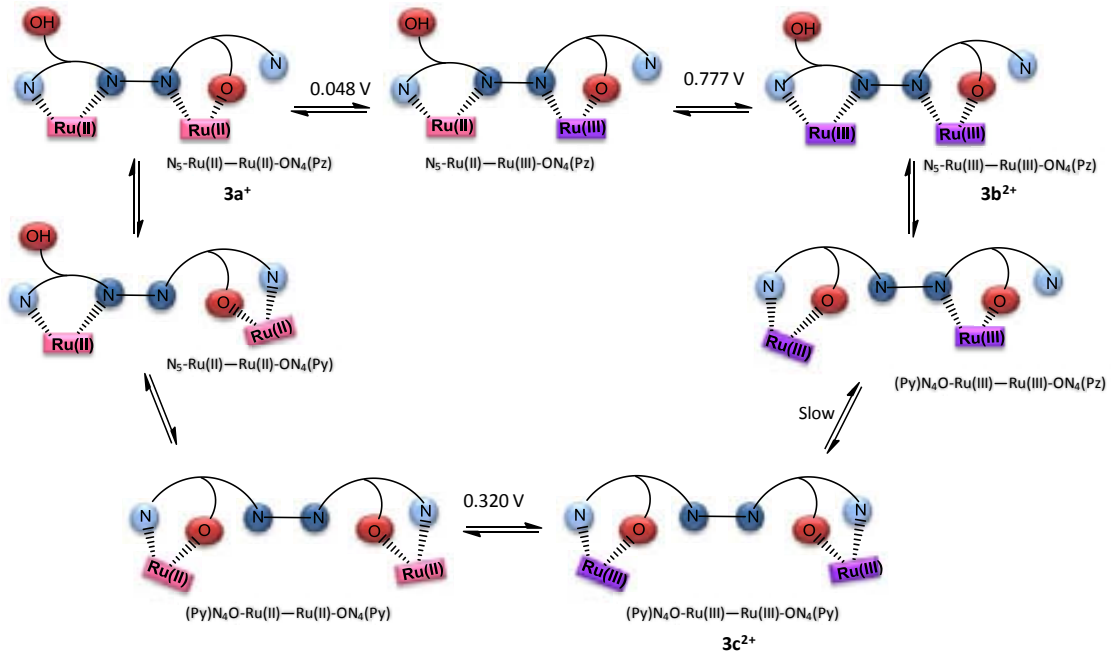

Scheme 6. Schematic representation of the different linkage isomerism processes in the dinuclear complex **3a**$^{+}$.

III.2.5. Catalytic activity

III.2.5.1. Water oxidation

The mononuclear complex **2a**$^{2+}$ has been preliminarily tested as a water oxidation catalyst showing very low activity and the cogeneration of O_2 and CO_2 due to the oxidative bimolecular deactivation pathway described in the chapter III.1. (Figure 22). In this case, the non-coordinating part of the ligand could be the most activated and accessible region for the initiation of a catalytst-catalyst oxidative process.

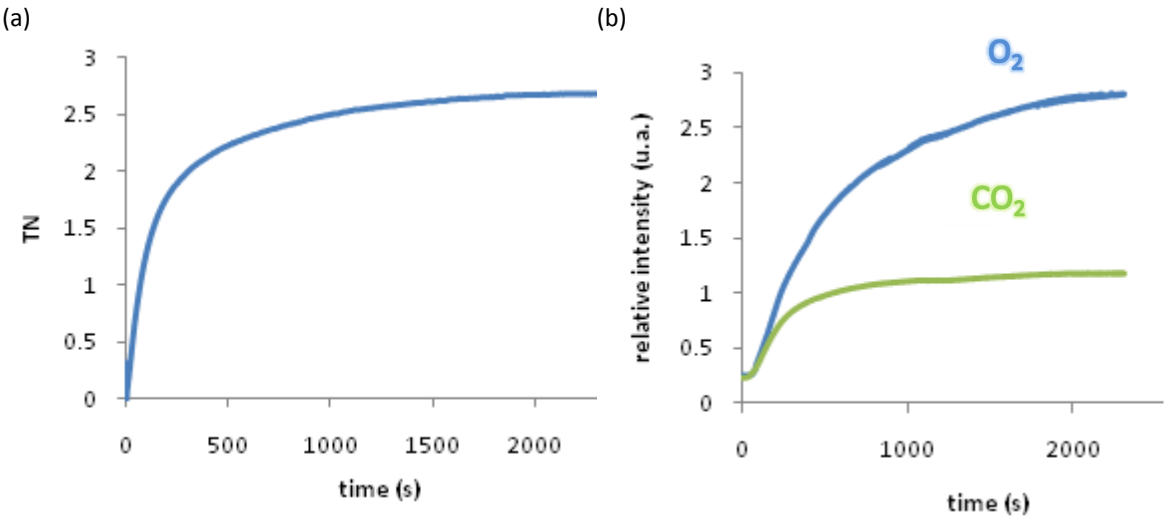

Figure 22. Monitoring of the catalytic gases generated during the water oxidation reaction as function of time: Cat (**2a**$^{2+}$) 1 mM/Ce 100 mM/0.1 M triflic acid with a total volume of 2 mL at 25.0 °C. (a) Manometry profile, (b) Online mass spectrometry profile for **2a**$^{2+}$.

III.2.5.2. Organic oxidations.

Furthermore, complex **2a**$^{2+}$ has also been preliminary tested as catalyst for the epoxidation of *cis-β*-methyl styrene in dichloroethane and using diacetateiodosylbenzene as co-oxidant. Complex **2a**$^{2+}$ has shown to be an active catalyst towards this kind of organic oxidations. indicates that could be an efficient catalyst for different organic oxidations, but more work must be done in order to clarify the real performance of the system in this field.

III.2.6. References

[11] (a) Ghosh, A.; Bischoff, A.; Cappiello, J. *Eur. J. Org. Chem.* **2003**, 821-832. (b) Sachse, A.; Penkova, L.; Noël, G.; Dechert, S.; Varzatskii, O.; Fritsky, I.; Meyer, F. *Synthesis.* **2008**, 800-806.

[2] (a) Meth-Cohn, O.; Vuorinen, E.; Modro, T. A. *J. Org. Chem.* **1989**, *54*, 4822-4827. (b) Wulfman, D. *Tetrahedron* **1976**, *32*, 1257-1265.

[3] (a) Llobet, A.; Curry, M. E.; Evans, H. T.; Meyer, T. J. *Inorg. Chem.* **1989**, *28*, 3131-3137. (b) Burchfield, D. E.; Richman, R. M. *Inorg. Chem.* **1985**, *24*, 852-857.

[4] Pérez-Trujillo, M.; Nolis, P.; Parella, T. *Org. Lett.* **2007**, *9*, 29-32.

[5] Sens, C.; Rodríguez, M.; Romero, I.; Llobet, A.; Parella, T.; Benet-Buchholz, J. *Inorg. Chem.* **2003**, *42*, 8385-8394.

[6] (a) Hu, Y.-Z.; Xiang, Q.; Thummel, R. P. *Inorg. Chem*. **2002**, *41*, 3423. (b) Brown, D.; Muranjan, S.; Jang, Y.; Thummel, R. *Org. Lett*. **2002**, *4*, 1253. (c) Wu, F.; Thummel, R. P. *Inorg. Chim. Acta* **2002**, *327*, 26. (d) Juris, A.; Prodi, L.; Harriman, A.; Ziessel, R.; Hissler, M.; El-Ghayoury, A.; Wu, F.; Riesgo, E. C.; hummel, R. P. *Inorg. Chem*. **2000**, *39*, 3590. (e) Wu, F.; Riesgo, E. C.; Thummel, R. P.; Juris, A.; Hissler, M.; El-Ghayoury, A.; Ziessel, R. *Tet. Lett*. **1999**, *40*, 7311.

[7] (a) Rodríguez, M.; Romero, I.; Llobet, A.; Deronzier, A.; Biner, M.; Parella, T.; Stoeckli-Evans, H. *Inorg. Chem*. **2001**, *40*, 4150. (b) Barkawi, K.; Llobet, A.; Meyer, T. J. *J. Am. Chem. Soc*. **1988**, *110*, 7751. (c) *Llobet, A. Inorg. Chim. Acta.* **1994**, *221*, 125-131.

[8] Huynh, M. H. V.; Meyer, T. J. *Chem. Rev.* **2007**, *107*, 5004–5064.

[9] DigiSim for Windows 95. Version 3.05. File type: CV. Bioanalytical Systems.

IV. SUMMARY AND CONCLUSIONS

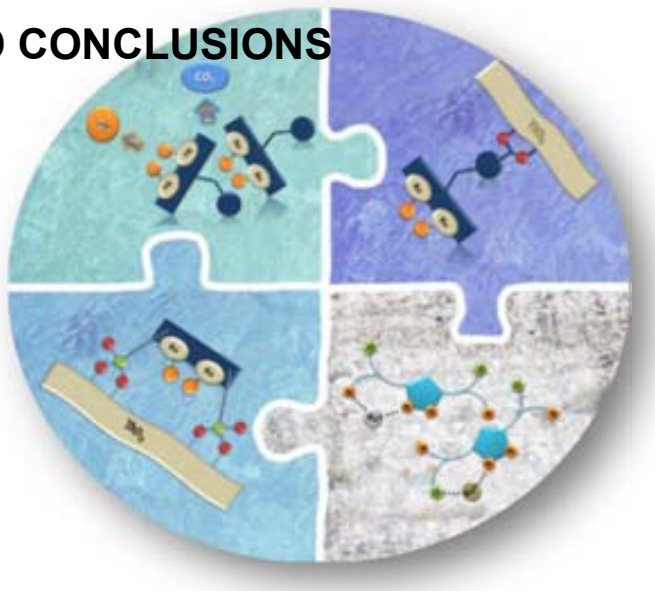

Considering the objectives described in Chapter II and the obtained results of this study, the following concluding remarks on this PhD thesis can be given:

Five new Hbpp-modified ligands (Hbpp-Bz, Hbpp-R_e, $(Hbpp)_2$-*p*-Xyl, $(Hbpp)_2$-*m*-Xyl, $(Hbpp)_2$-*o*-Xyl) have been synthesized and thoroughly characterized. Their dinuclear ($\{[Ru^{II}_2(trpy)_2(Y)](\mu\text{-}L)\}^{x+}$; L= Hbpp-Bz and Hbpp-$R_e$. When Y= Cl^- or Ac^- X=2+, and when Y=$(H_2O)_2$ X=3+) and tetranuclear ($\{[Ru^{II}_2(trpy)_2(Y)]_2(\mu\text{-}L)\}^{x+}$; L= $(Hbpp)_2$-*u*-Xyl. When Y= Cl^- or Ac^- X=4+, and when Y=$(H_2O)_2$ X=6+) complexes have been prepared and structurally, spectroscopically and electrochemically characterized.

These dinuclear and tetranuclear complexes have been tested as water oxidation catalysts. The results have shown the cogeneration of O_2 and CO_2, being the former the first gas evolved. Furthermore, the O_2/CO_2 ratio has been evaluated and proved dependent on catalyst concentration and benzylic CH_2 accessibility. Analizing the results we can arrange the complexes in increasing order of their benzylic CH_2 accessibility: $\{[Ru^{II}_2(trpy)_2(H_2O)_2]_2(\mu\text{-}(bpp)_2\text{-}o\text{-}Xyl)\}^{6+}$ < $\{[Ru^{II}_2(trpy)_2(H_2O)_2]_2(\mu\text{-}(bpp)_2\text{-}m\text{-}Xyl)\}^{6+}$ < $\{[Ru^{II}_2(trpy)_2(H_2O)_2]_2(\mu\text{-}(bpp)_2\text{-}p\text{-}Xyl)\}^{6+}$ < $\{[Ru^{II}_2(trpy)_2(H_2O)_2](\mu\text{-}bpp)\}^{3+}$ and by their O_2/CO_2 production ratio: $\{[Ru^{II}_2(trpy)_2(H_2O)_2]_2(\mu\text{-}(bpp)_2\text{-}o\text{-}Xyl)\}^{6+}$ [3] < $\{[Ru^{II}_2(trpy)_2(H_2O)_2]_2(\mu\text{-}(bpp)_2\text{-}m\text{-}Xyl)\}^{6+}$ [2.5] < $\{[Ru^{II}_2(trpy)_2(H_2O)_2]_2(\mu\text{-}(bpp)_2\text{-}p\text{-}Xyl)\}^{6+}$ [2.5] < $\{[Ru^{II}_2(trpy)_2(H_2O)_2](\mu\text{-}bpp)\}^{3+}$ [1]. By comparing these series, we can conclude that as the benzylic accessibility increases the O_2/CO_2 ratio decreases. Therefore, this dependence points out the benzylic CH_2 as the starting point of CO_2 production.

The Hbpp-R_e containing complex, after hydrolysis to Hbpp-R_a, has been supported onto a TiO_2 rutile surface and its capacity to oxidize water in heterogeneous phase with Ce(IV) as chemical oxidant has been tested. O_2 and CO_2 evolution has been online monitored and compared. All data indicates that the origin of this CO_2 is the same for the homogeneous and the heterogeneous systems.

From these experimental results, both in homogeneous and heterogeneous phase, we can conclude that one of the principal deactivation pathways for these WO catalysts is the intermolecular catalysts-catalyst oxidative degradation. The high

reactivity that presents the Ru(IV)-O group is the responsible of this oxidation of the organic part of the catalysts. The oxidation process starts from the less hindered and activated (electron rich) part of the ligand, which in these cases is the CH_2 of the benzyl moiety, and continues to the rest of the ligand.

In order to improve these results, the electrocatalytic activation of the catalysts has been tested to replace the strong and indiscriminate Ce(IV) as chemical oxidant for an specific and controlled potential. To accomplish that, the synthesis of new complexes containing trpy-P_e has been developed. Their hydrolysis has been carried out in order to obtain trpy-P_a, which can be used as anchoring moiety. This complex and the Hbpp-R_a containing one have been supported onto FTO-TiO_2 conducting films. All the newly generated species have been structurally, spectroscopically and electrochemically characterized. In addition, the anchoring processes have also been studied and optimized.

The FTO-TiO_2-$[Ru^{II}_2(trpy\text{-}P_a)_2(H_2O)_2(bpp)]^+$ and FTO-TiO_2-$[Ru^{II}_2(trpy)_2(H_2O)_2(bpp\text{-}R_a)]^{2+}$ modified electrodes have shown a displacement of their electrocatalytic WO waves to higher potentials. Nevertheless, they have been tested as water oxidation catalysts applying 1.6 and 1.7 V potentials, respectively. In both cases oxygen evolution could not be detected in the employed conditions. For the FTO-TiO_2-$[Ru^{II}_2(trpy\text{-}P_a)_2(H_2O)_2(bpp)]^+$ case this lack of catalytic activity can be attributed to the hydrophobic nature of the formed cavity between the catalysts and the solid surface. The later could prevent the H_3O^+ entrance to the active sites. When FTO-TiO_2-$[Ru^{II}_2(trpy)_2(H_2O)_2(bpp\text{-}R_a)]^{2+}$ is used, catalyst leaching together with the interaction between its active sites and the solid surface could prevent O_2 formation. This interaction could be caused by the prolonged anchoring time needed to anchor this complex in non-coordinating methanol as solvent.

For further works it is important to take into account that the position of the anchoring group and the anchoring process have big influence on the final properties and catalytic activity of these hybrid systems. Furthermore, the higher stability of the phosphonate moiety in comparison with the carboxylate one in these catalytic conditions has been demonstrated.

Despite all these new compounds are not efficient catalysts to oxidize water, it has been demonstrated that they are suitable catalysts to perform organic oxidations. The homogeneous complexes have been used as catalysts in the epoxidation of *cis*-β-methyl styrene , using $PhI(OAc)_2$ as chemical oxidant. The complexes supported onto FTO-TiO_2 conducting films have shown catalytic activity towards the electrocatalytic ethanol oxidation.

The synthesis and characterization of a new tetradentate bridging ligand (Hpbl) with O/N different coordination sites has been carried out. This new ligand is inspired on the structurally related and more rigid N-donor Hbpp [3,5(bispyridyl)pyrazole] ligand. The Hpbl contains extra sp^3 carbon atoms with alcoholic functions between the pyrazol and pyridine groups, that allowing a linkage isomerism between the pyridilyc or pyrazolic nitrogen atoms and the alcoholic oxygens.

The mononuclear $[RuX(Hpbl)(trpy)]^{y+}$ (X=Cl, y=+1; X=H_2O, y=+2) and dinuclear $[Ru_2Cl_2(bpl)(trpy)_2]^+$ Ru(II) complexes have been synthesized. In solution, all these complexes have been characterized spectroscopically (UV-vis and NMR) and electrochemically (CV). In the solid state, monocrystal X-ray diffraction analyses have been carried out for two linkage isomers of the dinuclear complex $[Ru_2(trpy)_2(pbl)Cl]^{2+}$ and for the mononuclear $[Ru^{III}(trpy)(pbl)(OH)]$ or $[Ru^{II}(trpy)(pbl)(H_2O)]$ complex.

The linkage isomerism processes occurring for the mononuclear aqua complex has been studied as function of pH and redox potential. Therefore, three different coordination environments around the Ru-OH_2/Ru-O basic structure have been identified: (1) the ruthenium metal centre coordinated by 5 nitrogens atoms of the ligands (three from the trpy and two from the Hpbl) [Ru-N_5]; (2) coordination to Ru through one alkoxo oxygen an four nitrogen atoms (three from the trpy and one from the pyridyl group of Hpbl), [Ru-ON_4(Py)]; and (3) coordination taking place again *via* one alkoxide oxygen and four nitrogen atoms (three from trpy but now one from the pryrazol Hpbl scaffold), [Ru-ON_4(Pz)]. The combination of them allows us to explain the redox-dependent linkage isomerism of the dinuclear complexes observed in the solid state (X-ray Crystallography) and CV experiments.

The application of these new complexes in different biologically and technologically relevant catalytic oxidation processes is currently under development in our laboratories.